Mudslides during Hurricane Ivan and an Assessment of the Potential for Future Mudslides in the Gulf of Mexico

by

Mary C. Nodine, Jeong Yeon Cheon, Stephen G. Wright, and Robert B. Gilbert,

The University of Texas at Austin

E.G. Ward, Offshore Technology Research Center

Phase II Project Report

Prepared for the Minerals Management Service

Under the MMS/OTRC Cooperative Research Agreement

1435-01-04-CA-35515

Task Order 39239

MMS Project Number 552

October 2007

OTRC Library Number: 10/07C185

For more information contact:

Offshore Technology Research Center

Texas A&M University

1200 Mariner Drive

College Station, Texas 77845-3400

(979) 845-6000

or

Offshore Technology Research Center

The University of Texas at Austin

1 University Station C3700

Austin, Texas 78712-0318

(512) 471-6989

A National Science Foundation Graduated Engineering Research Center

EXECUTIVE SUMMARY

This study involves the examination of wave-induced submarine mudslides caused by recent major hurricanes in the Mississippi Delta region of the Gulf of Mexico, including the development of a model that can be used to analyze and predict these mudslides. Reports of mudslides caused by Hurricane Ivan in 2004 and Hurricane Katrina in 2005 were collected and studied to determine locations of mudslide activity. A simple limit equilibrium model was adapted to calculate a factor of safety against mudslide occurrence given the soil shear strength, the water depth, the slope angle, and the wave height and period at a site. The limit equilibrium model was verified using a more rigorous deformation model, and parametric analyses were performed to determine the sensitivity of the model to changes in input parameters. The limit equilibrium model was validated by comparing model predictions with reported occurrences and non-occurrences of mudslides in Hurricanes Katrina and Ivan as well as Rita, Lili, and Andrew. Finally, the limit equilibrium model was incorporated into a risk assessment methodology to quantify and analyze the risk associated with offshore mudslides in the Mississippi Delta.

The following major conclusions are drawn from this study:

- Mudslides caused by recent large hurricanes occurred in or very near to the mudslide prone area delineated by Coleman et al. (1980). Most mudslides occurred in the mudflow lobe areas within the mudslide prone area, while a few occurred in the mudflow gully area.
- In most parts of the Mississippi Delta region of the Gulf of Mexico, mudslides can only be caused by very large storm waves and are therefore infrequent events. Only three major storms (Camille, Ivan, and Katrina) caused significant and widespread mudslide activity in the past 40 years.

- Hurricanes Ivan and Katrina probably caused similar amounts of mudslide activity.
- Wave period is an important factor in mudslide vulnerability. Waves in Hurricanes Ivan caused significantly more mudslide activity than other storms of its magnitude due to its very long wave periods.
- Slope angle is not a significant factor in mudslide vulnerability except in the deeper parts of the mudslide prone area (water depths greater than about 300 feet).
- Site-specific analyses of mudslide vulnerability are challenging due to substantial variations in soil shear strength over distances as short as a few hundred feet; analyses need to incorporate these possible variations in shear strength to be realistic.
- Mudslides are localized features, on the order of several thousand feet in lateral extent and about 50 to 150 feet deep. The areal extent and depth of mudslides are related to the lengths and widths of the storm waves that cause them. Mudslides are not likely to lead to large-scale, regional mudflows due to the very flat slopes in the mudslide prone area and the large amount of local variation in soil shear strength.
- The return periods for mudslides impacting facilities range from less than 10 years to greater than 1,000 years and depend strongly on location. The risk for mudslides increases as the water depth decreases, the slope of the bottom increases, and the amount of infrastructure in a particular area increases. Project-specific risk analyses should incorporate all available site-specific information on metocean conditions, bathymetry and soil properties.

TABLE OF CONTENTS

LIST OF TABLES AND FIGURES

TABLES

FIGURES

I. INTRODUCTION

Hurricane Wave-Induced Mudslides and their Consequences

Waves generated by large hurricanes in the Gulf of Mexico can cause significant damage to offshore oil and gas infrastructure. Not only do these waves generate forces on structures, they also generate significant pressures on the ocean floor in shallow water (up to about 400 feet). In the Mississippi Delta region of the Gulf of Mexico, where the rapidly-deposited sediment can be very weak, wave-induced pressures can be large enough to trigger submarine slope failures, commonly referred to as "mudslides."

The consequences of submarine mudslides were first documented after Hurricane Camille in 1969, when one offshore oil platform was destroyed and at least one other was severely damaged by a mudslide in South Pass Lease Block 70 (Sterling and Strobeck, 1973). Significant mudslide activity was not observed again until 35 years later, when Hurricane Ivan occurred in September 2004. The Minerals Management Service (2005) published reports of 24 incidents of damage to pipelines caused by mudslides during Hurricane Ivan, and reports indicated that one platform in Mississippi Canyon Lease Block 20 was toppled by a mudslide. Coyne et al. (2005) and Thompson et al. (2005) described in detail incidents where pipelines were severed and moved out of alignment by mudslides.

In August 2005, less than one year after Hurricane Ivan, Hurricane Katrina struck the Gulf of Mexico. Though the most dramatic damage caused by Hurricane Katrina occurred onshore in the vicinity of New Orleans, Louisiana, the storm caused 299 damage incidents to pipelines (MMS, 2006). Seven of these damage incidents were attributed to mudslides, but discussion with representatives from Shell Oil Company (Wrzyszczynski and Coyne, 2007) indicates that additional cases of damage that may have been caused by mudslides were discovered since that MMS report was compiled. Mudslide activity is expected to occur in future large hurricanes with tracks crossing over or near the Mississippi Delta region of the Gulf of Mexico. Unless pipelines are routed

around mudslide prone areas or are constructed to withstand mudslides, continued damage to pipelines is expected.

Motivation

After the mudslide in South Pass Lease Block 70 caused by Hurricane Camille in 1969, a significant amount of research was devoted to studying mudslides and developing models that could be used to predict them. Little research was performed after the mid-1980's, however, because no new data were available to study wave-induced mudslide activity. The mudslide activity caused by Hurricanes Ivan and Katrina provide an excellent opportunity to re-examine the areas of the Gulf of Mexico that are expected to be vulnerable to mudslides, to verify the existing models used to predict mudslides, and to develop methods for assessing the risk for future mudslides at a site.

Objectives

The objectives of this research include using reports of wave-induced mudslides, bathymetric data, soil shear strength data, and oceanographic data to analyze mudslide vulnerability in the Mississippi Delta region of the Gulf of Mexico.

The tasks for Phase I as outlined in the project proposal are as follows.

> ***Task 1:*** Review existing data on seafloor movements, including pipeline movements and failures, during Hurricane Ivan to identify the locations where movements occurred and the extent of movements.
>
> ***Task 2:*** Review pre-Ivan soil data including data on soil properties (unit weights, undrained shear strength) for selected areas where large soil movements were observed or expected.
>
> ***Task 3:*** Select representative sites for analyses and further study based on the

locations of movements and the available soil data. Also select and include a nearby site where the seafloor appeared to remain stable during Ivan.

Task 4: Determine wave conditions during Ivan at the selected sites. Obtain Hurricane Ivan oceanographic data.

Task 5: Analyze seafloor stability at the representative sites selected in Task 3 to predict the potential for instability and soil movements. Data assembled in Task 1, 2 and 4 will be used in these analyses.

Task 6: Final Report on Phase 1.

The final report on Phase I was issued in October, 2006. The tasks for Phase II as outlined in the project proposal are as follows:

Task 7: Areas of interest will be selected for a study of potential soil movements in future hurricanes. The sites could include the routes of existing and/or expected future pipelines. Areas of future interest will be defined in consultation with the MMS and industry.

Task 8: Analyze the potential for seafloor movements in future hurricanes. The validated models will be used to analyze the potential for seafloor movements due to future hurricanes. Parametric studies of seafloor movement due to hurricane waves will be conducted for sites representing these areas of interest. The Parametric study will use seafloor properties estimated from best available sources. Wave conditions will include the range of those that can be expected in future hurricanes.

Task 9: Probabilistic analyses of these results will provide estimates of the potential and likelihood for future seafloor movements throughout the areas of interest. These results can then be used to identify areas where either seafloor

movements are likely or where more detailed investigations will be needed before hazards and risks can be established.

Task 10: This task is devoted to preparation of the final project report. The final report will summarize the analyses, results, and data used in this study and include appropriate maps of the Gulf of Mexico identifying areas of potential seafloor movement due to future hurricanes. A final meeting with MMS representatives and industry will be held to discuss study results.

Scope

This report presents results of the research for MMS Project 552 as outlined in Tasks 1-10, listed above. Investigation of mudslides caused by Hurricane Katrina was not included in the original proposal, because at the time the project was proposed, Hurricane Katrina had not yet occurred. Oceanographic data and information on reported mudslides from Hurricane Katrina were incorporated into this study as they became available.

Equations for a simple limit equilibrium model that can be used to analyze mudslide vulnerability are presented. The model is verified using a more complex layered continuum model. Two simple tools are presented that can be used to apply the limit equilibrium model. One is a chart that can be used to find the factor of safety against mudslide initiation for a site where the undrained shear strength increases linearly with depth, and the other is an Excel spreadsheet computer program that can be used to calculate the factor of safety for sites with more complicated shear strength profiles. The various forms of data that are necessary to implement the limit equilibrium model are then presented. These data include reports of mudslide activity, bathymetry, oceanographic data, and soil shear strength data. Analyses performed using the limit equilibrium model are then presented. Parametric analyses were performed to explore the sensitivity of the limit equilibrium model to different input variables. Analyses of mudslide activity in the Mississippi Delta region of the Gulf of Mexico in Hurricanes Ivan and Katrina were also performed to determine how well results found using the simple limit equilibrium model agreed with reports of mudslide activity. Finally, a risk

analysis investigating the potential risk of future mudslides in the Mississippi Delta region of the Gulf of Mexico is presented.

Publications

Nodine, M.C., Wright, S.G., Gilbert, R.B., and Ward, E.G. (2006), "Mudflows and Mudslides During Hurricane Ivan," *Proc. Offshore Technology Conference*, Houston, Texas, OTC Paper No. 18328.

Nodine, M.C., Gilbert, R.B., Wright, S.G., Cheong, J.Y., Wrzyszczynski, M., Coyne, M., and Ward, E.G. (2007), "Impact of Hurricane-Induced Mudslides on Pipelines," *Proc. Offshore Technology Conference*, Houston, Texas, OTC Paper No. 18983.

II. BACKGROUND

Characteristics of Water Waves

This section defines the important terms related to water waves that will be used in this report. For most of the calculations performed for this study, it was assumed that the assumptions of first-order linear wave theory applied (Wiegel, 1964). A two-dimensional schematic of a water wave with important parameters labeled is shown in Figure 1. Waves were generally assumed to be sinusoidal in shape and were assumed to be infinitely long in the direction perpendicular to the direction of wave propagation.

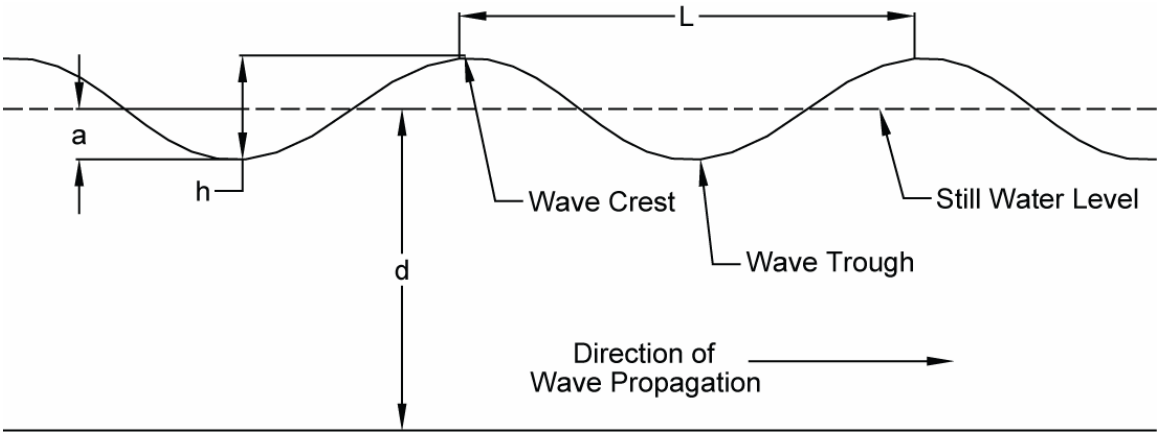

Figure 1. Schematic of an ocean wave

The wave height (*h*), amplitude (*a*), wavelength (*L*), and water depth (*d*) are labeled in Figure 1. The wave height is the distance from the crest to the trough of the wave. The wave amplitude is the distance from the still water level to the peak or trough, or half of the wave height. The wavelength is the distance from the crest of one wave to the crest of the next wave. The wave period (*T*) is the time that it takes for the wave to travel the distance of one wavelength. The water depth is the distance from the still water level to the ocean floor. In all calculations for this study, the ocean floor was assumed to be rigid.

Mudslide Mechanism

Hurricanes can generate very large waves in the Gulf of Mexico, and recent hurricanes have caused particularly large waves. The highest waves recorded to date in the Gulf of Mexico were measured during Hurricane Katrina and had a maximum wave height of about 100 feet (Cardone et al, 2005). During Hurricane Ivan in 2004, the maximum measured wave height was about 95 feet. Prior to 2004, the maximum measured wave in the Gulf of Mexico was about 72 feet, measured in 1969 in Hurricane Camille (Patterson, 1974).

In shallow water (less than 400 feet), large storm waves can cause significant increases and decreases in the pressure on the ocean floor. The pressure on the ocean floor increases beneath the wave crest and decreases beneath the trough. As a wave moves along the ocean surface a corresponding pressure wave moves along the ocean floor. The amplitude of the pressure wave becomes greater with larger wave heights and longer wave periods, and becomes smaller with an increase in water depth. When the water depth is greater than about 400 feet, the change in pressure on the seafloor due to the waves at the water surface is essentially inconsequential. A schematic of the pressure wave on the ocean floor caused by waves on the ocean surface is shown in Figure 2.

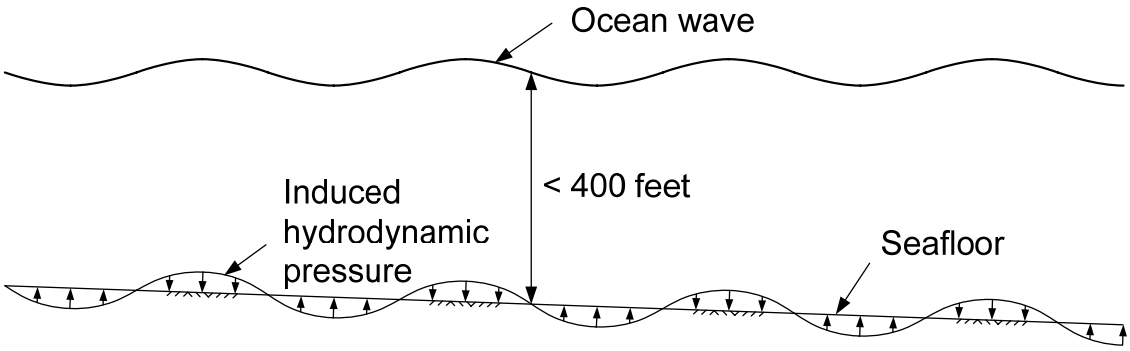

Figure 2. Schematic of the pressure wave on the ocean floor caused by waves on the ocean surface (from Wright et al. 2007)

The soil in the Mississippi Delta region of the Gulf of Mexico tends to be very soft due to its rapid deposition. The soil has often not reached a degree of consolidation of 100%

under the current overburden. Soils such as these are often referred to as underconsolidated clays. These characteristics result in the soil having very low undrained shear strength, which increases its vulnerability to slope failures. In shallow water the pressure change caused by storm waves can produce a driving moment sufficient to cause slope failure in these soft soils, even on very flat slopes (Henkel, 1970). Researchers have performed experimental studies confirming the ability of large waves to produce seafloor movements (e.g. Doyle, 1973).

Mudslide Prone Area

In the late 1970's, a project was undertaken by the United States Department of the Interior to map the bathymetry and geologic features in the Mississippi Delta region of the Gulf of Mexico (Coleman et al. 1980). Mudslide features mapped from side-scan sonar data are delineated in Map 5 from Coleman et al. (1980), entitled "Seafloor Morphology" and shown in Figure 3. In this map, regions containing six different types of seafloor features are delineated. These features include collapse depressions, mudflow gullies, mudflow lobes, slightly disturbed seafloor, reef, and undisturbed seafloor. The various types of features as explained by Coleman et al. (1980) are described in the following section.

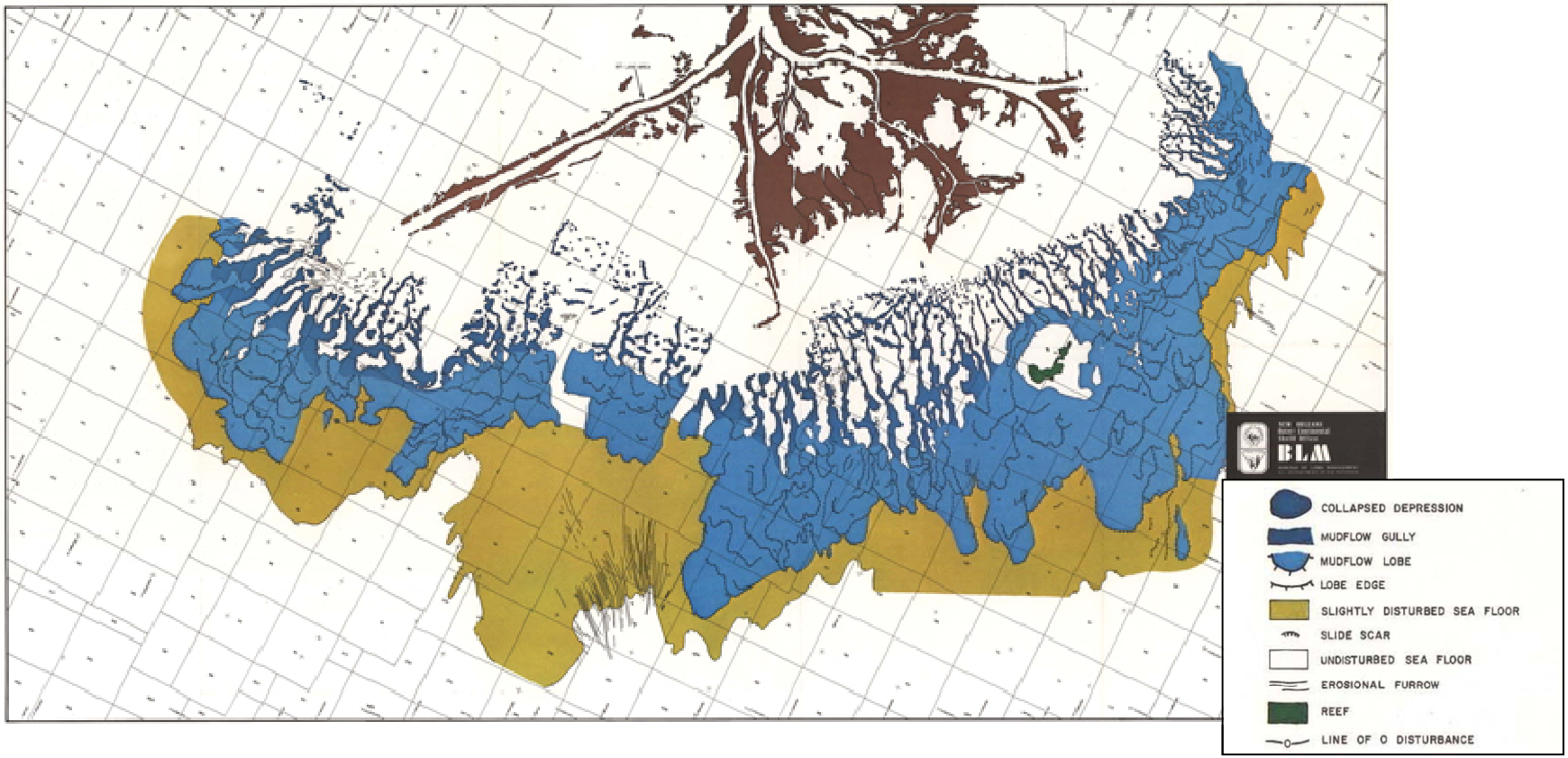

Figure 3. Geologic features in the Mississippi Delta region of the Gulf of Mexico (Map 5 from Coleman et al, 1980)

Collapse Depressions

Collapse depressions occur in water depths up to about 50 feet and on very flat slopes, ranging from less than 0.1° to about 0.4°. These features are relatively small, on the order of 120 to 500 feet in areal extent. Collapse depressions are bowl-shaped areas that have been displaced vertically, surrounded by scarps up to 9 feet high. The central portion of collapse depressions tends to have a blocky, hummocky surface (Coleman et al, 1980). Collapse depressions are included in the "Mudflow Gully" area in most of the maps shown in this report. The small, rounded, individual regions closest to shore are collapse depressions, while the elongate regions connected to the rest of the mudslide prone area are mudflow gullies.

Mudflow Gullies

Mudflow gullies are narrow, sinuous features typically four to six miles long occurring in water depths from 20 to 300 feet. According to Coleman et al. (1980), disturbed or remolded sediment follows the path of mudflow gullies, starting at collapse depressions and other features upslope and terminating at the mudflow lobes in deeper water. The floors of mudflow gullies may be 10 to 60 feet below the adjacent ocean floor (Coleman et al, 1980). A few of the wave-induced mudslides that were reported after Hurricanes Ivan and Katrina occurred in the mudflow gully region.

Mudflow Lobes

The region of mudflow lobes begins where mudflow gullies terminate, and is characterized by multiple overlapping lobes of sediment. Each lobe has a relatively flat surface with a sharply inclined "nose" downslope composed of discharged debris. The mudflow lobes can be more than 75 feet thick. As episodic slope failures occur in the mudflow gully and mudflow lobe regions, the mudflow lobes pile on top of one another, often resulting in very deep deposits of disturbed sediment (Coleman et al, 1980). The

dynamic nature of the mudflow lobe region and the mudflow gully region upslope, due both to sediment deposition from the Mississippi River and mudslide activity, causes the soil properties in this area to be extremely variable. Most of the wave-induced mudslides discussed in this study occurred in the mudflow lobe region.

Slightly Disturbed Seafloor

The zone of slightly disturbed seafloor around the edge of the mudflow lobes has a somewhat irregular surface and is typically less than 10 to 15 feet thick. It lies above well-stratified deposits that do not appear to have undergone movement (Coleman et al, 1980). Few wave-induced mudslides have been reported in or along the border of this region.

Reef

A reef exists in South Pass Lease Blocks 60-67. This reef is not believed to be living, but it protrudes above the soft sediments that surround it (Coleman et al, 1980). No wave-induced mudslides have been reported, nor are they expected to occur, in the reef area.

Undisturbed Seafloor

The remaining area on the Seafloor Morphology Map is called Undisturbed Seafloor. This region was not studied in detail by Coleman et al. (1980) for their mapping project, and it is not specifically described in their report. Presumably this region consists of well-stratified deposits that have not been disturbed by the various types of seafloor movement that occur in rest of the Mississippi Delta region.

Together, the regions with mudflow gullies, mudflow lobes, and slightly disturbed seafloor make up what is referred to in this study as the “mudslide prone area.” Both in

this study and historically, no strong evidence of ocean wave-induced mudslides has been reported for locations outside the mudslide prone area. Therefore, this study focuses almost exclusively on data from and events that occurred within the mudslide prone area. Figure 4 shows all of the oil and gas pipeline routes in the mudslide prone area as reported by the Minerals Management Service (2006). Hundreds of pipelines cross this area in a variety of directions, so the potential for pipelines to be impacted and damaged by mudslides that occur during large hurricanes is very high.

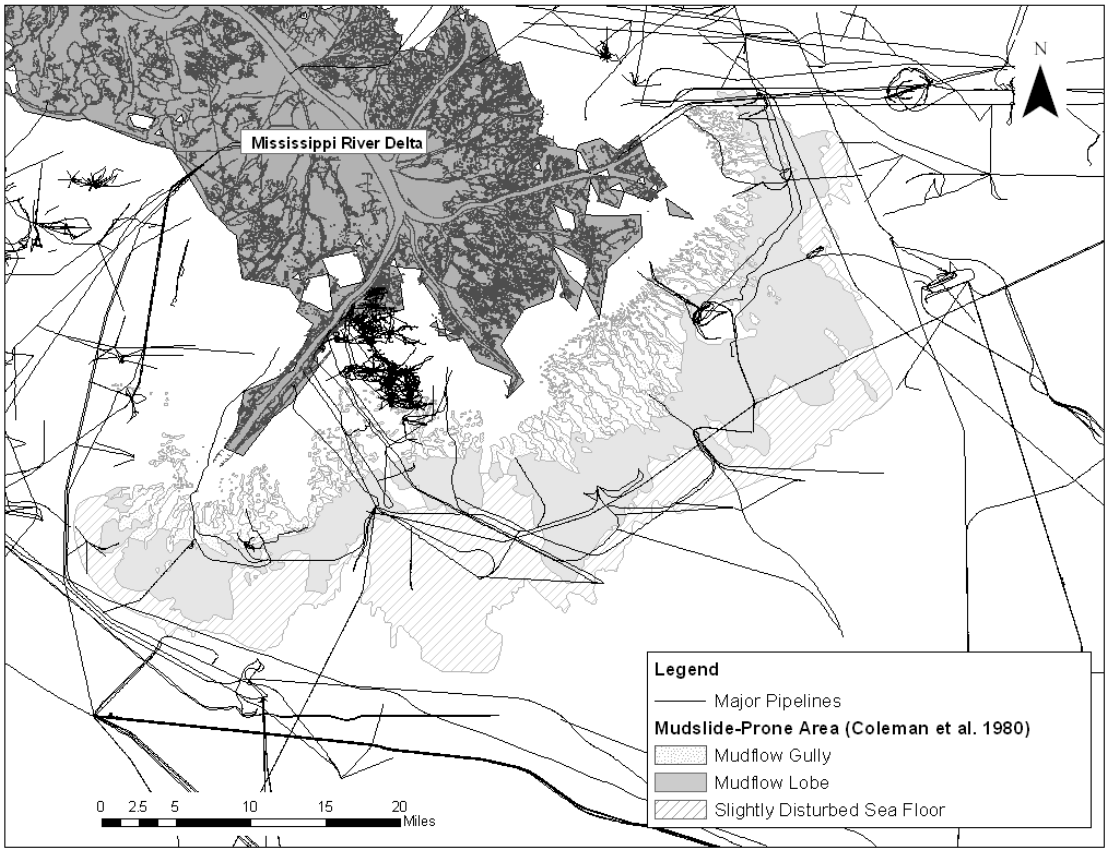

Figure 4. The mudslide prone area delineated by Coleman et al. (1980), shown with all major pipeline routes as reported by the Minerals Management Service in 2006

Previous Studies of Mudslide Vulnerability

Numerous studies have been performed, mostly in the 1970's and 1980's, to investigate and model storm wave-induced slope failures in the Mississippi Delta region of the Gulf of Mexico. These studies generally used one of three types of models: limit equilibrium, layered continuum, or finite element. Each model is described briefly in the following sections, and examples of the use of each model are provided.

Limit Equilibrium Models

Limit equilibrium models are used to calculate a factor of safety against slope instability, usually represented as the sum of the resisting moments divided by the sum of the driving moments. If the factor of safety is less than 1.0, the slope is expected to be unstable. The limit equilibrium model was first used to analyze ocean wave-induced submarine mudslides by Henkel (1970). Henkel assumed a circular failure surface with moments summed about the center of the circle. The driving moments consist of the weight of the soil and the pressures imparted on the ocean floor by the wave on the ocean surface. The resisting moment comes from the shear strength of the soil. Henkel used the undrained shear strength of the soil due to the relatively rapid load rate of the wave pressures that cause the soil to fail.

Researchers have also applied the limit equilibrium model to non wave-induced submarine mudslides using an infinite slope analysis and drained shear strengths. Prior and Suhayda (1978) used this method to investigate the effect of pore water pressures on sediment stability in the Mississippi Delta, indicating that increases in pore water pressures due to gas generation, sediment buildup, and cyclic wave loading could cause shallow slope failures.

Layered Continuum Models

Unlike limit equilibrium models, layered continuum models provide information on the extent of soil movement. The most common layered continuum model is that developed by Schapery and Dunlap (1977, 1978). This model represents the soil profile as a series of parallel layers with different material properties. The soil is assumed to be linear and viscoelastic. Schapery and Dunlap (1977, 1978) were able to use their model to couple the motions of ocean waves with the corresponding motion of soil to determine how much wave energy is dissipated by the soil. This model has been used by others since its development, including Bea et al. (1981) and Hooper (1996, 2005) to analyze the slope stability of various sites. Another layered continuum model developed by Pabor (1981) uses a nonlinear hysteretic soil model.

Finite Element Models

Finite element models model the soil with discrete (finite) elements. Soil properties are represented by nonlinear stress-strain relationships. Like layered continuum models, finite element models can be used to determine stresses and movements in a soil mass. Finite element models were employed by Arnold (1973), Kraft (1976), Wright et al. (1972) to analyze submarine slope stability. All of these studies model the wave loading as an instantaneous static stress on the ocean floor. Later finite element models included the effects of gravity-induced stresses on soil movements (Wright, 1976).

Bea et al. (1980) used limit equilibrium, layered continuum, and finite element models to analyze a mudslide in South Pass Lease Block 70 after Hurricane Camille in 1969. The authors found that results of all three models agreed well with observed soil movement, both in terms of the prediction of failure and in terms of the extent and depth of movement. The limit equilibrium model proposed by Henkel (1970) was used for most

of the analyses performed for this study. Equations for the limit equilibrium model are presented on page 21 . In one case, results obtained using the limit equilibrium model were compared with those obtained using a layered continuum model, and the results of the two methods were found to agree well (see page 89).

III. REPORTED MUDSLIDE OCCURRENCES DURING HURRICANES

Sources of Information

Numerous mudslides were reported after Hurricanes Ivan and Katrina. The majority of these mudslides were reported because they damaged or moved a pipeline. Information on mudslide occurrences during Hurricanes Ivan and Katrina came from various sources, including the Minerals Management Service (MMS) pipeline damage lists (MMS 2006), published reports (Walsh et al. 2006; Thompson et al. 2005; and Coyne et al. 2005), and discussions with oil industry personnel (Coyne and Wrzyszczynski, 2006). Details on each source of information are described in the following sections.

Minerals Management Service Pipeline Damage Lists

The main source of information about pipeline damage caused by mudslides was a pipeline damage list (MMS, 2006). This list is in the form of a Microsoft Excel spreadsheet and includes all reports of damage to pipelines after each hurricane in the Gulf of Mexico. It includes such information as the pipeline segment number, its size, operator, and location, the cause and location of damage, and a description of the damage. A portion of the pipeline damage list for Hurricane Ivan is shown in Table 1.

Table 1. Sample entries from the MMS pipeline damage list for Hurricane Ivan

SEGMENT	SIZE	PROD	Operator	ORIGIN			DESTINATION			Age	CAUSE		Damage	Damage Location	Location
				AREA	BLK	ID NAME	AREA	BLK	ID NAME		Prmry	Secndry			
5625	10	G/O	CHEVRON PIPE LINE COM	SP	49	capped end	SP	50	end	26	NH	Mud Slide	Apart	Departing Riser	Other
5750	26	GAS	TENNESSEE GAS PIPELIN	SP	77	A	SP	55	A	25	NH	Mud Slide	Other	Submerged Pipe	
5750	26	GAS	TENNESSEE GAS PIPELIN	SP	77	A	SP	55	A	25	NH	S/H	Apart	Departing Riser	
5773	10	BLKO	CHEVRON USA INC	SP	77	capped end	SP	77	end	26	NH	Mud Slide	Apart	Receiving Riser	Other
5781	04	BLKO	MARLIN ENERGY OFFSHO	ST	21	#111	ST	21	D	26	NH	S/H	Apart	Departing Riser	Zone

REPORT DATE	Damage Description
27-Sep-04	Mudslide caused safety joint to break at SP 49 A and pipe is broken in SP 45. No pollution.
17-Sep-04	Pipeline has a leak about 100 yards from the SP 77 platform. Break away joint must be replaced and an investigation is underway to determine extent of damage.
18-Mar-05	As a result of a mudslide, the PBSJ separted from SP77A structure, located 200 feet from the platform.
15-Dec-04	Due to mudslide pipeline separated and can only be located by divers 1500' from SP 77 A.
15-Oct-04	During an attempt to verify integrity of p/l prior to returning it to service, a leak was detected in the riser @ ST 21, No. 111.

For this study, mudslides were assumed to have occurred in the locations of where "Mud Slide" was listed as the cause of damage in the 13th column of the MMS pipeline damage list (see Table 1).

However, it should be recognized that the MMS damage report largely represents a compilation of preliminary damage reports submitted by different operators for their pipeline segments. There are potential inconsistencies between individual damage reports. Some can arise from different reporting formats and practices. Methods for determining the cause of damage are not always consistent. Operators may have had difficulty determining the exact cause of damage. There may be instances where an operator interpreted that the damage was caused by a mudslide when in fact it was caused by bottom currents or some other mechanism. And the reverse could also happen. The MMS database is certainly valuable, but for the above reasons it should not be interpreted as a collection of consistent and comprehensive data entries, and should be used with care.

Because of these potential inconsistencies, the descriptions of damage shown in the final column of the MMS pipeline damage lists were examined to gain further insight into the probable causes of damage. Some descriptions of damage were very complete and helpful, and others were sparse, unclear, or nonexistent. In general, the descriptions of damage for pipelines damaged by Hurricane Ivan were more complete than those for Hurricane Katrina. In some cases we determined, based on the description and location of damage, that a mudslide was likely the cause of a damage incident even though "Mud Slide" was not listed as the cause. Some damage reports, for example, did not include a detailed damage description, but the damaged pipeline segments they described were located in the mudslide prone area near where other pipelines had reportedly been damaged by mudslides. Other reports did not list mudslides as a cause of damage, but the pipeline was located in the mudslide prone area and was described as being "severed" and/or "buried," which may be indicative of mudslide activity. Locations of pipelines such as these were classified as "possible" mudslide locations. All entries from the pipeline damage list that were used as data for this study are listed in Appendix A, and

explanations are provided regarding the rationale for choosing locations of "possible" mudslides.

The pipeline damage list indicates which pipelines were damaged, and in some instances it also provides information on a more exact location of the damage. For instance, if the Damage Location is listed as "Receiving Riser," the damage must have occurred at the destination end of the pipeline. Sometimes the damage descriptions provided the location of damage by indicating the lease block in which the damage occurred (for long segments of pipelines). These pieces of information were helpful in locating mudslides, though in some cases the exact location of damage along the pipeline was not known and had to be estimated.

Thompson et al. (2005)

A mudslide occurred in Main Pass Lease Block 73 during Hurricane Ivan and was described by Thompson et al. (2005). The mudslide at this location moved the Main Pass Oil Gathering (MPOG) pipeline slightly but did not cause any damage. Damage to this pipeline in deeper water was included in the MMS damage lists, but the mudslide incident was not reported. Thompson et al. (2005) indicated that side-scan sonar and subbottom profiler data showed "disturbed bottom conditions indicative of mudslide activity" at this location, and figures were provided showing the exact location of the mudslide. Further confirmation of mudslide activity was provided through personal communication with BP personnel (BP, 2007).

Coyne et al. (2005)

Mudslides occurred during Hurricane Ivan in Main Pass Lease Block 151 and Main Pass Lease Block 70 and were described by Coyne et al. (2005). Further details on these mudslides were provided through personal communication with one of the authors and a colleague from Shell Oil Company (Coyne and Wrzyszczynski, 2006). The mudslide in Main Pass Lease Block 151 severed a connection in the Nakika pipeline line owned by Shell. Coyne and Wrzyszczynski (2006) indicated through personal communication that the mudslide was about 6000 feet long and that it covered the pipeline with 12 to 15 feet

of soil. The mudslide traveled parallel to the pipeline in the southeasterly direction, moving generally in the direction of the steepest slope and parallel to the direction of travel of the storm waves. The mudslide in Main Pass Lease Block 70 caused a leak in the Odyssey 12" pipeline owned by Shell Oil Company. Coyne et al. (2005) indicate that mudflows prior to Hurricane Ivan buried this pipeline about 15 feet deep, and surveys showed that Hurricane Ivan caused additional mudflows. The author indicated through personal communication that the area of mudslide activity at this location is about 150 feet wide. Both incidents discussed by Coyne et al. (2005) were listed in the MMS damage reports, but mudslides were not listed as the cause of damage.

Walsh et al. (2006)

A mudslide occurred in West Delta Block 108 caused by Hurricane Katrina and is described by Walsh et al. (2006). Walsh et al. (2006) took shallow core samples in this area and performed a multibeam sonar survey soon after Hurricanes Katrina and Rita. The morphology of the mudflow is visible in the image shown in Walsh et al. (2006). Also, the lack of stratification and presence of overconsolidated clasts and gas bubbles in portions of the core samples indicated mudflow deposits. This mudslide was not listed on the damage spreadsheet because there are no pipelines in this vicinity, so it did not cause any damage.

Personal Communication

Two representatives from Shell Oil Company, Michael Coyne of Coyne et al. (2005) and Mark Wrzyszczynski, provided information on additional mudslides from both Hurricane Ivan and Hurricane Katrina (Coyne and Wrzyszczynski, 2006).

Hurricane Ivan

Coyne and Wrzyszczynski (2006) indicated that a mudslide occurred in South Pass Lease Block 60 during Hurricane Ivan and broke a pipeline. This incident was included in the pipeline damage lists, but a mudslide was not listed as the cause of damage.

Hurricane Katrina

Coyne and Wrzyszczynski (2006) also indicated that a mudslide occurred in Main Pass Lease Blocks 148 and 151 during Hurricane Katrina that caused no damage, but moved the Nakika pipeline 350 feet to the east over a few thousand feet and buried the pipeline 15 feet deep. This incident was not listed in the MMS damage reports. The Shell representatives also reported that a mudslide caused a leak in the Odyssey 12" pipeline in Main Pass Lease Block 70. They indicated that there has been damage to this pipeline caused by mudslides four times in the past ten years and that after Hurricane Katrina the pipeline was re-routed to avoid the mudslide area. The damage to this pipeline was reported in the MMS damage lists, but a mudslide was not listed as the cause. Coyne and Wrzyszczynski (2006) also reported that a mudslide occurred in South Pass Lease Block 38 during Hurricane Katrina and caused a leak in Shell Oil Company's Cognac pipeline. The mudslide buried the pipeline more than 20 feet deep and was 1000 feet wide. This incident was not reported in the MMS damage lists because it was not discovered until a year after Hurricane Katrina.

Personal communication with Coyne and Wrzyszczynski (2006) from Shell Oil Company was extremely helpful in this research project. These contacts provided information on mudslides that were not reported to MMS, as well as details on some mudslides that were reported. The fact that the representatives from Shell Oil Company reported so many damage incidents caused by mudslides that were either not reported at all or were not

attributed to mudslides in the MMS damage lists indicates that Hurricanes Ivan and Katrina may have caused other mudslides in the mudslide area that were not reported.

Coyne and Wrzyszczynski (2006) reported three mudslide incidents caused by Hurricane Katrina that were not reported in the MMS damage lists (MMS, 2006). This figure increases the total number of reports of mudslide damages by nearly 50%, as only seven damage incidents on the MMS damage lists (MMS, 2006) were reportedly caused by mudslides during Hurricane Katrina. If similar numbers of unreported mudslides affected infrastructure owned by all the oil companies with pipelines in the mudslide prone area, the total number of mudslides affecting pipelines could be many times that reported in the MMS damage lists. There are also regions in the mudslide area where no pipelines exist, and there were probably unreported mudslides in some of these locations as well. Therefore, the mudslides reported after Hurricanes Ivan and Katrina most likely represent only a small percentage of the number of mudslides caused by these hurricanes.

Locations of Reported Mudslide Damage

The locations of all reported wave-induced mudslides described in Section 3.1 and the locations of pipelines damaged by mudslides are shown in Figure 5 and Figure 6 for Hurricanes Ivan and Katrina, respectively. Mudslide locations are distinguished by symbols depending on the source in which they were reported. Each marked location corresponds to a single area of mudslide activity, rather than a single damage report; in some areas multiple incidents of pipeline damage were reported.

Pipelines designated in Figure 5 and Figure 6 as “Pipelines Possibly Damaged by Mudslides” and damage locations designated as “Possible Mudslide Locations” indicate locations where a mudslide was not reported as a cause of damage on the MMS damage lists (MMS, 2006) but that, based on the description of damage and the location of the incident, it is believed that a mudslide may have occurred. The remaining locations of

mudslides shown in Figure 5 and Figure 6 from the MMS damage lists are locations of pipeline damage for which “Mud Slide” was listed as a cause.

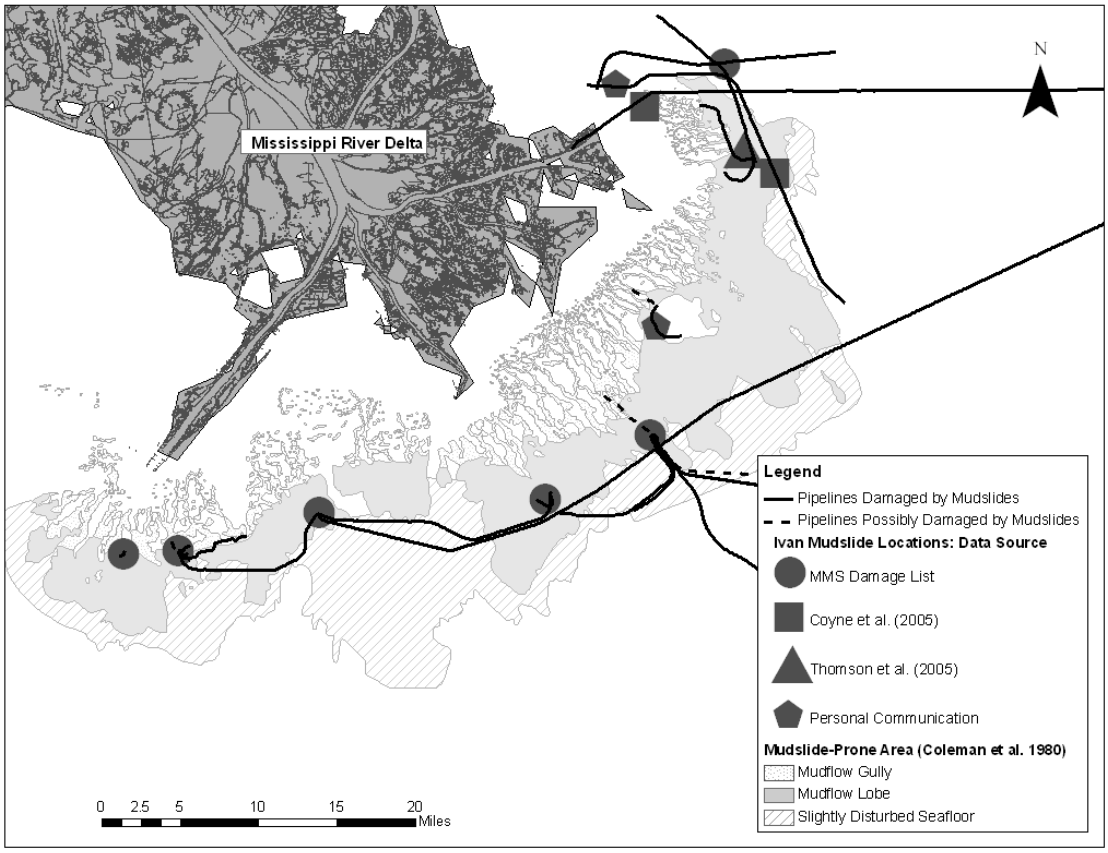

Figure 5. Locations of reported mudslides caused by Hurricane Ivan

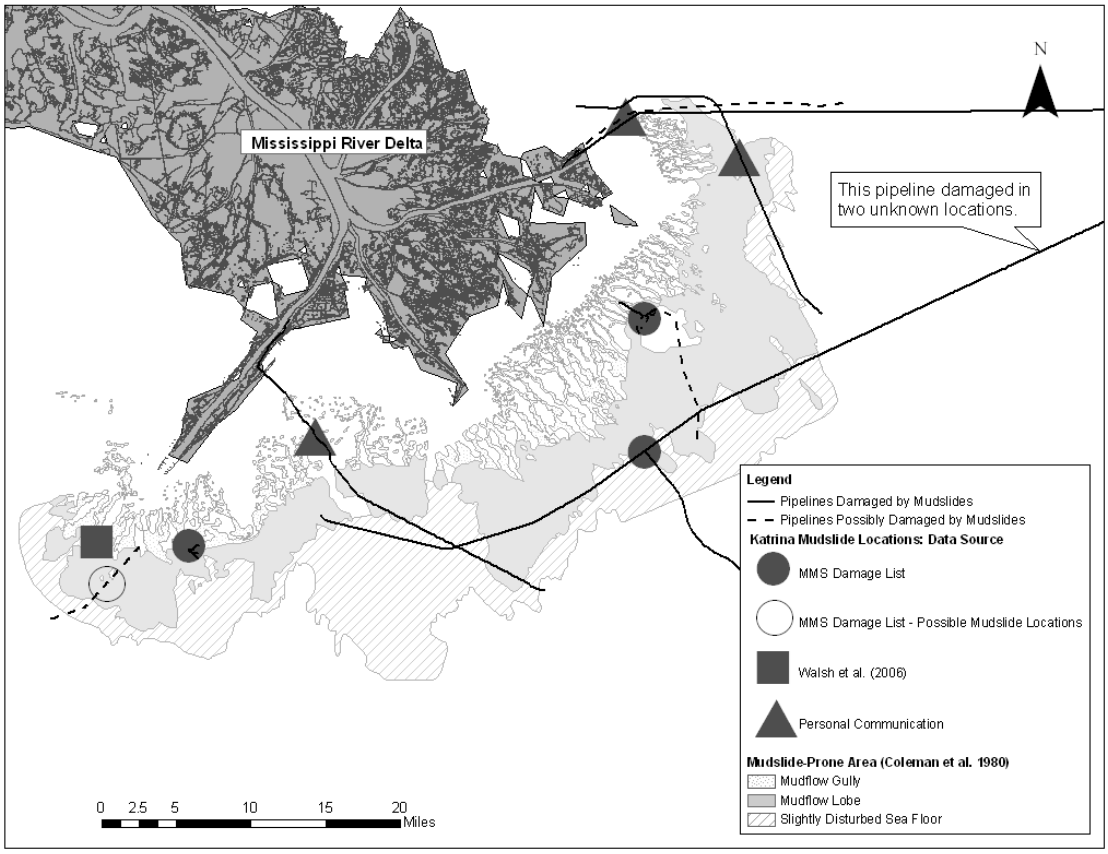

Figure 6. Locations of reported mudslides caused by Hurricane Katrina

The numbers of mudslide locations shown in Figure 5 and Figure 6 are similar for Hurricanes Ivan and Katrina. The overall amount of mudslide activity caused by each storm was probably similar as well. At some locations, mudslides occurred in both Hurricanes Ivan and Katrina. These areas may be especially vulnerable to mudslides in future large hurricanes. It is also evident in the above figures that almost all of the reported mudslides occurred within the mudslide prone area designated by Coleman et al. (1980), with the majority of the mudslides occurring in the area of mudflow lobes.

IV. LIMIT EQUILIBRIUM SLOPE STABILITY MODEL

The simple limit equilibrium model proposed by Henkel (1970) was used for most of the analyses in this study. This model assumes a rigid seafloor rather than considering the stresses and displacements in the water to be coupled with those in the underlying soil. The equilibrium equation is written by summing moments about the center of a circular slip surface. The driving moments include that due to the change in water pressure on the sea floor caused by the ocean wave and that produced by the weight of the soil and a sloping seafloor. The pressure on the sea floor represents the change in pressure from the mean hydrostatic value and depends on the water depth, ocean wave height, and wave period (or wavelength). The resisting moment is provided by shear stresses (τ) developed along the length of the circular slip surface.

Equations for the Limit Equilibrium Model

The geometry for the simple model of limit equilibrium is shown in Figure 7. The location of the potential slip circle is defined by its radius (R) and height (h) expressed as the perpendicular distance from the slope to the center of the circle. The center of the circle is assumed to lie on a line perpendicular to the slope at the "null" point where the induced wave pressures are zero.

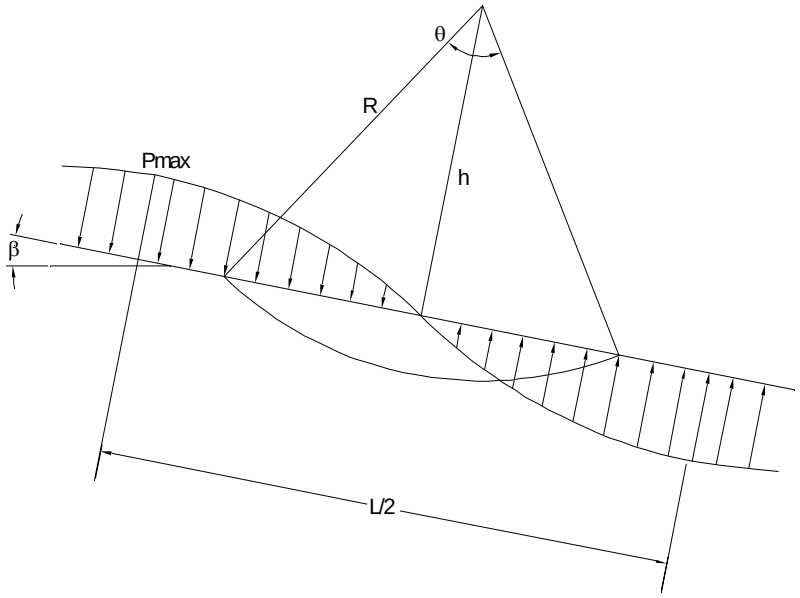

Figure 7. Geometry of the limit equilibrium model

A factor of safety is defined as the ratio of the developed shear stresses to the undrained shear strength of the soil:

$$F = \frac{c}{\tau} \tag{1}$$

where "c" represents the undrained shear strength. The factor of safety in the following equations is calculated for a soil with a finite undrained shear strength at the ground surface and a linear increase in strength with depth.

For the slope in Figure 7, the driving moment due to soil weight, M_w, is equal to:

$$M_w = W_s a \tag{2}$$

where W_s is the weight of soil and a is the moment arm of soil weight.

The weight of the soil inside the slip circle, W_s, is equal to:

$$W_s = \gamma'_s \left(\pi R^2 \theta - h\sqrt{R^2 - h^2} \right) \tag{3}$$

where γ'_s is the submerged unit weight of the soil. The submerged unit weight of the soil for this study was assumed to be 35 pcf, which is a reasonable value for the Mississippi Delta region of the Gulf of Mexico (Quiros 2003). The moment arm, *a*, is the horizontal distance from the center of gravity of the soil weight to the center of the circle. This value is equal to:

$$a = \frac{2}{3} R \frac{\sin\left(\frac{\theta}{2}\right)^3}{\left(\frac{\theta}{2}\right) - \sin\left(\frac{\theta}{2}\right)\cos\left(\frac{\theta}{2}\right)} \sin\beta \tag{4}$$

Ocean wave-induced pressures also contribute to the driving moment. The limit equilibrium model includes the assumptions that the pressure wave induced by an ocean wave is sinusoidal and that it has the same wavelength as the ocean wave. The moment due to induced seafloor pressures, M_{wave}, is calculated as:

$$M_{wave} = 2 p_{\max} \left[\left(\frac{L}{2\pi} \right)^2 \sin\left(\frac{2\pi X}{L} \right) - \frac{LX}{2\pi} \cos\left(\frac{2\pi X}{L} \right) \right] \tag{5}$$

where p_{max} is the maximum wave-induced pressure and L is the wavelength of the ocean wave. The length X is the chord length defined as:

$$X = R \sin\left(\frac{\theta}{2}\right) \tag{6}$$

The maximum wave-induced pressure on the ocean floor is directly proportional to the height of the wave and the unit weight of the water, but because the pressures dissipate as they pass through water, it is also dependent on the water depth and the wavelength. The pressures increase with an increase in wavelength, and they decrease with an increase in water depth. A simple way to calculate wave-induced pressures to assume linear wave theory (Weigel, 1964), in which the waves are assumed to be infinitely long in the direction perpendicular to the direction of propagation, and they are assumed to move in

a straight line. The equation for the wave-induced bottom pressure in this case, expressed as a difference from hydrostatic pressure, is:

$$p_{\max} = \frac{\gamma_w}{2}\left(\frac{H}{\cosh\left(\frac{2\pi}{L}d\right)}\right) \tag{7}$$

Where γ_w is the unit weight of sea water (assumed in this study to be 64 pcf), H is the wave height and d is the water depth. The wavelength, L, can also be calculated based on linear wave theory (Weigel, 1964) using the relationship:

$$L = \frac{gT^2}{2\pi}\tanh\frac{2\pi d}{L} \tag{8}$$

where g is the acceleration of gravity, T is the wave period in seconds, and d is the water depth.

The total driving moment due to the soil weight and the wave-induced bottom pressures, M_d, is equal to:

$$M_d = M_w + M_{wave} \tag{9}$$

The resisting shear force, S, is equal to:

$$S = \left(c_0 - c_z\gamma'_s R\cos\left(\frac{\theta}{2}\right)\right)R\theta + 2c_z\gamma'_s R^2\sin\left(\frac{\theta}{2}\right) \tag{10}$$

where c_0 is the undrained shear strength at the ground surface (mudline) and c_z is equal to the rate of change in soil shear strength with effective stress $(dc/dz)/\gamma'_s$. The undrained shear strength of the soil at a given depth, c, is equal to:

$$c = c_0 + c_z\gamma'_s z \tag{11}$$

where z is the depth below the ground surface, measured perpendicular to the slope. The resisting moment is then equal to:

$$M_r = SR \tag{12}$$

A factor of safety can be calculated as the ratio of the resisting moment to the driving moment:

$$F = \frac{M_r}{M_d} \tag{13}$$

The factors of safety calculated based on Equation 13 are identical to those expressed earlier by Equation 1 in terms of shear strength. The equations developed for this study are in a slightly different form than that shown in Henkel (1970), but the resulting factors of safety calculated are equal.

For cases where the undrained shear strength varies with depth, as it does for the actual strength profiles considered in this study, piecewise linear variations in strength were assumed and integration was performed to calculate the resisting shear force. An example of a piecewise linear strength profile with three linear segments is shown in Figure 8.

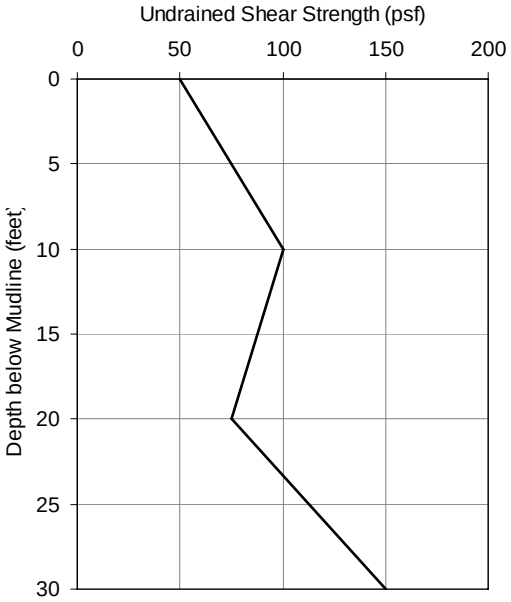

Figure 8. Example of a piecewise linear strength profile

To determine the factor of safety for a site with the shear strength profile shown in Figure 8, the contribution of each of the three linear segments of the profile to the resisting moment would be calculated. The contribution of the three segments would then be summed to determine the total resisting moment, and the total resisting moment would be divided by the sum of the driving moments to determine the factor of safety against mudslide initiation. In the spreadsheet program included with this report, the factor of safety is calculated in this manner. A user's manual for the spreadsheet program is presented in Appendix B.

V. TOOLS FOR ANALYSIS

Two user-friendly tools have been developed for this study to calculate the factor of safety against mudslide initiation at a site. The first, a spreadsheet program, allows the user to calculate the factor of safety by entering site parameters into Microsoft Excel. The second is a nondimensional chart solution that can be used for preliminary calculations for soil profiles with a linear increase in shear strength with depth. To use these tools, the user must know the slope angle (β), water depth (d), wavelength (L), wave height (h), submerged unit weight of soil (γ'_s), unit weight of water (γ_w), the shear strength of the soil at the mudline (c_0), and the increase in shear strength with depth (c_z) at the site.

Limit Equilibrium Model Spreadsheet Program

A spreadsheet program that can be used to analyze the mudslide vulnerability of a submarine site is included with this report as a Microsoft Excel file. The spreadsheet program calculates the factor of safety against mudslide initiation for any location with a piecewise linear shear strength profile. The spreadsheet calculates the minimum factor of safety for a site by calculating the factors of safety for various slip circles of different sizes (center point location and radius). A user's guide to accompany the spreadsheet program is attached in Appendix B.

Nondimensional Solution and Stability Chart

A chart has been developed that can be used to calculate the factor of safety against mudslide initiation for any location, assuming that the soil shear strength increases linearly with depth. The chart is shown in Figure 9. The chart was developed using dimensionless parameters derived from the equations for the limit equilibrium method shown on pages 21-23.

The factor of safety against mudslide initiation is calculated using the chart in Figure 9 and the following steps:

1. Calculate the maximum pressure on the sea floor, p_{max}, using the following formula based on linear wave theory (Weigel 1964):

$$p_{\max} = \frac{\gamma_w}{2}\left(\frac{H}{\cosh\left(\frac{2\pi}{L}d\right)}\right).$$

   The pressure can be reduced if desired to account for the shape of the storm waves, as described later in the section entitled "Ocean Wave Data."

2. Calculate the dimensionless constant: $\frac{\gamma L \tan\beta}{p_{\max}}$ using the known quantities.

3. Calculate the dimensionless constant: $\frac{c_z L}{c_0}$.

4. Using the values of $\frac{\gamma L \tan\beta}{p_{\max}}$ and $\frac{c_z L}{c_0}$, calculated in steps 2 and 3 respectively, determine a value of $N_z = \frac{c_z L}{p_{\max} F}$ from the chart in Figure 9. If necessary, interpolate between lines for intermediate values of $\frac{c_z L}{c_0}$.

5. Calculate the factor of safety as $F = \frac{1}{N_z}\left(\frac{c_z L}{p_{\max}}\right)$ using N_z from the chart in Figure 9 and known values of c_z, L and p_{max}.

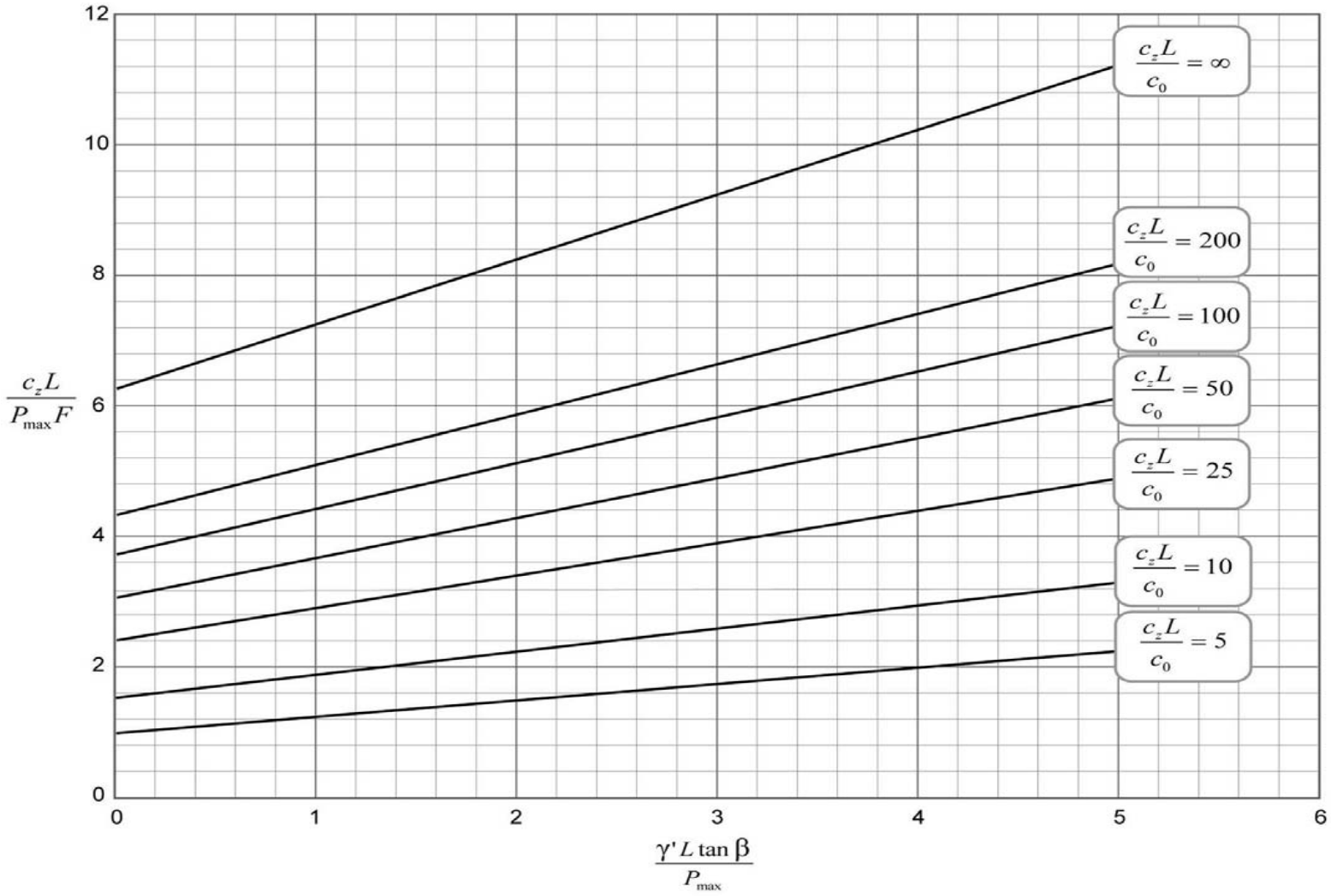

Figure 9. Stability chart for the limit equilibrium slope stability model

Examples Using Stability Chart

Shear strength profiles at South Pass Lease Block 70 and Mississippi Canyon Block 63 and the linear strength profiles used to approximate them are shown in Figure 10. Sample chart calculations for these sites are shown in Table 2.

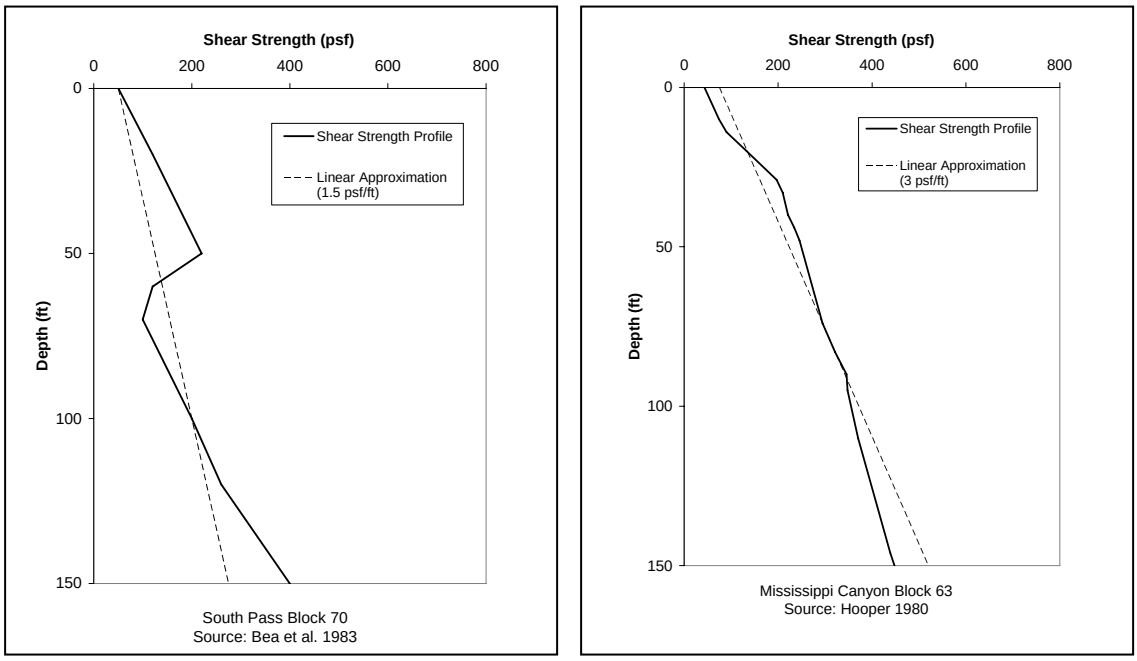

Figure 10. Shear strength profiles and corresponding linear profiles for example sites

Table2. Sample factor of safety calculations using stability chart

Lease Block	Slope Angle (radians)	Water Depth (ft)	Wavelength (ft)	Wave Height (ft)	Submerged Soil Unit Wt. (pcf)	Water Unit Wt. (pcf)	Pmax (psf)	$\gamma L \tan\beta / p_{max}$
SP-70	0.0023	335	1341	73	30.0	64	931.9	0.100
MC-63	0.0167	495	1260	69	30.0	64	371.4	1.696

Lease Block	c_z (psf/ft)	c_0 (psf)	$c_z L/c_0$	$c_z L/(P_{max} F)$	F (from chart)	F (using original model)	Percent Difference (%)
SP-70	1.5	50	40.2	3.0	0.72	0.76	5.3
MC-63	3	75	50.4	4.1	2.48	2.43	2.1

The factors of safety calculated using the charts at these locations are within about 5% of those calculated using the limit equilibrium model with piecewise linear profiles. For locations with more variable strength profiles, the chart calculations are less accurate, because it is difficult to approximate these profiles by a simple linear increase in strength with depth. Caution and conservatism should be used when approximating shear strength profiles with a linear increase in strength, because features such as high-strength crusts and other strength variations can significantly change the behavior of the soil. For sites with non-linear soil profiles, a linear profile representing a lower bound strength can safely be used as a first conservative estimate of the factor of safety. However, it is recommended that the limit equilibrium model with the full piecewise linear strength profile be used in cases where the strength profile is variable, as presented in the attached spreadsheet program and described in Appendix B.

VI. GEOTECHNICAL PROPERTIES OF SUBMARINE CLAYS

The shear strength of the soil provides the resisting force and moment in the limit equilibrium model. Undrained shear strengths of the soil were used in this study. Values were derived from the results of in-situ vane tests, miniature vane tests, and unconfined compression tests as reported in published and unpublished sources. A discussion of the relevance of undrained shear strength to the study of submarine mudslides and descriptions of the soil shear strength properties specific to the Mississippi Delta region of the Gulf of Mexico are presented in this section.

Relevance of Undrained Shear Strength

Undrained shear strength is typically used in the analysis of wave-induced mudslides because the loading of the storm waves that cause mudslides is rapid compared with the time it takes for the cohesive sediments to drain (Henkel, 1970). However, the tests used to measure undrained shear strengths do not model exactly what happens when a submarine slope fails because they do not take into account the effects of the anisotropy of the soil or the stress path followed prior to failure.

The problem of ocean-wave induced mudslides is similar to the problem of rapid drawdown or earthquake loading of a slope on land. The soil is first consolidated under anisotropic stresses that include shear stresses due to gravity. Later, the soil is subjected to loading by ocean waves. If the initial shear stresses in the soil at the time of consolidation are large, they will increase the undrained strength of the soil. However, most of the slopes in the Mississippi Delta region of the Gulf of Mexico are relatively flat (less than 1.5% grade), so the initial shear stresses are much less significant than they would be in a typical earth dam subjected to rapid drawdown or earthquake loading. These stresses do have some effect on the undrained strength, however, so neglecting them is a source of error in the analysis of submarine mudslides. In the areas of the

Mississippi Delta region of the Gulf of Mexico where slopes are steeper (up to about 3% grade), this error would be more significant. Also, when the strength of the soil is measured, the strength reported is that on the failure plane at which the soil fails during the test, which is not necessarily at the same orientation as that when the soil fails in a mudslide. Because the soil is consolidated anisotropically, the strength found in a test is most likely not the same as the strength acting to resist slope failure.

The fact that the soil in the Mississippi Delta region of the Gulf of Mexico is expected to have anisotropic strength due to the nature of its consolidation indicates that the use of the undrained shear strength measured by standard field and laboratory tests in analyses of submarine mudslides is probably not a rigorous way to approach the problem. However, an attempt to describe the strength of the soil exactly would be inconvenient and expensive, and it would be impossible to eliminate all sources of error. Undrained shear strengths are widely available for soil in this region, and they have been used successfully in this and past studies to predict and analyze the occurrence of wave-induced submarine mudslides. They appear to work well as an index property to compare the resistance to wave-induced bottom pressures for soil in one area to that in another. For these reasons, the undrained shear strength of the soil was considered a reasonable parameter for use in all analyses in this study.

Data Sources

Shear strength data for the Mississippi Delta region of the Gulf of Mexico were obtained from Bea et al. (1983), Dunlap et al. (2004), Hooper (1980, 1996) and Roberts et al. (1976), as well as from two proprietary sources. Shear strength data were in the form of profiles showing the variation in shear strength with depth. Where shear strength data were not available to a depth of 150 feet or more, regional data on shear strength versus depth were obtained from a proprietary source and used to approximate the soil shear strength profiles up to a depth of 150 feet. These proprietary data are in the form of

contour maps of shear strengths at various depths below the mudline in the Gulf of Mexico, and were created by a geotechnical consulting company for the purpose of offshore project planning.

Locations of all borings from which shear strength data were obtained, including those obtained from proprietary sources, are shown in Figure 11. Locations for some of the borings are approximate because published reports did not always include coordinates or detailed location maps for borings.

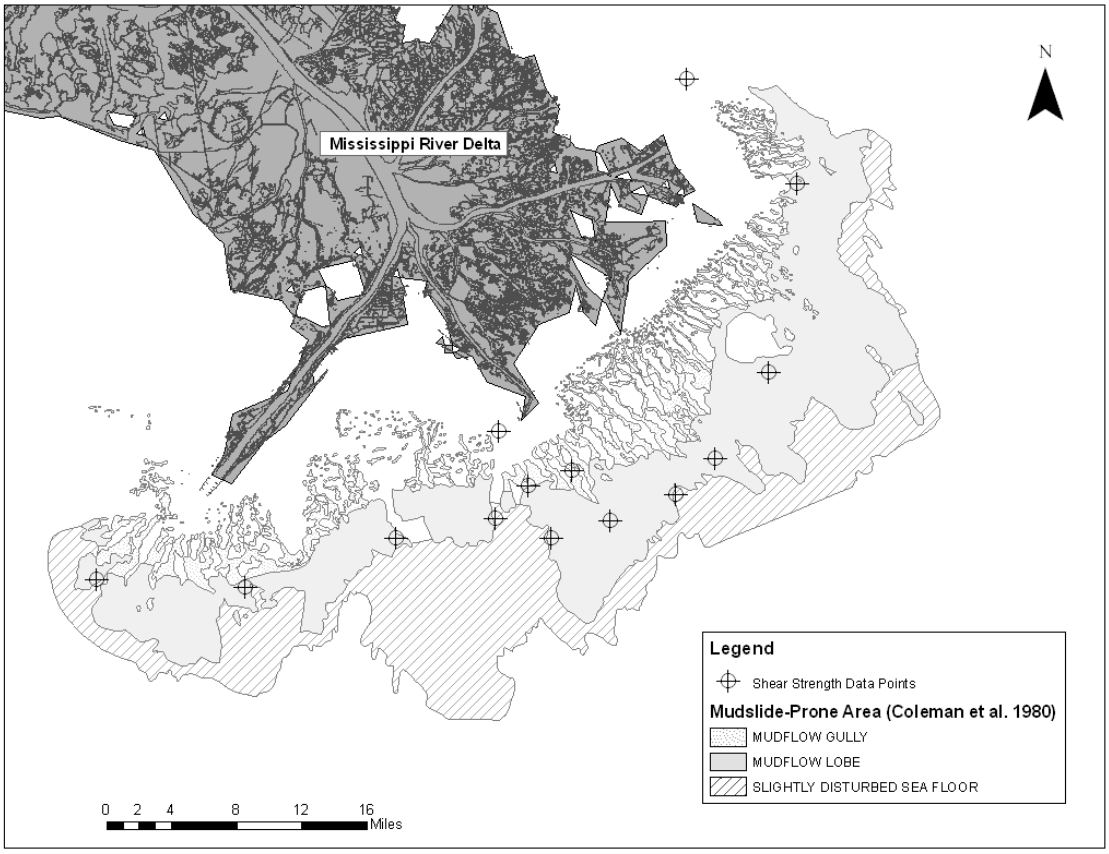

Figure 11. Locations of borings from which shear strength data were obtained

Shear Strength Correction Factors

Shear strength data used in this study were obtained using various testing and sampling methods, all of which affect the value of undrained shear strength reported. It was

therefore necessary to correct the data to remove the effects of the testing and sampling methods. Data for all strength profiles were corrected with the modification factors used by Dunlap et al. (2004), which adjust strengths obtained from all testing methods to the reference strength of an unconfined compression test performed on a sample obtained using a 3-inch thin-walled sampler pushed into the soil. In general, measured strengths for tests in which the sample was more disturbed than in an unconfined compression test were increased, and strengths for tests in which the sample was less disturbed than an unconfined compression test were decreased. The correction factors are shown in Table 3.

Table 3. Correction factors used to relate all measured undrained shear strengths to the strength measured with an unconfined compression test from a pushed sample

Sampler Type	Method of Insertion	Strength Test	Modification Factor, $su/su_{measured}$
2.25" thin-walled	percussion	unconfined compression	1.5
2.25" thin-walled	percussion	miniature vane	1.1
3" thin-walled	push	unconfined compression	1
3" thin-walled	push	miniature vane	0.8
In-Situ Measurement:		remote vane	0.7

In many cases, multiple types of strength measurements were available. The strengths chosen for use in this study were typically those for which the most data existed for any given soil shear strength profile. Most often, either miniature vane or remote vane strengths were used. The method of sampler insertion was not always stated on the boring logs from which shear strength profiles were obtained. Because push sampling

methods generally replaced percussive sampling methods around 1982, percussive sampling methods were assumed for borings taken before 1982, and push sampling methods were assumed for more recent borings.

Plots of shear strength profiles

The strength profiles used in this study are shown in Figures 12 through 15 with the exception of strength profiles in Mississippi Canyon Lease Block 20 and South Pass Lease Block 77, which were obtained from proprietary sources. The bold, solid lines represent shear strength data obtained from public boring logs. The bold, broken lines represent proprietary data used to complete strength profiles that did not extend to depths of 150 feet or more. Profiles that were completed in this manner include South Pass 54, West Delta 107, Main Pass 70, Main Pass 77, and South Pass 30. The data obtained from the contour maps of shear strengths for depths of 60 feet to 150 feet are shown on all soil profiles for comparison, with the exception of Mississippi Canyon Block 63, as the contour maps did not include this location.

Linear strength profiles increasing at 2 psf per foot and 8 psf per foot, corresponding to typical normally consolidated and remolded clays in the Gulf of Mexico, respectively (Quiros et al, 1983) are shown on each of the soil shear strength profiles for reference. The linear strength profiles are represented by lightweight, dotted lines.

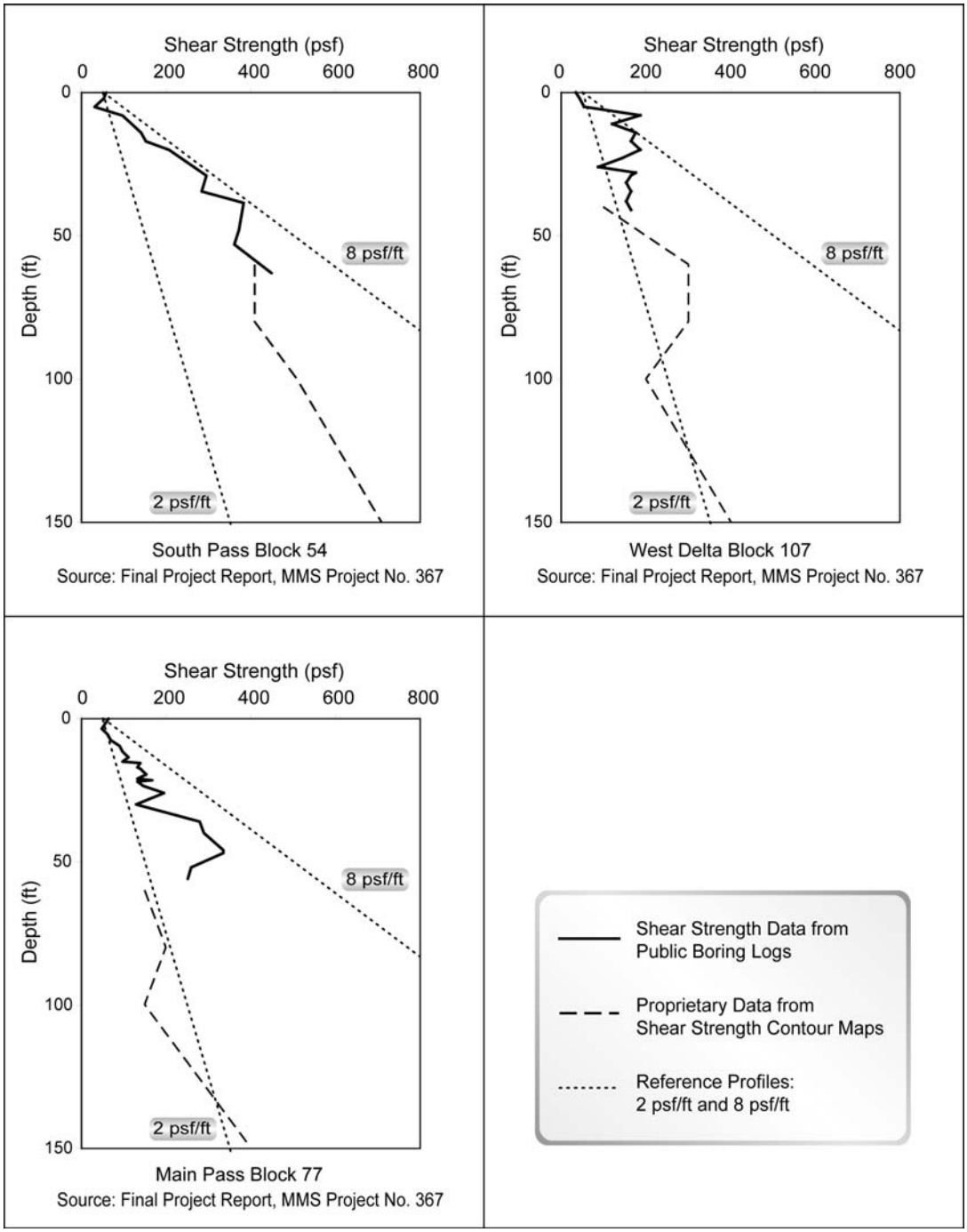

Figure 12: Soil shear strength profiles in the Mississippi Delta Region of the Gulf of Mexico

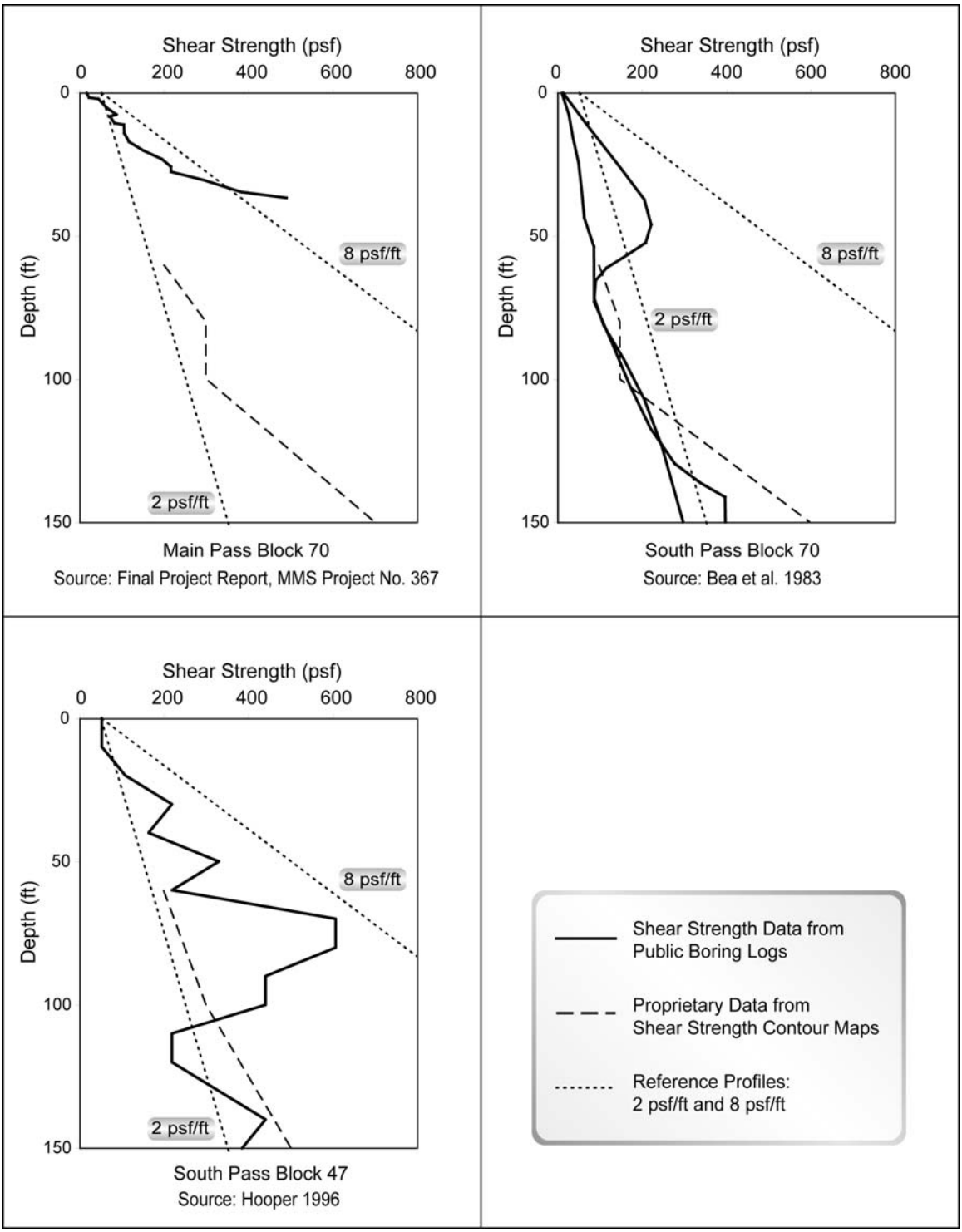

Figure 13: Soil shear strength profiles in the Mississippi Delta Region of the Gulf of Mexico

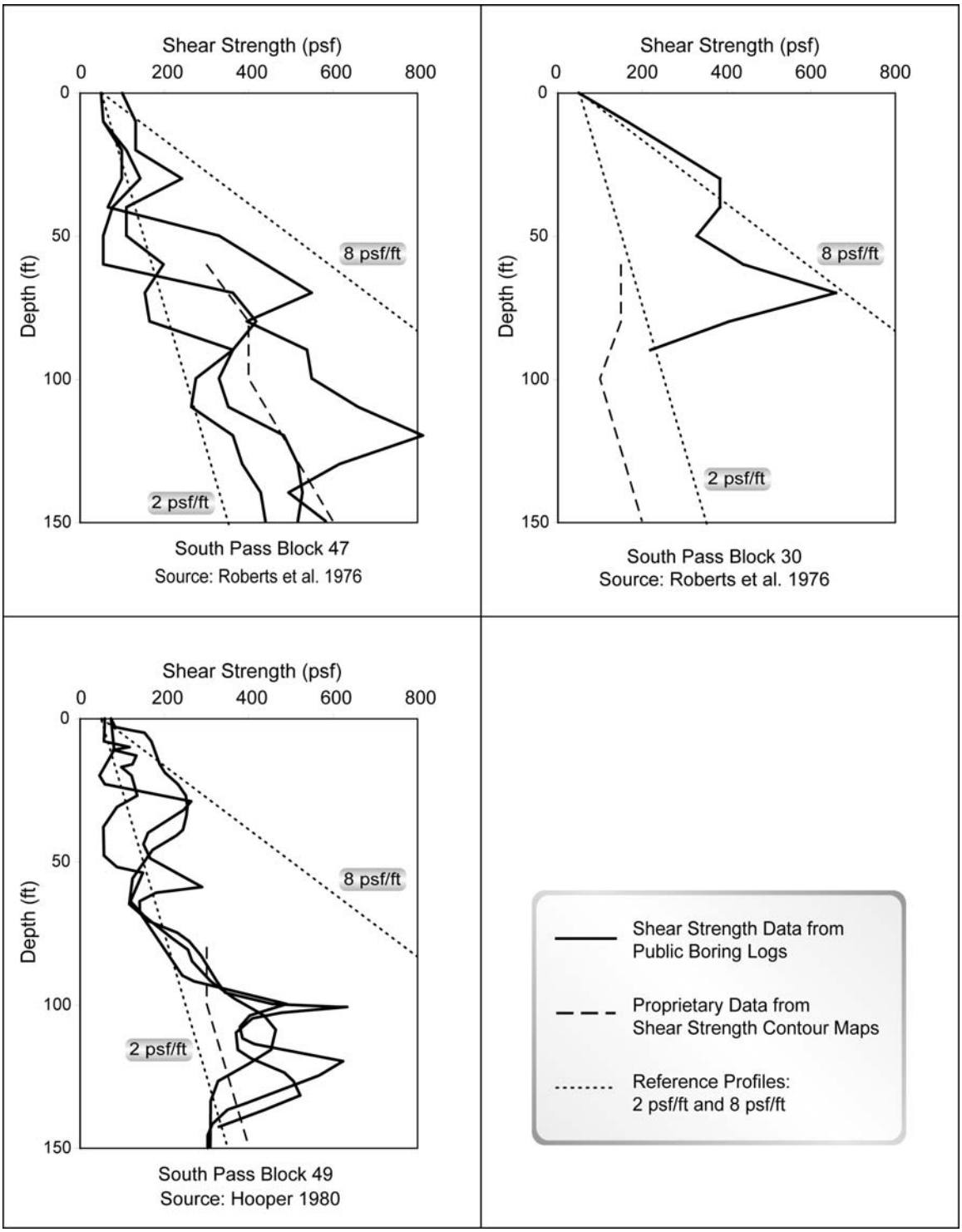

Figure 14: Soil shear strength profiles in the Mississippi Delta Region of the Gulf of Mexico

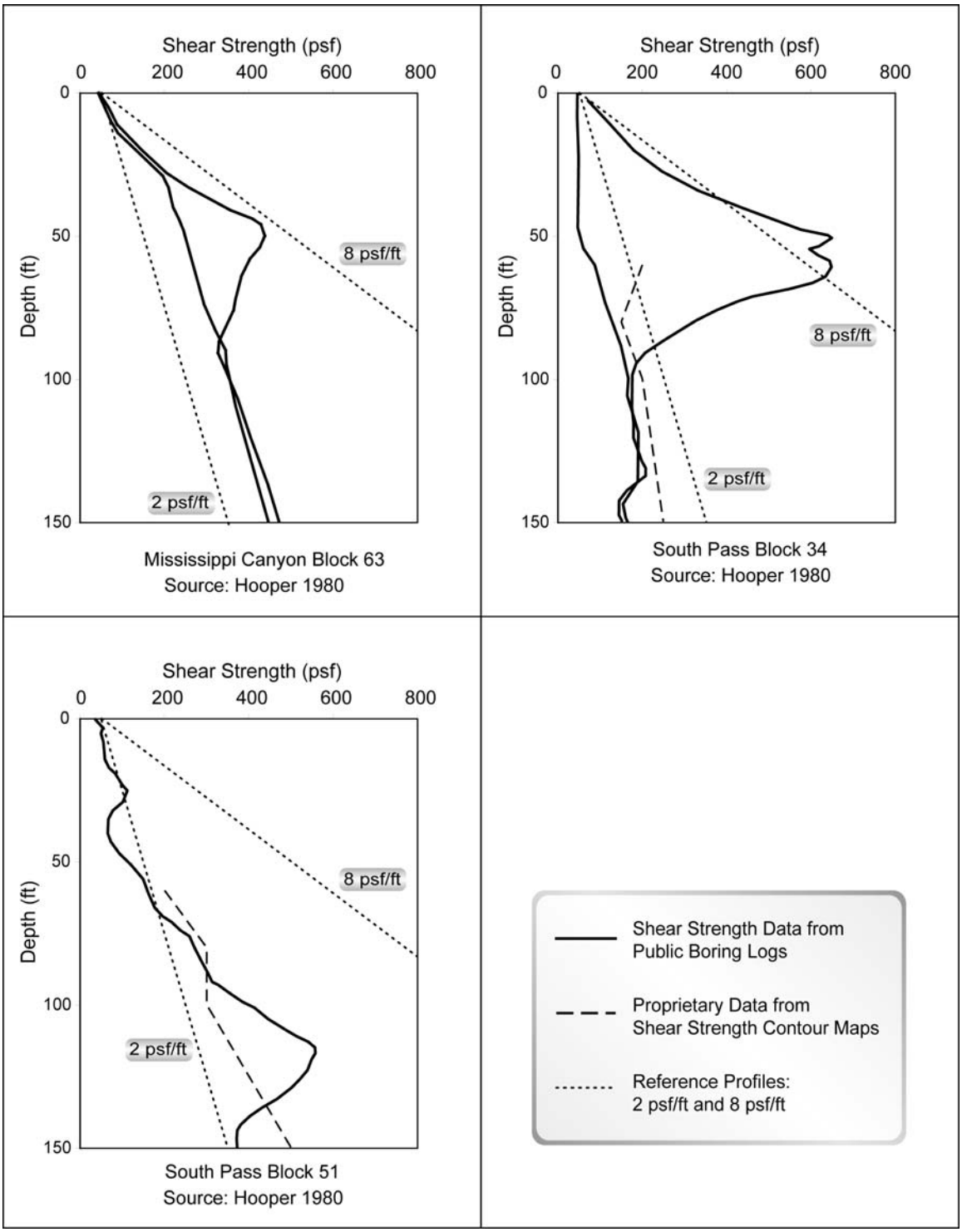

Figure 15: Soil shear strength profiles in the Mississippi Delta Region of the Gulf of Mexico

Typical Strength Properties

The soil in the Mississippi Delta region generally has much lower strengths than soil in other parts of the Gulf of Mexico. Most of the soil in the Mississippi Delta Region has undrained shear strength significantly lower than a typical normally consolidated profile for the Gulf of Mexico, which increases in strength at a rate of about 8 psf per foot (Quiros et al, 1983). In some locations, undrained shear strengths increasing at a rate of less than 2 psf per foot have been measured, as shown in the borings for South Pass Lease Block 70 and South Pass Lease Block 34 in Figure 13 and Figure 15, respectively (Bea et al, 1980, and Hooper, 1980).

Though the soil in the Mississippi Delta region of the Gulf of Mexico is very weak in some areas, it is also extremely variable, both regionally and locally. The rapid deposition of sediment results in soft, underconsolidated strength profiles in some locations. In other locations, however, the soil has a stronger upper "crust" overlying weaker material beneath. According to Hooper (1980), these crusts may form for a variety of reasons. They may be caused by consolidation of the upper layer of soil after deposition. Crusts may also consist of large blocks of stiff soil that traveled from another location during a mudslide. Crustal layers may exist at some depth if softer soil is deposited on top of an already overconsolidated crust (Hooper, 1980). The mechanisms that form crustal zones apparently act on a local level, and they contribute significantly to the variability in soil shear strength in the Mississippi Delta region.

Hooper (1980) presents examples of three sites in which the shear strength varies dramatically within a small area. These examples are shown in Figures 14 and 15. In one example, three borings were drilled 500 feet apart (see profile for South Pass Lease Block 49 in Figure 14). All of these borings show crustal features at depths less than 50 feet, but the depths of the crusts are different and the strengths vary widely at any given depth. Two other examples shown by Hooper (1980) reveal borings with profiles of

weak, linearly varying strengths less than three thousand feet from borings with crustal profiles (see profiles for Mississippi Canyon Block 63 and South Pass Lease Block 34 in Figure 15). Roberts et al. (1976) present three strength profiles within about 10,000 feet of one another (see profiles for South Pass Lease Block 47 in Figure 14). These profiles vary widely in strength in the upper 150 feet. Bea et al. (1980) also present two nearby profiles (exact scale not shown), one with a crustal layer and one without (see profiles for South Pass Lease Block 70 in Figure 13).

The significant variation in soil shear strength over short distances in the Mississippi Delta region of the Gulf of Mexico makes it difficult to determine the mudslide vulnerability in this area. The area of study is over 60 miles in extent, but soil shear strength may vary so much over just thousands of feet that the factor of safety against mudslide initiation may vary by a factor of 2. Therefore, even if soil shear strength data exist near a location of interest, they may not represent the soil shear strength at the location of interest. Soil shear strength may also vary over the areal extent of a single mudslide. In this study, some site-specific analyses of mudslide vulnerability were performed, but emphasis was placed on analyses that took the potential strength variations of the soil into account.

VII. BATHYMETRY

Bathymetric data were used to establish the water depth and slope angle for the limit equilibrium analyses. Both of these input parameters affect the driving moment in the model. Shallower water increases the pressure on the seafloor caused by a wave, thereby increasing the driving moment and decreasing the factor of safety. A steeper slope also increases the driving moment and decreases the factor of safety, as well as increasing the portion of the driving moment caused by the soil weight.

Sources of Bathymetric Data

The map identified as "Map 4" in the series produced by Coleman et al. (1980) was the main source of bathymetric data used in this study. The map shows depth contours measured in the period between 1977 and 1979 at intervals of 10 feet up to a depth of 600 feet, and intervals of 50 feet thereafter. All of the maps by Coleman et al. (1980) were digitized by William Lettis and Associates, and made available to researchers in this study in shapefiles readable in ArcMap, a GIS program created by ESRI. A map showing the depth contours derived from Map 4 is shown in Figure 16. Approximate contour labels are shown in Figure 16 for reference.

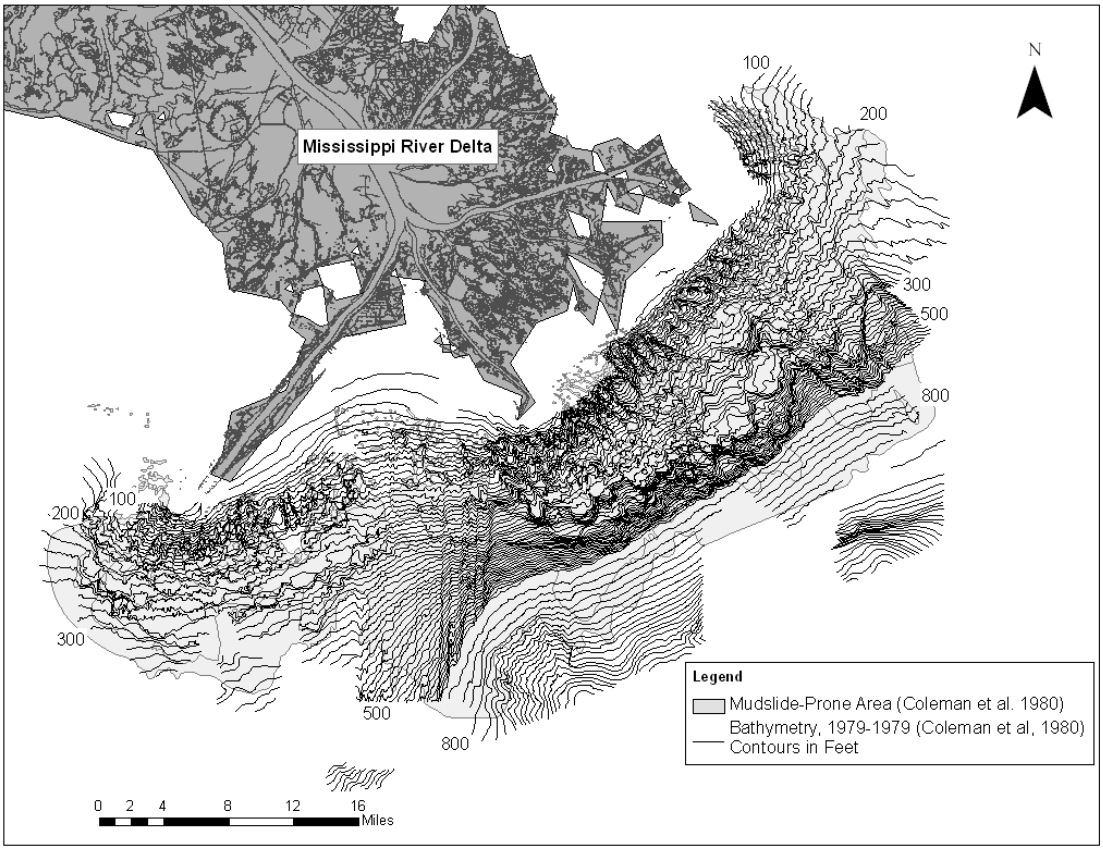

Figure 16. Depth contours (in feet) from Map 4 by Coleman et al. (1980)

Other depth information was available to the researchers during this study from the hurricane hindcast data. Water depth is used to compute the shallow water effects (refraction, shoaling, friction, and breaking) during the propagation of waves across the shelf. The bathymetry for the Hurricane Katrina hindcast (Cardone et al. 2006) and the the Hurricane Ivan hindcast (Cox et al, 2005) were on different grids and were not always in agreement at a give location. The exact dates of these bathymetric data are unknown, but the measurements are more recent than the bathymetry from Coleman et al. (1980). The bathymetry for the Hurricane Ivan hindcast was based on the General Bathymetric Chart of the Oceans (GEBCO, Inc., 2007), and the bathymetry for Hurricane Katrina was based on the IPET report (USACE, 2006). However, the resolution of the hindcast grid

and associated bathymetry available is relatively coarse (about 0.6 miles for Hurricane Katrina and even coarser for the Hurricane Ivan hindcast). Thus, the bathymetry available from the hurricane hindcasts is significantly less detailed than the bathymetry illustrated in Figure 16 and was not adequate for calculating slope angles at specific locations.

Relevance of Bathymetric Data Sources

The bathymetry used in this study affects both the water depth and the slope angle used in limit equilibrium analyses. The nature and magnitude of the effects of the bathymetry on these two parameters are described in detail in the following sections.

Effect on Water Depth

To determine the differences among the bathymetry data presented by Coleman et al. (1980) and the bathymetry data associated with the Hurricane Ivan and Katrina hindcasts (Cox et al, 2005 and Cardone et al, 2006), the depths from the three sources were compared. Differences in reported bathymetry could be due to soil movement, survey errors, or other factors. Figures 17 and 18 show the differences in water depths between Coleman's data (1979) and depths from the Hurricane Ivan hindcast (2005) and the Hurricane Katrina hindcast (2006), respectively, calculated by subtracting the water depths shown in Coleman et al. (1980) from the water depths in the hindcast models.

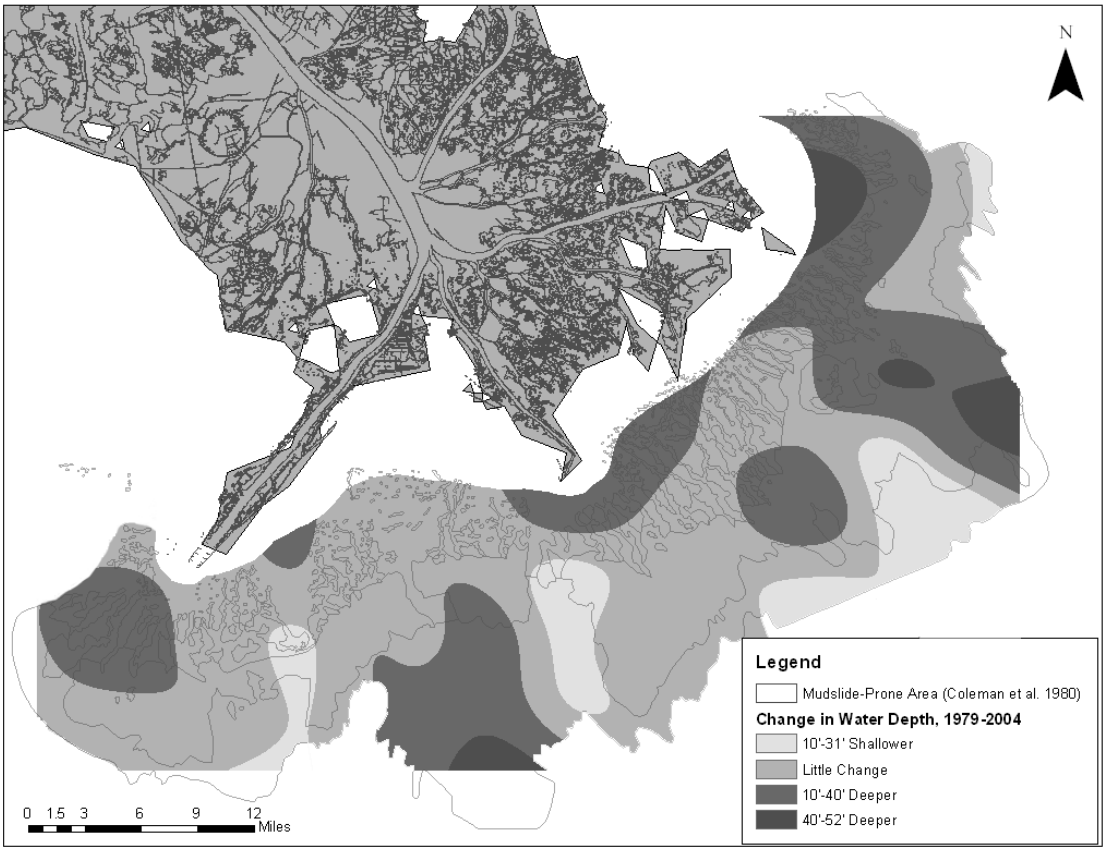

Figure 17. Differences in bathymetry between Coleman et al. (1980) and Cox et al (2005)

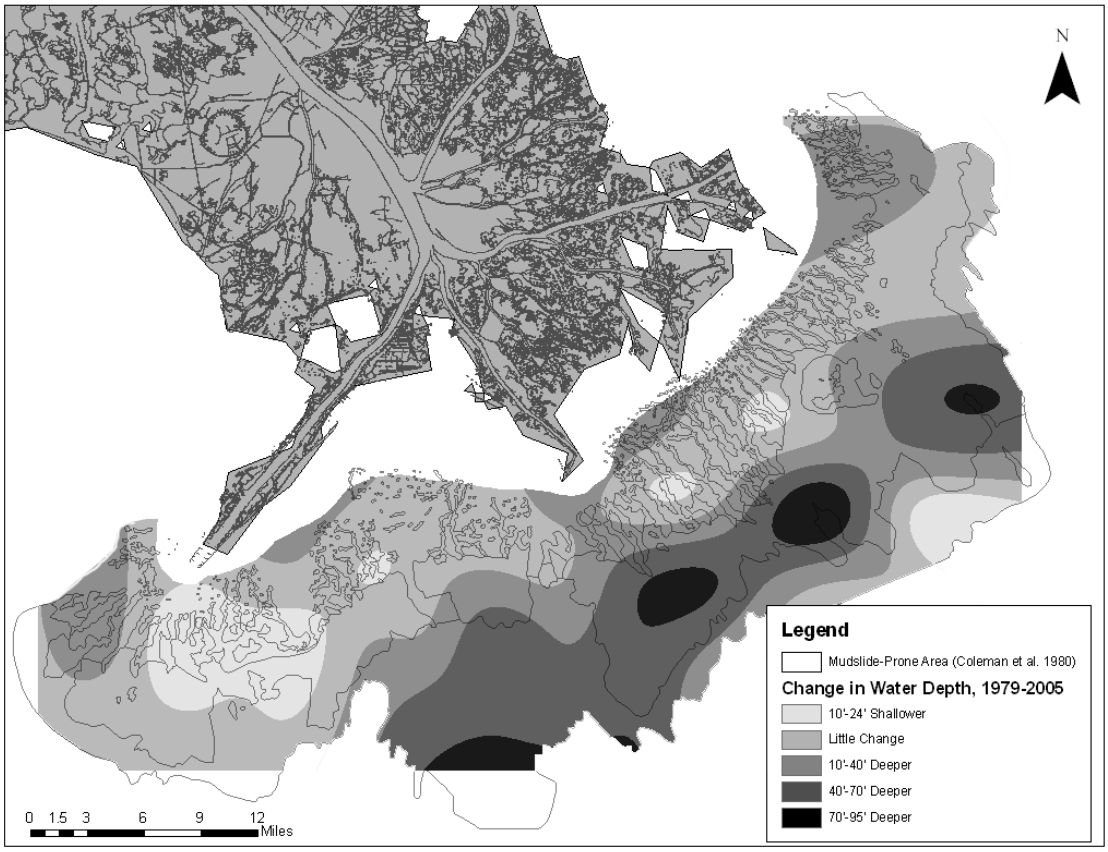

Figure 18. Differences in bathymetry between Coleman et al. 1980 and Cardone et al (2006)

It can be seen in Figures 17 and 18 that over most of the mudslide prone area, the difference between the bathymetry from Coleman et al. (1980) and the bathymetry from the hindcasts (Cox et al, 2005 and Cardone et al, 2006) is small. Where there is a difference in depths, deeper depths were generally reported in the Hurricane hindcasts than were reported by Coleman et al. (1980). The depths from the Hurricane Katrina hindcast show large differences of up to 95 feet, particularly in deeper water. It is possible that some of the difference in water depth is due to soil movement over time. However, if soil movement were the only cause, one would expect little net change in depth on a regional scale. From a practical standpoint, it is difficult to imagine an increase in depth of 100 feet in 25 years at any given location.

Most of the difference in water depths among the surveys is most likely due to error in the surveys or gridded depths. In order to investigate potential error in the surveys, as-built water depths were obtained from the Minerals Management Service website for two platforms that were damaged in Hurricanes Ivan and Katrina (MMS, 2007) within the mudslide prone area. The as-built water depth for one platform, in 190 feet of water, was found to match closely with the bathymetry from all sources. The as-built water depth for the other platform, however, which was in 475 feet of water, was found to match closely with the bathymetry from Coleman et al. (2005) and with the depths from the Hurricane Ivan hindcast (Cox, 2005), but it did not agree well with the depths from the Hurricane Katrina hindcast (Cardone, 2006). As-built depths for a few platforms outside the mudslide prone area (and outside the limits of the bathymetry by Coleman et al, 1980) were also checked against the depths from the Katrina Hindcast (Cardone, 2006). To the west of the mudslide prone area, depths agreed well, but to the east of the mudslide prone area, the depths from the Hurricane Katrina hindcast were up to 185 feet deeper than the reported platform depths. These depth discrepancies were reported to the authors of the hindcasts, but at the time this report was completed, no information was available to determine the reason for the discrepancy in depths. They did note that isolated errors in depths would likely have little impact on hindcast wave heights since shallow water effects generally occur relatively slowly as a wave propagates. (Cox, personal communication).

Another factor contributing to differences between the hindcast bathymetry and the bathymetry by Coleman et al. (1980) is that the hindcast bathymetry is described by grid averaged depths that represent the average depth in the area surrounding each grid point rather than the actual depth at the grid point. The grid averaged depths are suitable for determining the growth, dissipation, and propagation of the waves as they pass through the area around the grid point. The differences between the grid resolutions and the difference in the baseline bathymetry sources for the Hurricane Ivan and Katrina hindcasts contribute to the differences in the hindcast bathymetries, and the grid

averaging contributes to the differences between as-built platform depths and the depths associated with the hurricane hindcasts.

Because the bathymetry by Coleman et al. (1980) matched well with the as-built platform depths, and because the depths associated with the hindcast data points do not represent the actual depths at those points due to grid averaging, the bathymetry by Coleman et al. (1980) was used to find the water depths for most of the analyses in this study. In a few analyses, the water depths from the Hurricane Ivan and Katrina hindcasts (Cox et al, 2005 and Cardone et al, 2006) were used in areas where they matched well with the bathymetry from Coleman et al. (1980). In these cases, factors of safety were being calculated at the locations of hindcast data points, and the depths from the hindcasts were used for ease of calculation.

Effect on Slope Angle

Due to the lack of detail in the bathymetry associated with the Hurricane Ivan and Katrina hindcast data (Cox et al, 2005 and Cardone et al, 2006) and the potential error in all the bathymetric surveys, it was not possible to assess whether the slope angle at any given site changed over time. In order to investigate the possible magnitude of slope changes, information from Hitchcock et al. (2006) were used to estimate the maximum possible change in slope at one location due to slope movement over the course of about two decades. Hitchcock et al. (2006) presented a figure showing detailed changes in measured bathymetry over the course of about twenty years at a site in an unknown location within the mudslide prone area. The change in bathymetry was found by subtracting the water depths found from a recent, presumably very detailed survey, from those shown in Map 4 by Coleman et al. (1980, Figure 16).

The figure from Hitchcock et al. (2006) shows a decrease in water depth of about 40 feet at one location and an increase in water depth of about 40 feet at a location about 7,900

feet away. These changes in water depth could be due to error in the surveys, but it also could potentially represent sediment deposition from mudslides. Assuming the changes in depth do represent sediment deposition, and assuming the initial slope at the site was 3 percent (about the maximum slope in the mudslide prone area), the final slope would be approximately 1.6 percent based on the distance between the two locations and the net change in depth. Assuming the soil has a submerged unit weight of 35 pcf and assuming a typical bottom pressure increase of 500 psf caused by a hurricane wave, this change in slope would increase the factor of safety against a mudslide by about 20 percent if the soil shear strength remained the same. Thus, soil movement over time may affect site-specific slope stability. On a regional scale, however, slope movements may cause steepening in some areas and flattening in others. It is therefore unlikely that the effect of soil movements on slope angles would significantly effect the mudslide vulnerability of the Mississippi Delta region as a whole. In addition, most of the slopes in the Mississippi Delta region of the Gulf of Mexico are 1.5 degrees or flatter, so a change in bathymetry would have a less significant effect on the slope and the factor of safety than that shown in the example above. For the purposes of this study, the bathymetry presented by Coleman et al. (1980) and shown in Figure 16 was considered sufficient for calculating the slope angles at the sites analyzed.

VIII. OCEAN WAVE DATA

Data from hurricane hindcasts on the wave height and wavelength were used to perform analyses with the limit equilibrium model. The wave height and wavelength determine the magnitude of the pressure on the ocean floor and the geometry of the pressure distribution, thereby affecting the driving moment. A larger wave height or wavelength increases the driving moment, decreasing the factor of safety against mudslide initiation.

Sources of Ocean Wave Data

Data on wavelengths and wave heights were obtained from hurricane hindcasts completed by Oceanweather, Inc. for Hurricane Andrew (Cardone et al. 1992), Hurricane Lili (Cardone et al. 2002), Hurricane Ivan (Cox et al. 2005), and Hurricanes Katrina and Rita (Cardone et al. 2006). Hurricane hindcasts are created with complex models that use meteorological and oceanographic data to calculate wind, wave and current information. Data for storm waves is reported in each hindcast for locations in a grid throughout the Gulf of Mexico. The spacing between grid points varies among hurricanes. The hindcast grid point spacing is 0.2 decimal degrees for Hurricane Andrew (about 14 miles), 0.05 decimal degrees for Hurricanes Ivan and Lili (about 3.1 miles), and 0.01 decimal degrees for Hurricanes Katrina and Rita (about 0.6 miles). Because Hurricanes Andrew, Lili, and Rita did not cause significant amounts of reported mudslide activity, most of the analyses performed for this study focused on Hurricanes Ivan and Katrina.

The hindcast data include wind, wave, and current information for each grid point. Though each hindcast contains information on the sea state for every 15 minutes throughout the storm, the maximum values given are the maxima that would be expected to occur if that sea state continued for three hours, because extreme sea states in the Gulf of Mexico typically are sustained for approximately three hours (Haring and Heideman, 1978). The three-hour projected maximum significant wave height, peak spectral period,

and vector mean direction for the sea state every 15 minutes are available for all data points in each hindcast. Directional spectra are available for about 5% of the data points for each hurricane. The directional spectra describe the wave energy distribution over a range of directions and frequencies (the inverse of the wave period). An example of the available data for one 15-minute time increment at one location from the Hurricane Ivan hindcast is shown in Table 4. The location and depth data for the point are listed in the first row of the table. The date and time and the peak wave, wind, and current data are listed in the second and third rows. The remainder of the table contains information for the directional spectra.

Table 4. Example of peak wave data and directional spectra from the Hurricane Ivan hindcast

Latitude	28.9500,	Longitude	-88.8500,	Angle	0.0000,	Depth	255.7778m																	
CCYYMM	DDHHmm	LPoint	WD	WS	ETot	TP	VMD	ETotSe	TPSe	VMDSe	ETotSw	TPSw	VMDSw	Mo1	Mo2	HSig	DomDr	AngSpr	Inline	Tau				
200409	152015	57105	27.2	29.921	11.159	16.892	289.7	3.889	10.912	247.9	7.27	16.906	308.8	6.321	4.456	13.362	298.7	0.7934	0.7217	0				
freq	0.039	0.0429	0.0472	0.052	0.0572	0.063	0.0693	0.0763	0.084	0.0924	0.1017	0.112	0.1233	0.1357	0.1493	0.1643	0.1809	0.1991	0.2191	0.2412	0.2655	0.2922	0.3216	anSpec
127.5	0	0	0	0	0	0	0	0	0	0	0	0	0	0	0	0	0.0001	0.0001	0.0001	0.0001	0.0001	0.0002	0.0013	0.0021
142.5	0	0	0	0	0	0	0	0	0	0	0	0	0.0003	0.0003	0.0003	0.0004	0.0005	0.0013	0.0014	0.0008	0.0006	0.0006	0.0029	0.0094
157.5	0	0	0	0	0	0	0	0.0001	0.0002	0	0	0.0002	0.0007	0.0027	0.0019	0.0036	0.0033	0.0052	0.0044	0.0025	0.0013	0.0012	0.005	0.0324
172.5	0	0	0	0	0	0.0001	0.0002	0.0005	0.0008	0.0011	0.0021	0.001	0.0016	0.0141	0.0136	0.0089	0.0058	0.0079	0.0061	0.0046	0.0025	0.0019	0.0062	0.079
187.5	0	0	0	0.0001	0.0002	0.0003	0.0006	0.002	0.004	0.0012	0.0021	0.0084	0.0263	0.0269	0.0222	0.0154	0.0089	0.0092	0.0083	0.0059	0.0032	0.0024	0.007	0.1546
202.5	0	0	0.0001	0.0002	0.0004	0.0005	0.0016	0.0041	0.0082	0.0038	0.0565	0.0389	0.0312	0.037	0.0286	0.023	0.012	0.0096	0.0089	0.0061	0.0034	0.0026	0.0075	0.2843
217.5	0	0.0001	0.0001	0.0003	0.0007	0.0012	0.0046	0.0098	0.0207	0.0556	0.1126	0.0665	0.0304	0.0309	0.0333	0.0246	0.0121	0.0098	0.009	0.006	0.0034	0.0026	0.0077	0.4422
232.5	0	0.0001	0.0002	0.0004	0.0014	0.0037	0.0116	0.0221	0.0311	0.0563	0.1134	0.0849	0.0402	0.0268	0.0359	0.0248	0.0122	0.0095	0.0091	0.0061	0.0034	0.0026	0.008	0.5037
247.5	0.0001	0.0001	0.0004	0.0015	0.0042	0.0108	0.0276	0.0955	0.0564	0.1383	0.1165	0.0853	0.0424	0.0325	0.0346	0.0246	0.0123	0.0091	0.0091	0.0062	0.0034	0.0025	0.008	0.7215
262.5	0.0002	0.0006	0.0025	0.0064	0.014	0.0241	0.0452	0.1869	0.0969	0.1535	0.1322	0.0888	0.0424	0.0296	0.0334	0.0241	0.0119	0.0085	0.0088	0.0061	0.0033	0.0023	0.0077	0.9296
277.5	0.0007	0.0035	0.0149	0.0264	0.0409	0.1062	0.2528	0.1508	0.1103	0.1539	0.1323	0.0764	0.0379	0.0266	0.0328	0.023	0.011	0.0079	0.0085	0.0057	0.003	0.0021	0.0072	1.2346
292.5	0.0012	0.0093	0.0557	0.1131	0.1916	0.3386	0.2705	0.1515	0.0964	0.1458	0.103	0.0485	0.0345	0.0246	0.0324	0.0215	0.0104	0.0072	0.0079	0.0053	0.0026	0.0018	0.0063	1.6798
307.5	0.0013	0.0048	0.0657	0.3266	0.554	0.5043	0.2563	0.1511	0.0891	0.0706	0.0625	0.0236	0.0311	0.0241	0.0297	0.019	0.0092	0.0065	0.0072	0.0048	0.0023	0.0015	0.0055	2.2508
322.5	0.0007	0.0024	0.0153	0.194	0.4683	0.4738	0.158	0.1315	0.0587	0.0704	0.0624	0.0226	0.0159	0.0254	0.0244	0.0132	0.0071	0.0056	0.0064	0.0042	0.002	0.0012	0.0047	1.7683
337.5	0.0003	0.0024	0.0096	0.0888	0.2718	0.0688	0.0899	0.0659	0.0538	0.0377	0.0535	0.0187	0.0144	0.0157	0.0157	0.0069	0.0042	0.0048	0.0053	0.0036	0.0015	0.0009	0.0041	0.8385
352.5	0.0001	0.0008	0.0025	0.0028	0.0024	0.0012	0.0641	0.0364	0.0051	0.0112	0.0117	0.0097	0.008	0.0076	0.0059	0.0033	0.0024	0.0045	0.0039	0.0026	0.001	0.0005	0.0035	0.1914
7.5	0	0.0001	0.0003	0.0001	0.0001	0.0001	0.0001	0.0002	0.0031	0.0016	0.0116	0.0006	0.001	0.0015	0.0016	0.0011	0.0006	0.0013	0.0013	0.0006	0.0003	0.0002	0.0027	0.0303
22.5	0	0	0	0	0	0	0	0.0001	0	0.0015	0.0001	0.0002	0.0005	0.0002	0.0002	0.0002	0.0001	0.0002	0.0001	0.0001	0	0.0001	0.0018	0.0053
fSpec	0.0047	0.0244	0.1673	0.7606	1.5502	1.534	1.1833	1.0086	0.6351	0.9027	0.9725	0.5743	0.3588	0.3265	0.3473	0.2375	0.124	0.1081	0.1059	0.0713	0.0375	0.0271	0.0971	11.159
dens	1.27	5.92	36.92	152.47	282.34	253.84	177.91	137.77	78.82	101.79	99.63	53.46	30.35	25.09	24.24	15.07	7.15	5.66	5.04	3.08	1.47	0.97	0.9	

An example plot of a directional spectra from the Hurricane Ivan hindcast is shown in Figure 19. The plot depicts the amount of wave energy corresponding to each combination of wave period and direction. The wave periods and directions with the most energy are the dominant periods and directions for the sea state that the spectra is describing.

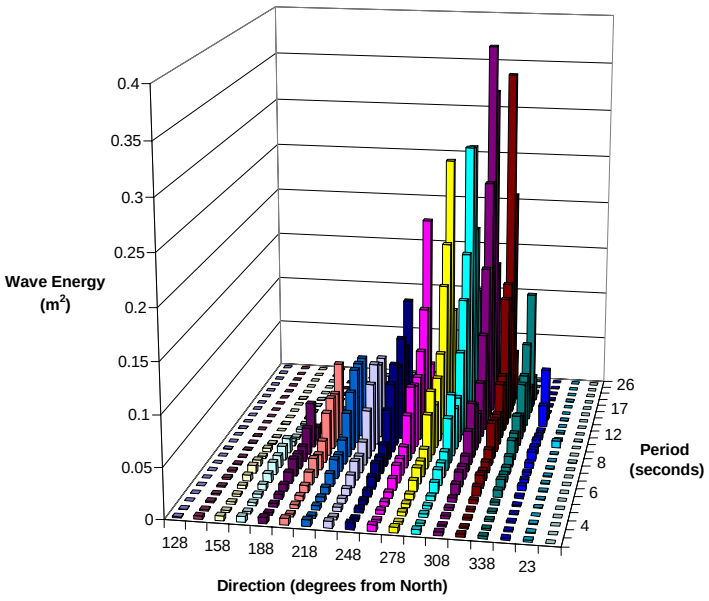

Figure 19. Example plot of a directional spectra from Hurricane Ivan hindcast

Uses of Ocean Wave Data in this Study

Two methods were used in this study to analyze mudslide vulnerability, each using different ocean wave data from the hurricane hindcasts. In the first method, directional spectra from the hindcast were used as input into a wave simulation program that calculated wave heights and pressures on the ocean floor (Zhang, 1999). The output from the simulation program was subsequently used to calculate factors of safety against mudslide initiation. In the second, simpler method, three-hour projected maximum wave height and period data were used to calculate factors of safety against mudslide initiation assuming linear wave theory (Wiegel, 1964).

Directional Spectra (Method 1)

Directional spectra from the hurricane hindcasts were analyzed using an irregular wave prediction program written by Dr. Jun Zhang from Texas A&M University. Details of the program are described by Zhang et al. (1999). Input to the program includes a directional spectra composed of wave frequencies, wave directions, and the amount of energy associated with each combination of wave frequency and direction. Output includes the wave amplitude (measured from the still water level, or sea level, to the wave peak or trough) and the pressure caused by the waves, (expressed as a change from hydrostatic pressure) as they vary with time. The program is based on the assumption of a rigid seafloor. The pressures and wave amplitudes can be calculated for any location, expressed in xyz coordinates, with the origin located on the ocean surface at the location for which the directional spectrum was calculated. In order to calculate pressures exerted by the waves on the ocean floor, typically referred to as the "bottom pressure", the water depth is entered as a negative z-coordinate. A schematic of the coordinate system used by the prediction program is shown in Figure 2020.

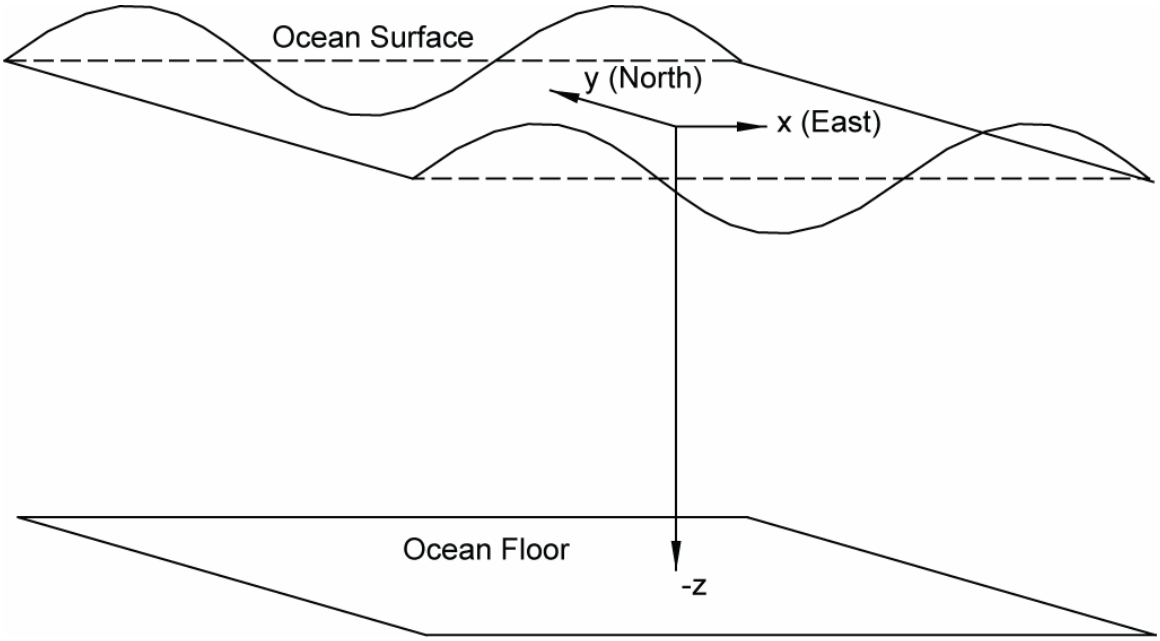

Figure 20. Coordinate system used by the irregular wave prediction program (Zhang, 1999).

The variation of wave amplitude and bottom pressure in space and time is simulated by running the prediction program for various x-y locations. Renderings of the wave amplitudes and bottom pressures over a 1000-square-meter area at one instant in time during the peak of Hurricane Ivan are shown in Figure 21 and Figure 22, respectively. The renderings are shown for a location in 259 feet of water in the mudslide prone area. Animations showing the wave amplitudes and bottom pressures as they vary with time during Hurricane Ivan are included electronically with this report (see Appendix C).

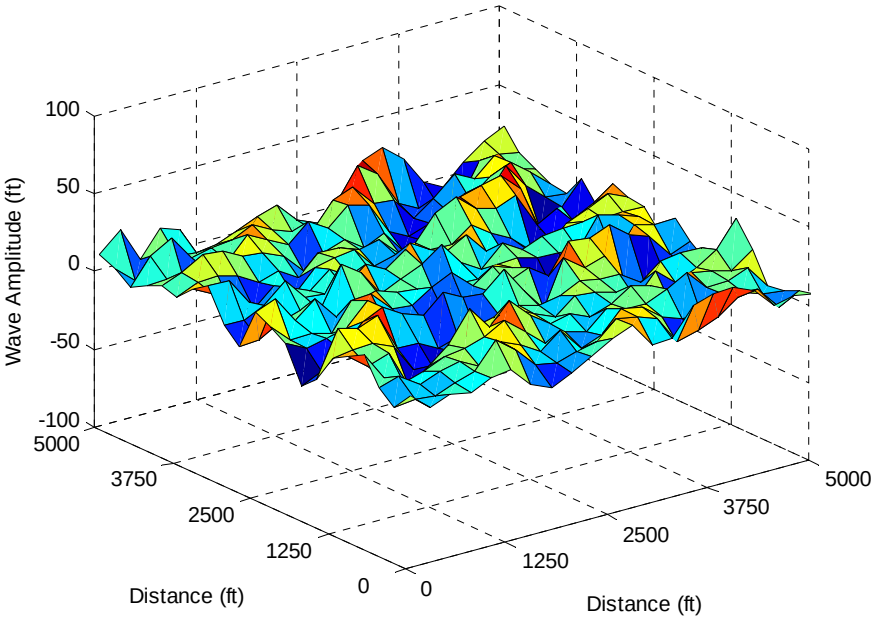

Figure 21. Spatial variation of wave amplitude at an instant in time during the peak of Hurricane Ivan, found using the prediction program by Zhang et al. (1999)

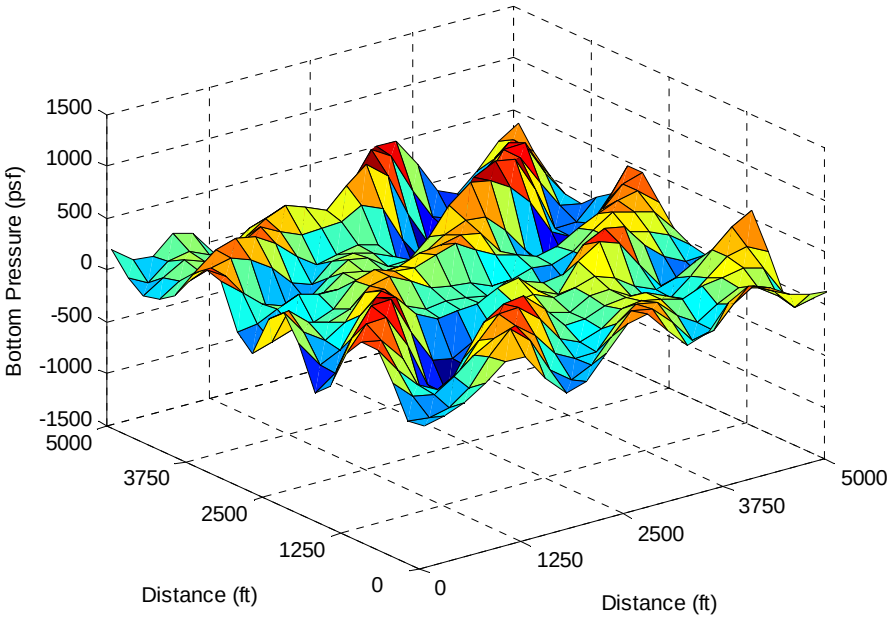

Figure 22. Spatial variation of bottom pressure at an instant in time during the peak of Hurricane Ivan, found using the prediction program by Zhang et al. (1999)

It can be seen in Figure 21 and Figure 22 that waves on the ocean surface (Figure 21) produce corresponding pressure "waves" on the ocean floor (Figure 22). In order to calculate the factor of safety at a site using a limit equilibrium analysis, it is necessary to know the magnitude and wavelength of this bottom pressure wave. The bottom pressure, p_{max}, required to calculate the factor of safety is the difference between hydrostatic pressure and the peak pressure. Because the pressure wave is not symmetric about the still water level, this value was approximated as half of the pressure difference between the peak and trough of the pressure wave as it moved over a point with time.

Because of the nonlinearity of the simulated waves, it was impractical to calculate the wavelength of each pressure wave created using the prediction program. The program determined the magnitude of the bottom pressure at a point, but the variations in directions and magnitudes of the wave with time (see animations included with this report and described in Appendix C) made determination of the maximum wavelength difficult. The wavelengths used to calculate factors of safety with the limit equilibrium analysis were estimated by using linear wave theory to calculate the wavelength corresponding to the peak spectral period for the spectrum being analyzed. This value for the wavelength was found to be a good approximation for the wavelengths of the largest pressure waves created using the prediction program. This agreement is illustrated by the following example. Contours of the pressures on the ocean floor at one instant in time during Hurricane Ivan are shown in Figure 23. The peak spectral period of the directional spectra used to simulate these pressure waves is 15.7 seconds. The site at which this directional spectra was calculated has a water depth of 259 feet. The wavelength of the largest waves as this site calculated using this water depth and peak spectral period and assuming linear wave theory (Equation 7) is 1128 feet. The measured wavelength of the largest wave in Figure 23 is approximately 1200 feet, which is similar to the value calculated using linear wave theory.

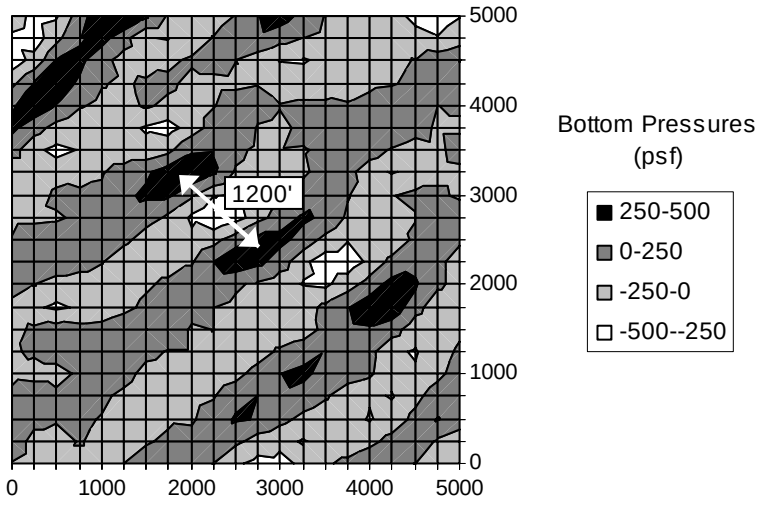

Figure 23. Contours of the pressures on the ocean floor at the peak of Hurricane Ivan, showing the wavelength of the largest pressure wave.

Once the maximum bottom pressure and wavelength were determined, these values were entered into the limit equilibrium equations presented previously to calculate the minimum factor of safety at a selected location for a given time period. This method for determining mudslide vulnerability is hereafter referred to as Method 1.

The irregular wave prediction program is more rigorous than techniques using linear wave theory because it includes nonlinear characteristics of the waves. It is, however, more time-consuming to calculate factors of safety using the irregular wave prediction program. It is also not possible to use the prediction program to calculate the factor of safety at all locations because directional spectra are not available at all locations. Because of these restrictions, factors of safety for most of the analyses performed in this study were calculated using the assumptions of linear wave theory. The irregular wave prediction program was used in a few cases to determine how the three-dimensional distribution of storm waves in space and time affects mudslide vulnerability, and to calibrate the results for bottom pressure found using linear wave theory. The procedure

for calculating factors of safety using linear wave theory is presented in the next section and is referred to as Method 2.

Peak Wave Data (Method 2)

In most of the analyses performed for this study, the goal was to determine whether a mudslide would have been expected during a hurricane at a given location or for a given set of parameters (slope angle, water depth, and soil shear strength). Therefore, it was typically only necessary to calculate the minimum factor of safety during the course of a storm. If the factor of safety was less than 1.0, a mudslide would be expected during the storm, and if it was greater than 1.0, a mudslide would not be expected.

In order to calculate the minimum factor of safety during a storm, it is necessary to know the most critical wave conditions that occurred during a hurricane event. The most critical wave height in terms of mudslide vulnerability is typically the maximum wave height, though mudslide vulnerability also depends on the wave period. Most of the hurricane hindcasts contained only information about the significant wave height, which is approximately the average of the highest 1/3 of all waves that occurred during the storm in a given time increment. The hindcast information for Hurricane Ivan also included the maximum wave heights at each location. Based on the relationship between the significant and maximum wave heights during hurricane Ivan and relationships reported in the literature (Ward et al, 1978), maximum wave heights in the other hurricanes analyzed were assumed to be equal to 1.8 times the maximum significant wave height.

The wave period is also an important aspect of the sea state in terms of mudslide vulnerability. Larger periods correspond to longer wavelengths, which increase the pressure on the seafloor and decrease the factor of safety. The hurricane hindcasts contain information about the peak spectral period, which is the period corresponding to

the highest energy component in the spectrum. While the peak spectral period is not precisely the period associated with the maximum wave height, the actual period of the highest wave is typically about 90% of the peak spectral period (Haring et al, 1976), and a 10% difference in period does not significantly affect calculations for the factor of safety. Therefore, it is reasonable to assume that the approximately the peak spectral period is the period of the largest wave.

In order to calculate the minimum factor of safety at a given location during a given storm, the maximum wave height during the course of the storm at that location was found from the hindcast, either directly (for Hurricane Ivan) or by multiplying the maximum significant wave height by 1.8 (for other storms). The wavelength and bottom pressure were calculated assuming linear wave theory (Wiegel, 1964) from the maximum wave height, the peak spectral period, and the water depth. The maximum bottom pressure calculated assuming linear wave theory is given by the equation:

$$p_{\max} = \frac{\gamma_w}{2}\left(\frac{H}{\cosh\left(\frac{2\pi}{L}d\right)}\right) \tag{14}$$

where γ_w is the unit weight of sea water, H is the wave height, L is the wavelength, and d is the water depth (Weigel, 1964). The wavelength calculated assuming linear wave theory is given by the equation:

$$L = \frac{gT^2}{2\pi}\tanh\frac{2\pi d}{L} \tag{15}$$

where g is the acceleration of gravity, T is the wave period in seconds, and d is the water depth (Weigel, 1964). The maximum bottom pressure increases linearly with wave height. The relationship among the maximum bottom pressure, wavelength, and water depth is shown in Figure 24. It can be seen in Figure 24 that the maximum bottom pressure decreases as the water depth increases, and that it increases as the wavelength increases.

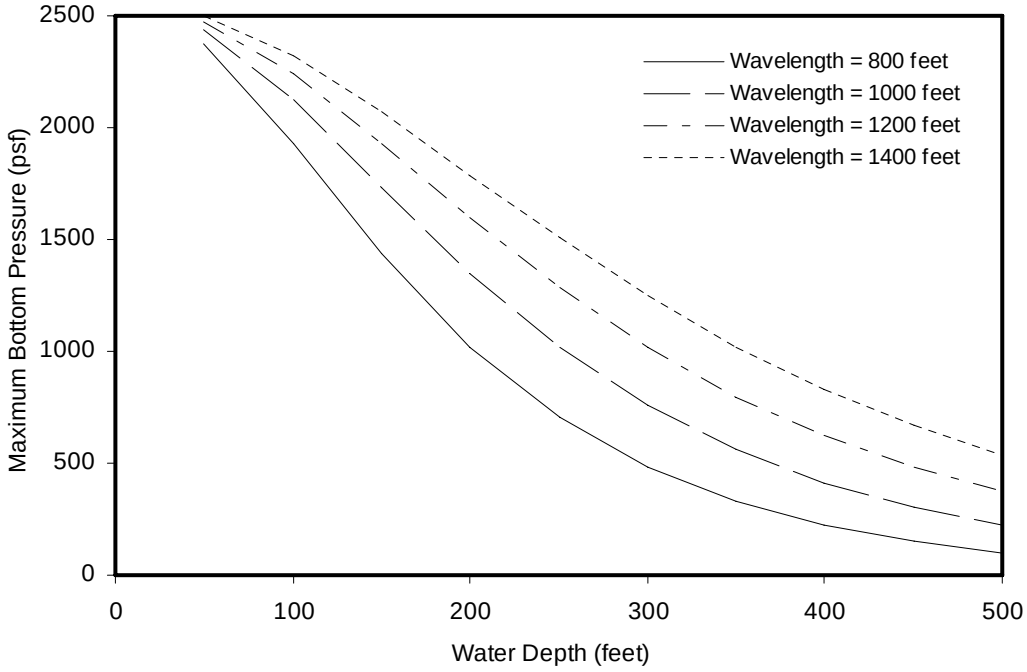

Figure 24. Relationship among maximum wave-induced bottom pressure, water depth, and wavelength

The bottom pressure, soil shear strength, wavelength, water depth, and seafloor slope were used to calculate the factor of safety. This method is hereafter referred to as Method 2.

Comparison of Methods 1 and 2

The wave heights and bottom pressures found using Method 1 (irregular wave prediction program by Zhang (1999) using directional spectra) and Method 2 (peak wave data assuming linear wave theory) were compared in order to determine how significant differences between results for mudslide vulnerability would be using the two methods. Values for wave height and bottom pressure found using Method 1 were the maximum values from a three-hour simulation. Values of wave height and bottom pressure were compared for all locations at which a directional spectra was available for Hurricanes Katrina and Ivan in the mudslide prone area. Because the hindcast for Hurricane Katrina

was developed with a finer grid than the hindcast for Hurricane Ivan, there are many more spectra available for Hurricane Katrina. The locations for which wave heights and bottom pressures were calculated and compared are shown in Figure 25.

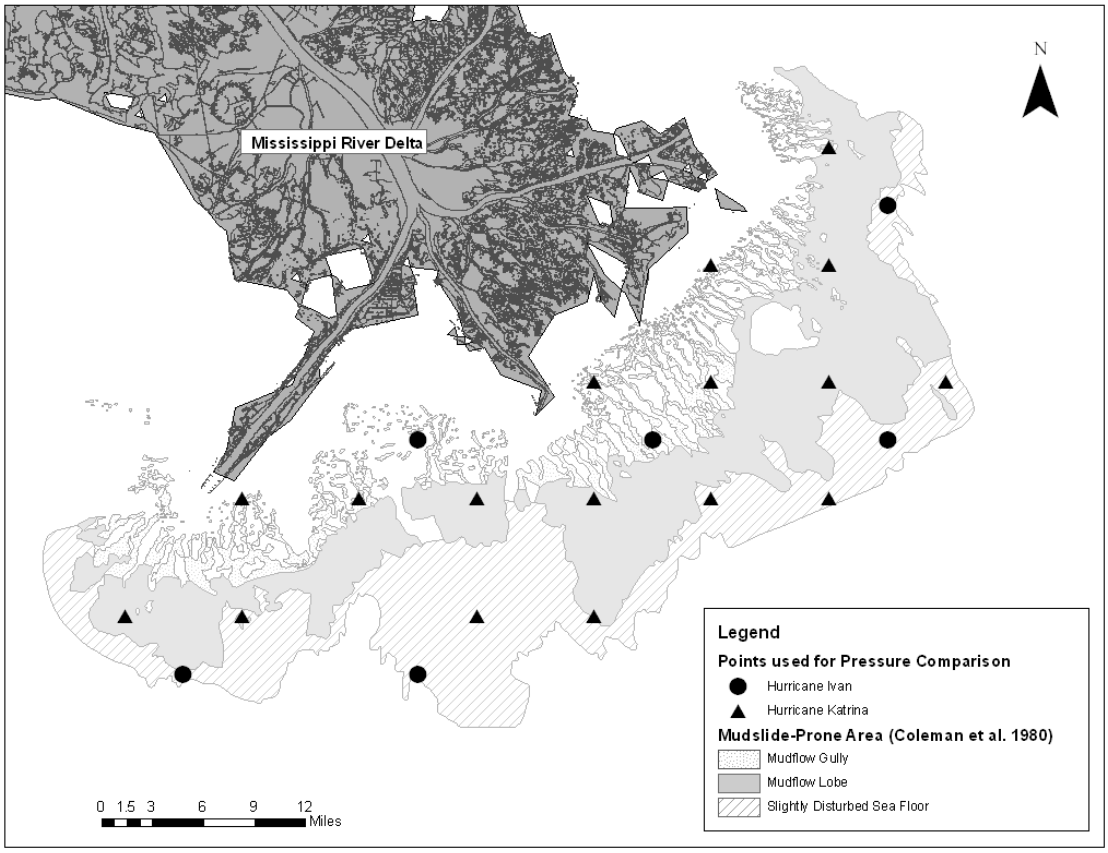

Figure 25. Locations for comparison of the two calculation methods for wave height and bottom pressure

The maximum wave heights and bottom pressures found using Methods 1 and 2 are shown in Table 5. Wave heights shown are the distances from the peak to the trough of the highest wave, and pressures shown represent the maximum increase from hydrostatic pressure. The ratios of each bottom pressures and wave height calculated using Method 1 to that calculated using Method 2 are also shown in Table 5.

Table 5. Comparison of wave heights and bottom pressures calculated using the irregular wave prediction program (Zhang, 1999) and with linear wave theory

						Maximum Wave Height (ft)			Bottom Pressure (psf)		
Hurricane	Grid Point	Water Depth (ft)	Maximum Significant Wave Height (ft)	Peak Spectral Period (sec)	Wavelength (ft)	Irregular Wave Prediction Program (Method 1)	Linear Wave Theory (Method 2)	Ratio (1/2)	Wave Prediction Program (Method 1)	Linear Wave Theory (Method 2)	Ratio (1/2)
Ivan	**57097**	**88**	**23.6**	**16.8**	**837**	**43**	**42**	**1.01**	**695**	**1109**	**0.63**
Ivan	**58017**	**240**	**37**	**15.9**	**1127**	**60**	**67**	**0.89**	**687**	**1058**	**0.65**
Ivan	**57101**	**259**	**36**	**15.7**	**1128**	**56**	**65**	**0.86**	**517**	**926**	**0.56**
Ivan	**56085**	**329**	**31**	**15.1**	**1112**	**45**	**56**	**0.80**	**344**	**543**	**0.63**
Ivan	56089	505	35	15.9	1277	55	63	0.87	214	334	0.64
Ivan	57105	839	44	16.9	1392	63	79	0.79	99	115	0.86
Katrina	6581	37	17	16.6	557	42	31	1.34	1008	922	1.09
Katrina	13204	50	36	14.8	566	128	66	1.96	2303	1811	1.27
Katrina	8796	66	41	15.7	684	101	73	1.37	1884	1971	0.96
Katrina	11043	73	37	15.4	699	92	67	1.38	1281	1752	0.73
Katrina	**8786**	**151**	**36**	**15.7**	**957**	**57**	**65**	**0.88**	**1070**	**1356**	**0.79**
Katrina	**14988**	**165**	**41**	**14.8**	**912**	**65**	**74**	**0.88**	**804**	**1377**	**0.58**
Katrina	**8806**	**180**	**43**	**15.6**	**1007**	**75**	**78**	**0.96**	**1055**	**1471**	**0.72**
Katrina	**8816**	**230**	**44**	**15.5**	**1074**	**73**	**80**	**0.92**	**735**	**1244**	**0.59**
Katrina	**14998**	**232**	**45**	**14.9**	**1015**	**67**	**81**	**0.83**	**790**	**1170**	**0.68**
Katrina	**11053**	**235**	**44**	**14.8**	**1008**	**73**	**80**	**0.91**	**769**	**1122**	**0.69**
Katrina	**13214**	**236**	**45**	**14.9**	**1019**	**72**	**82**	**0.89**	**801**	**1155**	**0.69**
Katrina	**6741**	**263**	**48**	**15.6**	**1122**	**76**	**87**	**0.87**	**792**	**1210**	**0.66**
Katrina	**6731**	**270**	**45**	**15.7**	**1140**	**75**	**81**	**0.92**	**794**	**1116**	**0.71**
Katrina	**8826**	**339**	**48**	**15.8**	**1206**	**82**	**86**	**0.95**	**559**	**918**	**0.61**
Katrina	**6751**	**363**	**50**	**15.6**	**1193**	**84**	**89**	**0.94**	**529**	**827**	**0.64**
Katrina	**13224**	**367**	**47**	**15.1**	**1129**	**74**	**85**	**0.88**	**522**	**691**	**0.76**
Katrina	11063	516	50	15.2	1174	90	89	1.01	286	359	0.80
Katrina	6761	601	48	15.6	1240	74	87	0.85	186	264	0.71
Katrina	8836	616	46	15.4	1210	72	83	0.87	169	216	0.78
Katrina	11073	727	49	15.3	1197	74	88	0.84	142	124	1.15
Katrina	6771	903	51	15.8	1278	86	92	0.93	93	70	1.34
Katrina	8846	943	50	15.1	1167	75	90	0.83	72	36	2.00
							Average =	0.98		Average =	0.82
							Average for depths of interest =	**0.90**		Average for depths of interest =	**0.66**

The average ratios of the maximum wave heights and bottom pressures calculated using Method 1 to those calculated using Method 2 are shown in Table 5. Average ratios were taken of maximum wave heights and bottom pressures for all the points shown in Table 5, and a second average was taken of only the maximum wave heights and bottom pressures for those points within the depths of the mudflow gully and mudflow lobe regions, where most mudslides occur (between 100 and 500 feet). These points are shown in bold in Table 5.

Results for Maximum Wave Height

The maximum wave heights in the depths of interest calculated using Method 2 are plotted against those calculated using Method 1 in Figure 26. A line with a slope of 1:1 is shown in Figure for comparison.

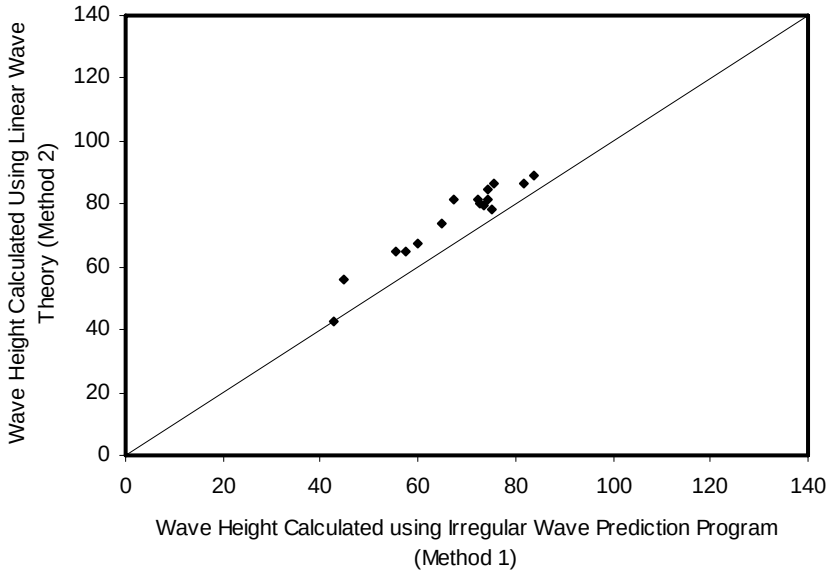

Figure 26. Comparison of maximum wave heights calculated using linear wave theory to those calculated using the irregular wave prediction program

The average ratio of the maximum wave heights calculated using Method 1 to the maximum wave heights calculated using Method 2 is 0.98 for all points and 0.90 for the points in the depths of interest. The small difference in calculated maximum wave heights between the two methods may be due to the random variation in the irregular wave prediction program. The irregular wave prediction program generates random phase angles for the waves, so results are somewhat different in every simulation. The amount of variability in the maximum wave heights found using the prediction program was explored by running ten three-hour simulations for the same site (Grid Point 57101 in Hurricane Ivan, also shown in Table 5) with the same directional spectra. Results of the maximum wave heights from the ten simulations are shown in Table 6.

Table 6. Results for the maximum wave height from ten simulations using the irregular wave prediction program, for Grid Point 57101 in Hurricane Ivan

Trial	Maximum Wave Height (feet)
1	49.3
2	53.8
3	58.9
4	59.5
5	62.0
6	60.5
7	57.3
8	54.1
9	57.7
10	55.6
Average:	56.9
Standard Deviation:	3.8
Standard Error:	1.2
Lower 95% Confidence Bound:	54.5
Upper 95% Confidence Bound:	59.2
Percent Error (%):	**8.2**

It can be seen in Table 6 that in ten three-hour simulations for the same site, the percent difference in the wave height based on the 95% confidence bounds is 8.2%. However, the maximum wave height calculated using Method 2 for Grid Point 57101 (see Table 5) is 65 feet, which is outside the 95% confidence bounds shown in Table 6. These results suggest that the difference of 10% between the wave heights calculated using Methods 1 and 2 in the depths of interest, as shown in Table 5, may be due in part to variation among simulations in the irregular wave prediction program (Zhang, 1999) but is mainly due to systematic differences between the two methods. The simple method of calculating the maximum wave height in Method 2 by multiplying the maximum significant wave height from the hurricane hindcast by 1.8 may contribute to this error, as this factor is not the same for all hurricanes. Overall, however, the difference in calculated maximum wave height between the two methods is small, so the results shown in Table 5 suggest that the irregular wave prediction program provides comparable results for maximum wave height with those reported in hindcast data.

Results for Bottom Pressure

The maximum bottom pressures in the depths of interest calculated using Method 2 are plotted against those calculated using Method 1 in Figure 27. A line with a slope of 1:1 is shown in Figure for comparison.

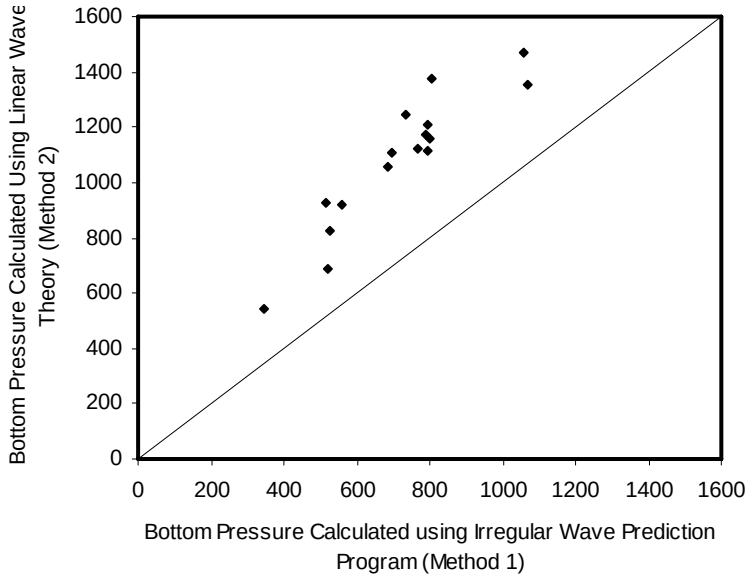

Figure 27. Comparison of maximum wave heights calculated using linear wave theory to those calculated using the irregular wave prediction program

The ratios of the bottom pressures show that the bottom pressures calculated using Method 2 are significantly larger than those calculated using Method 1. The average ratios of the bottom pressures calculated using Method 1 to those calculated using Method 2 (hereafter referred to as the "pressure ratio") are 0.82 for all points, and 0.66 for the points in the depths of interest. It is assumed that the bottom pressures calculated with Method 1, using the directional spectra and the irregular wave prediction program (Zhang et al, 1999), are more accurate than those calculated using Method 2. Method 2 involves linear wave theory, so it includes the assumption that bottom pressures are caused by one infinitely wide wave. The irregular wave prediction program (Zhang et al, 1999), on the other hand, takes into account the variation in direction and frequency of

the waves throughout the entire three hour simulation, making it more representative of the actual bottom pressures in a hurricane-like sea state. Pressures calculated using Method 2 must therefore be reduced if they are to accurately represent the pressures on the ocean floor during a hurricane.

The reason that smaller bottom pressures are caused by waves with finite lengths and widths compared to infinitely wide waves is that the stresses are dissipated three-dimensionally. The pressure caused by a wave on the ocean surface dissipates and spreads out as it is projected through the water, so the pressure it causes on the ocean floor covers more area than the wave on the ocean surface, but is smaller in magnitude. This effect is more pronounced in deeper water. If a wave is finite in both length and width, the pressure it causes dissipates in the direction of both its length and its width. However, if a wave is infinitely wide, the pressure it causes dissipates in the direction of its length, but it does not dissipate in the direction of its width. Therefore, the maximum bottom pressure caused by the infinitely wide wave will be larger than that caused by a wave that is finite in both length and width.

In order to reduce a value of bottom pressure calculated using Method 2 (linear wave theory) so it agrees with a value calculated using Method 1 (irregular wave prediction program), the value found using Method 2 can be multiplied by the pressure ratio defined above. In order to perform a calculation of bottom pressure using linear wave theory for any site, it must be possible to determine a value for the pressure ratio at locations where it is not possible to calculate the bottom pressure using the irregular wave prediction program. The relationship between the pressure ratio and other parameters was investigated in order to determine whether the pressure ratio might be estimated without knowledge of the directional spectrum. Plots of the pressure ratios from Table 5 against the maximum wave height, maximum wavelength, and the water depth are shown in Figure 28 through Figure 30.

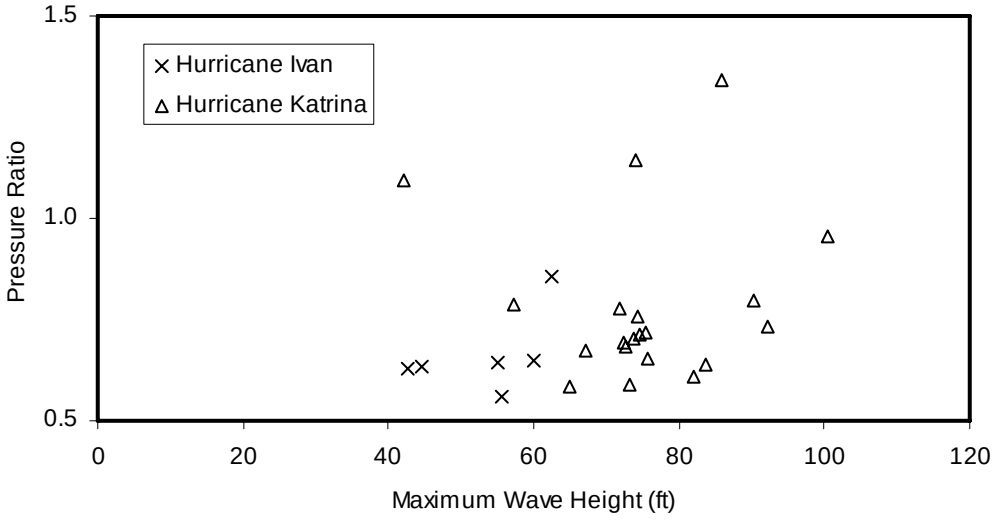

Figure 28. Pressure ratio versus maximum wave height for all points

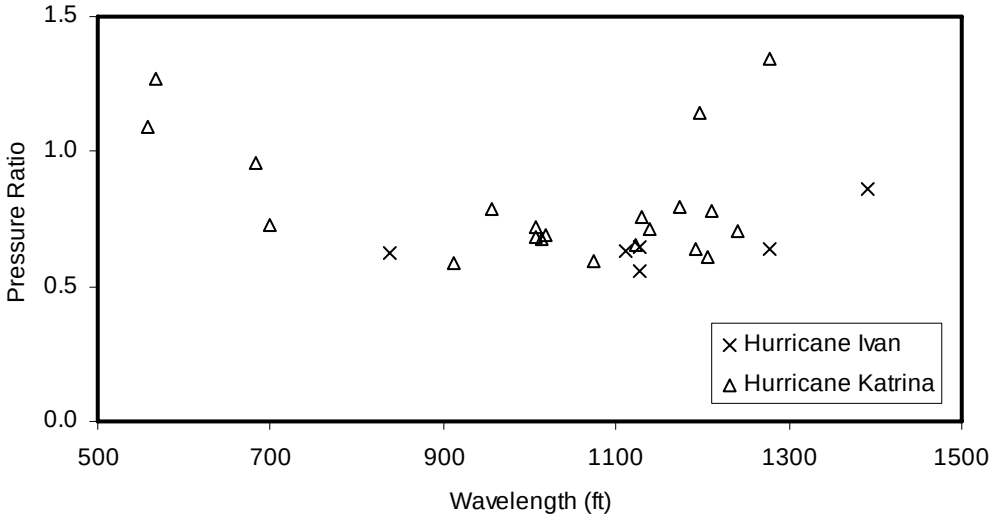

Figure 29. Pressure ratio versus wavelength for all points

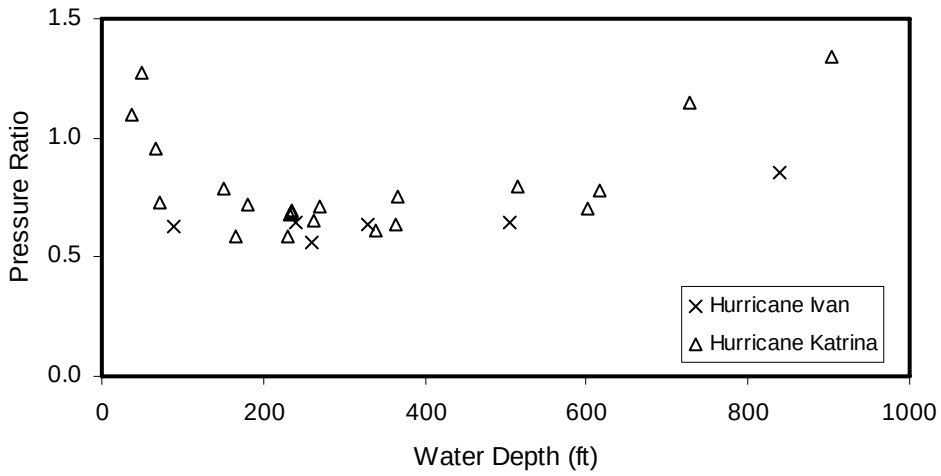

Figure 30. Pressure ratio versus water depth for all points

It can be seen in Figure 28 that the pressure ratio has no apparent correlation with wave height. The pressure ratio does appear to increase at high and low wavelengths (Figure 29) and at high and low water depths (Figure 30). The points with high pressure ratios at high and low wavelengths are the same points as those with high pressure ratios at high and low water depths, because wavelength generally increases as water depth increases.

Data for bottom pressure becomes questionable at high and low water depths for the following reasons. There is concern with extrapolating hindcast data into shallow water (less than 50-100 feet) due to interactions of the waves with the sea floor. In water deeper than about 400 feet, bottom pressures are so small that they have little influence on the ocean floor. Therefore, the apparent correlations of the pressure reduction factor with depth in very shallow and deep water were not considered relevant for this study. The relationship between bottom pressure and wavelength and between bottom pressure and water depth are plotted for points only within the depths of interest (100-500 feet) in Figure and Figure for wavelength and water depth, respectively.

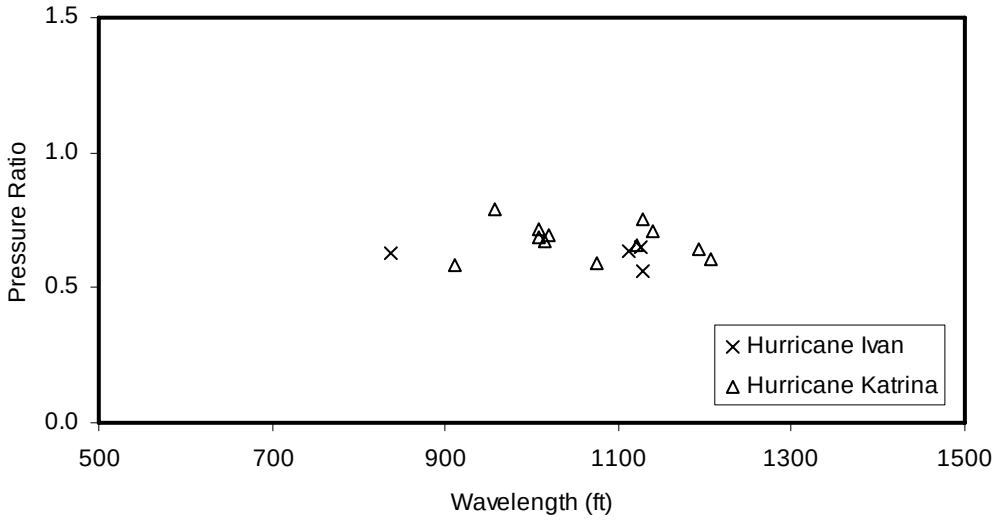

Figure 31. Pressure ratio versus wavelength for points in the depths of interest

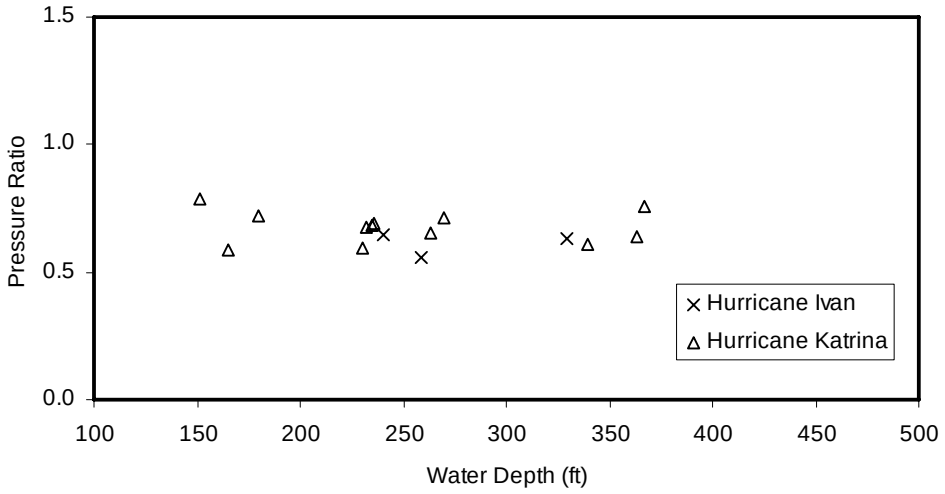

Figure 32. Pressure ratio versus water depth for points in the depths of interest

It can be seen in Figure 31 and Figure 32 that in the depth range of interest there is no apparent correlation between the pressure ratio and the wavelength or the water depth.

For the purposes of this study, all pressures calculated using linear wave theory (Method 2) were reduced by the average pressure ratio of 0.66, calculated for points within the

depth range of interest, so they would be closer to the more accurate pressures calculated using the irregular wave prediction program (Method 1). Further research is needed to determine if there is a more precise means of determining the maximum pressure on the sea floor during a hurricane when only the peak wave data are provided.

Due to the small number of directional spectra available and the significant calculation time required to obtain factors of safety using the irregular wave prediction program (Method 1), most of the calculations of factor of safety for this study were performed using linear wave theory (Method 2) with bottom pressures reduced by multiplying the pressures calculated using linear wave theory by an average pressure ratio of 0.66. Because the irregular wave prediction program is useful for examining the spatial variation of waves, Method 1 was used in one analysis to determine the areal extent and spatial distribution of mudslides. This analysis is described on page 83.

IX. EFFECTS OF INPUT VARIABLES ON MUDSLIDE VULNERABILITY AND ON THE CHARACTERISTICS OF MUDSLIDES

The simplicity of the limit equilibrium method makes it ideal for conducting parametric analyses of the effects of different input variables on mudslide vulnerability. In this section, the sensitivity of the limit equilibrium model to changes in the slope angle, water depth, wave height, and wave period are explored. The effect of the lateral extents of hurricane waves on the depth and areal extent of mudslides is also explored. A linear soil shear strength profile, with a strength of 50 psf at the surface and increasing at 2 psf per foot of depth, was used for most of the analyses presented in this section. This profile represents a remolded, or lower-bound, strength in the Gulf of Mexico. The weaker soil profiles measured in the mudslide prone area are close to or below 2 psf per foot (Figure 12 through Figure 15).

Slope Angle

Slope angles vary in the mudslide prone area from less than 0.5 percent to about 3 percent. A steeper slope lowers the factor of safety against mudslide initiation because it increases the driving moment due to the soil weight. The magnitude of the effect of the slope angle, however, is not the same at all sites. The effect of slope angle on the factor of safety for sites at two different water depths is shown in Figure 33. The Main Pass Lease Block 151 (MP-151) site has a water depth of 215 feet, while the Mississippi Canyon Lease Block 20 (MC-20) site has a water depth of 455 feet. Both sites are locations where mudslides were reported after Hurricane Ivan. The maximum wavelengths and peak spectral periods reported for these sites in the Hurricane Ivan hindcast (Cardone et al., 2005) were used for these analyses. The wave height and wavelength for the MP-151 site were 66 feet and 16.4 seconds, respectively. The wave height and wavelength for the MC-20 site were 71 feet and 16.1 seconds, respectively. The wave heights and wavelengths are similar at both sites and have little effect on the

difference in factors of safety. The soil was assumed to increase in strength linearly at 2 psf per foot.

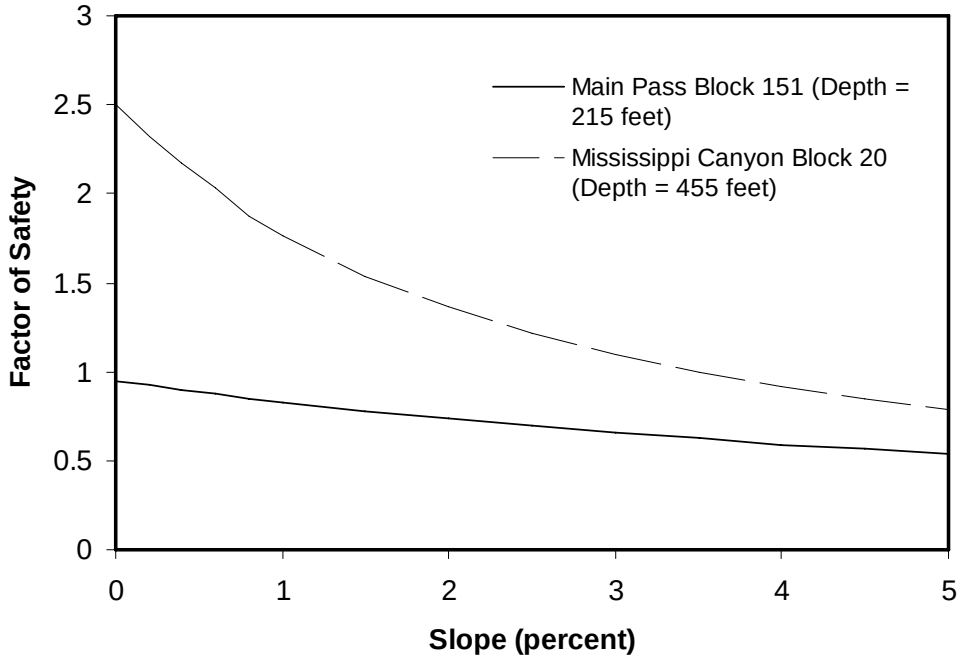

Figure 33. Factor of safety versus slope angle for sites of two mudslides caused by Hurricane Ivan, assuming a linear soil shear strength profile increasing at 2 psf/ft

It can be seen in Figure 33 that the slope angle has a much greater effect on the factor of safety in deeper water, at the MC-20 site. With an increase in slope from 0 to 3 percent, the factor of safety at the MP-151 site decreases from 0.95 to 0.66, a decrease of 31%. The same increase in slope at the MC-20 site decreases the factor of safety from 2.5 to 1.1, a decrease of 56%. In the limit equilibrium model, the driving moment is caused by a combination of the gravitational forces due to the soil weight and the pressures on the sea floor caused by large storm waves. The factor of safety at the shallower MP-151 site changes little with slope angle because the driving moment acting on the soil is dominated by the bottom pressures generated by hurricane waves. At the MC-20 site, which has water almost three times deeper than the MP-151 site, the effect of the

pressures generated by the waves is relatively less significant. The weight of the soil, and therefore the slope angle, proportionally has a much greater effect in this case.

The magnitude of the slope angle's effect is further illustrated in Figure 34, which shows the percentage of the driving moment as a function of the water depth for various slope angles. Curves are shown for slope angles of 0.5% (close to the flattest slope in the mudslide prone area), 1%, 2%, and 3% (close to the steepest slope in the mudslide prone area). The maximum wave assumed for this analysis was that caused by Hurricane Ivan at the MP-151 location, with a height of 66 feet and a period of 16.4 seconds. The wavelength was adjusted for the water depth assuming linear wave theory. The linear soil shear strength profile increasing at 2 psf per foot of depth was assumed for this analysis.

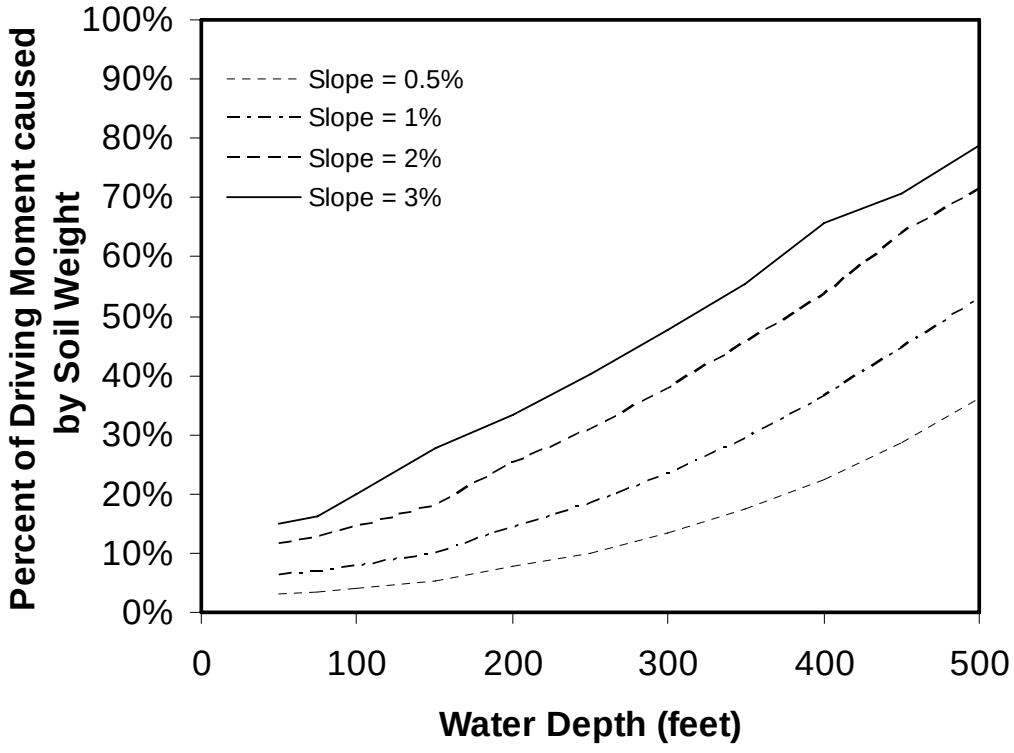

Figure 34. Percentage of the driving moment caused by soil weight as a function of water depth and slope angle, assuming a linear soil shear strength profile increasing at 2 psf/ft

It can be seen in Figure 34 that as the water depth increases, the percentage of the driving moment caused by soil weight increases, because the bottom pressures caused by the waves decrease. An increase in the slope angle also increases the percentage of the moment caused by soil weight, because increasing the slope angle increases the magnitude of the moment caused by the soil weight. In the deepest parts of the mudslide prone area where the slopes are steepest, such as at the Mississippi Canyon Lease Block 20 site, the soil weight accounts for as much as 80% of the driving moment. However, about 75% of the mudslide prone area is in water less than 300 feet deep, and nearly all of this area has slopes less than 1 percent (Hitchcock et al. 2006). Therefore, over most of the mudslide area, less than 25% of the driving moment is caused by the soil weight, making slope angle a relatively insignificant factor when compared with the pressures caused by storm waves.

Wave Height

The maximum wave height is an important factor in mudslide vulnerability at any location, because in most cases the driving moment acting on the soil mass is dominated by the pressure on the ocean floor caused by hurricane waves (Figure 34). In order to evaluate the size of hurricane waves required to initiate mudslides, the wave height required to cause a mudslide (or the wave height corresponding to a factor of safety of 1.0) was derived as a function of water depth for slope angle of 0.5%. The wave periods used for this analysis were the average periods corresponding to maximum wave heights. Hindcast hurricane wave data (Oceanweather, personal communication 2004) was used to derive the relationship between maximum wave heights and periods shown in Figure 35.

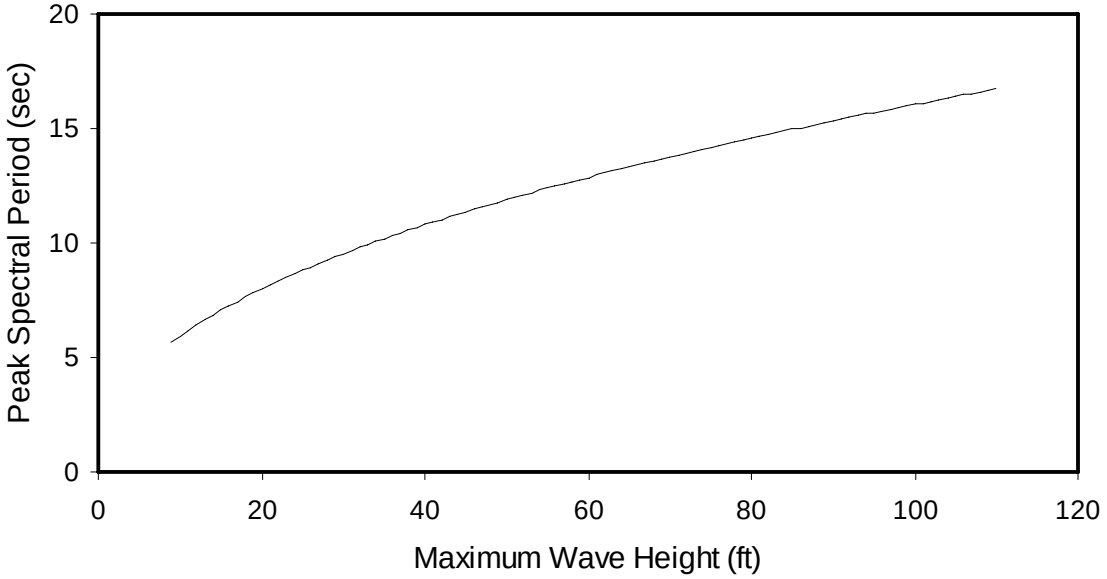

Figure 35. Relationship between maximum wave height and peak spectral period based on hindcasts of historical hurricanes

A soil shear strength profile with the strength increasing at 2 psf per foot of depth was assumed for this analysis. The relationship between maximum wave height required to cause failure and the water depth is shown in Figure 36. Note that the waves plotted in Figure 36 are the expected maximum wave heights for a three-hour sea state, which are approximately equal to 1.8 times the significant wave height, the value usually of interest in the hurricane hindcasts. The relationship between the water depth and the wave height required to cause failure is linear for a strength profile increasing linearly with depth, but this would not necessarily be the case if the soil strength profile did not increase linearly with depth.

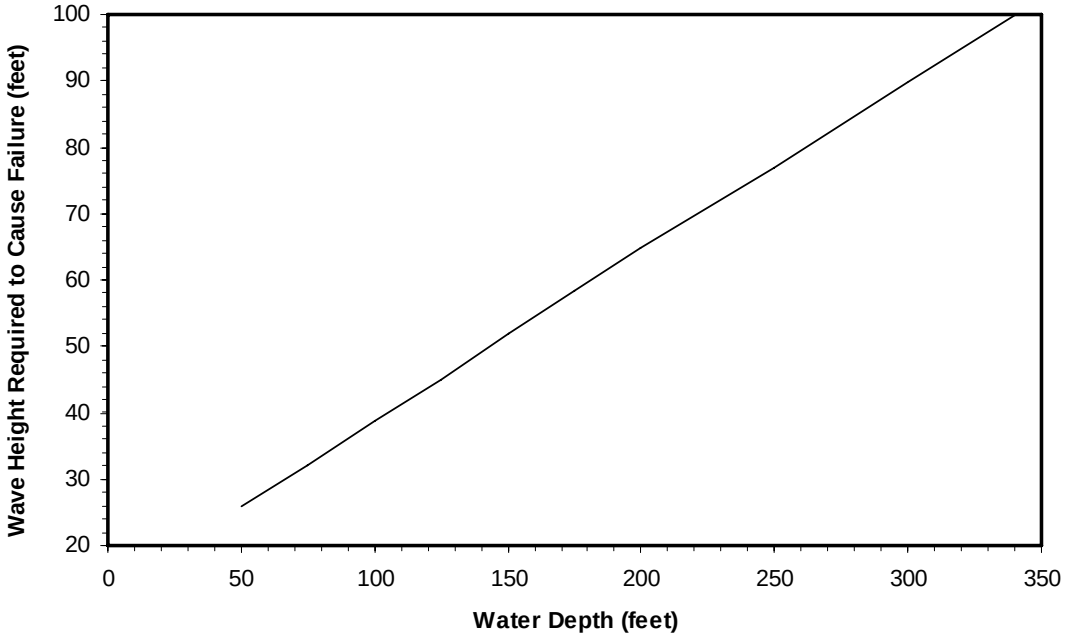

Figure 36. Maximum wave height required to cause failure as a function of water depth and slope angle, for a slope of 0.5% and a linear soil shear strength profile increasing at 2 psf/ft

It can be seen in Figure 36 that in a water depth of 50 feet, a maximum wave height of about 26 feet is necessary to cause failure. A maximum wave height of 26 feet corresponds to a significant wave height of about 14 feet, which is a large wave, but is below the value typically considered the threshold for a hurricane (a significant wave height of about 26 feet). Representatives from Shell Oil Company reported that mudslides have been known to damage pipelines during winter storms in shallow water (Coyne and Wrzyszczynski, 2007). Winter storms can be expected to produce maximum wave heights on the order of 30 feet in the Mississippi Delta region of the Gulf of Mexico (Suhayda, 1996), so it is feasible that winter storms could cause mudslides in shallow water (Figure). In water depths 150 feet and greater, the maximum wave height required to cause failure is 52 feet (significant wave height of 29 feet), which is above the threshold for a hurricane. Therefore, in most of the mudslide prone area, hurricane-sized

waves are required in order for mudslides to occur. As the water depth increases, increasingly large and therefore increasingly rare wave heights are required to cause mudslides. Widespread mudslide activity is only expected to occur in very intense hurricanes.

It is important to note that wave heights tend to decrease in shallow water due to attenuation, so the waves in the mudslide prone area during any storm will not be as large as those generated in the open water of the Gulf of Mexico. For example, for a storm to generate 60-foot high waves in the mudslide prone area, the storm must be larger, and therefore less likely to occur, than a storm that generates 60-foot high waves farther offshore. In order for a mudslide to occur, a storm must generate waves large enough to cause mudslides, and it must generate those waves in the vicinity of the Mississippi Delta where water is shallow and the shear strength of the soil is low. The occurrence of mudslides, then, is highly dependent on the track of and spatial variation of a hurricane, rather than just its size.

Wave Period

The period of a storm wave affects its wavelength, as shown previously in Equation 4.8, so mudslide vulnerability at a site is controlled in part by the periods of storm waves. The average relationship between hindcast maximum wave height (i.e, the maximum anywhere in the storm) and the associated peak spectral period for all Gulf of Mexico historical hurricanes was shown in Figure 35. The maximum wave heights and associated peak spectral periods at points throughout the mudslide prone area for Hurricanes Katrina and Ivan are superimposed on this plot in Figure 37. It can be seen in Figure 37 that the periods of waves in both hurricanes, and particularly in Hurricane Ivan, are longer than average. It seems reasonable to expect that while a hurricane's maximum wave height will be associated with the maximum wave period in the storm, there will local maximum wave heights at other locations that have the same peak spectral period. This behavior is seen in the Katrina data. The storm maximum height was ~ 97 feet (and on the curve representing the average maximum wave height versus

peak spectral period), and there were a number of points to the east and west of the northbound track that had lesser maximum heights. A similar trend is also seen for Ivan, but it must be remembered that the data shown are for locations in the mudslide prone area far to the west of the storm track and do not include the maximum wave height in the storm of ~96 feet.

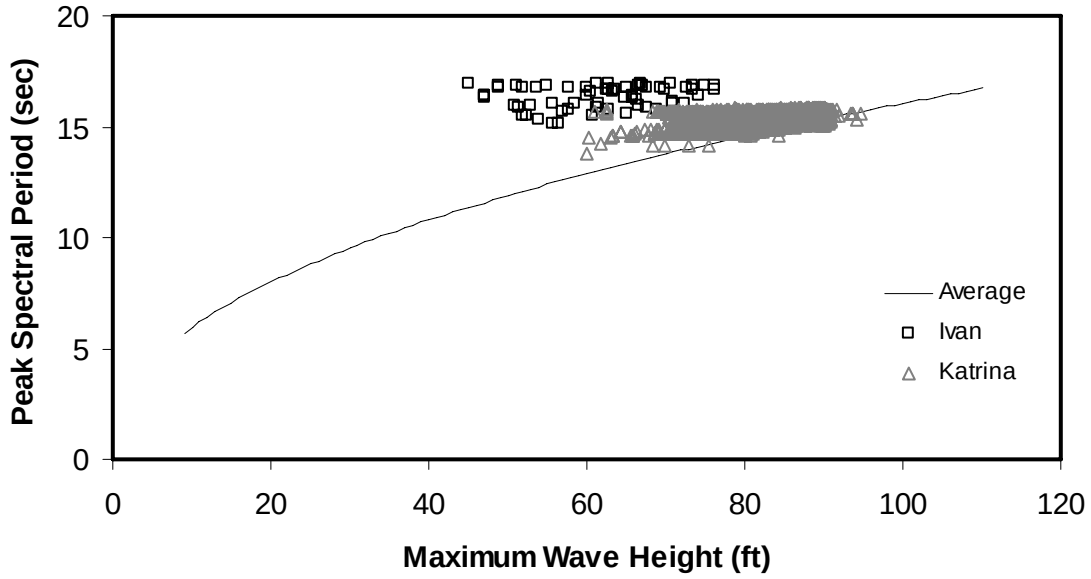

Figure 37. Relationship of peak spectral period with maximum wave height for Hurricanes Ivan and Katrina, and the average relationship for historical hurricanes

The effect of wave period on mudslide vulnerability is illustrated in Figure 38 using the site at Mississippi Canyon Lease Block 20 as an example. The water depth at this site is 455 feet, the slope angle is 2.3 percent, and the maximum wave height during Hurricane Ivan was 71 feet. The relationship between the peak spectral period and the factor of safety is shown in Figure 38. The period of this 71-foot high wave during Hurricane Ivan (16.1 seconds) and the period of a 71-foot wave in an average hurricane (13.8 seconds) as determined from the relationship shown in Figure 37 are also indicated in Figure 38. The site-specific strength profile for the Mississippi Canyon Lease Block 20 site was used in this analysis.

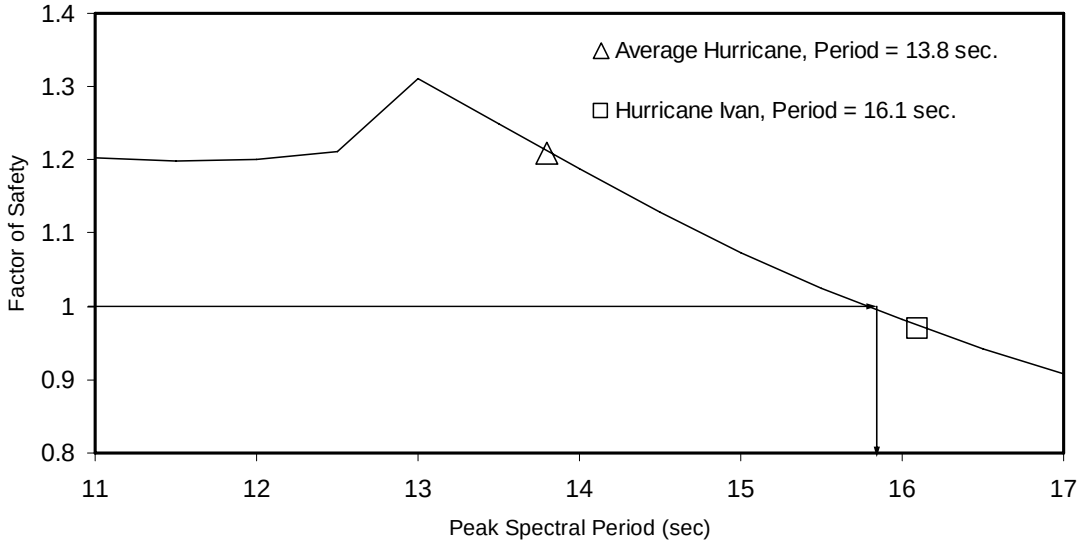

Figure 38. Factor of safety as a function of maximum peak spectra period for a 71-foot maximum wave height and the site parameters at the Mississippi Canyon Block 20 site (depth = 455 feet, slope = 2.3%)

It can be seen in Figure 38 that the long periods of the waves in Hurricane Ivan significantly lower the factor of safety when compared with the periods of an average hurricane. The reduction in period from 16.1 seconds to the average period of 13.8 seconds increases the factor of safety from 0.97 to 1.21, an increase of almost 25%. In fact, a mudslide reportedly destroyed a platform at this location during Hurricane Ivan (MMS, 2005). This incident, and much of the other mudslide activity caused by Hurricane Ivan, most likely would not have occurred in an average storm with wave heights in the Mississippi Delta region similar to those of Hurricane Ivan.

The slight decrease in factor of safety with a decrease in wave period below about 13.5 seconds occurs in Figure 38 because the strength profile used was not a linear strength profile, but rather the site-specific strength profile from Mississippi Canyon Lease Block 20 (from a proprietary source). This profile was nearly linear but had a few slight changes in slope. The decrease in factor of safety occurred because when the period decreased, resulting in a decrease of the maximum pressure on the ocean floor, a different

critical slip circle was found – in this case the critical slip circle became deeper with a smaller wave period. With a linear increase in shear strength, sudden changes in the depth of the slip circle will not occur with small changes in pressures, but with nonlinear strength profiles, locations in the profile with lower strength may change the geometry of the critical slip surface depending on the magnitude of the bottom pressure. This phenomenon can result in lower bottom pressures corresponding to lower factors of safety over a small range of bottom pressures, but in general the effect is small and does not result in large decreases in factor of safety. This example highlights the importance of determining the relationship between factor of safety and bottom pressure if a specific site is of interest, however, because the factor of safety will not vary at the same rate with bottom pressure for all soil profiles.

Relationship Between Size of Wave and Size of Mudslide

Mudslides in the Mississippi Delta region of the Gulf of Mexico are caused by storm waves, so it is logical to expect that their size might be related to the lengths and widths of the waves. (The width of the waves, or the dimension perpendicular to the direction of motion, is assumed to be infinite according to linear wave theory, but in reality this is not the case.) Analyses were performed in order to investigate the sizes of mudslides and compare them to the sizes of storm waves, both in terms of the depth of the failure surface and in terms of its areal extent.

Mudslide Depth

The depth of the failure surface predicted using the limit equilibrium model depends on the distribution of the shear strength of the soil with depth, and on the wavelength of the storm wave causing the mudslide. This relationship is shown in Figure 39 for linearly increasing shear strength profiles with a strength at the surface of 50 psf. It can be seen in Figure 39 that except in locations where the shear strength of the soil is extremely low, the depth of the failure surface (or the depth of the critical slip circle found from a limit

equilibrium analysis) is about 50 feet. This depth increases somewhat as the wavelength increases, but the effect of the wavelength is small. These results indicate that, in general, the depth of sliding will be about 5 to 10 percent of the wavelength of the largest waves. These results are consistent with the reports be Coleman et al. (1980) that the thickness of the mudflow lobes are up to 75 feet thick, indicating that some of the disturbed soil comprising mudflow lobes may have been deposited by wave-induced slope failures.

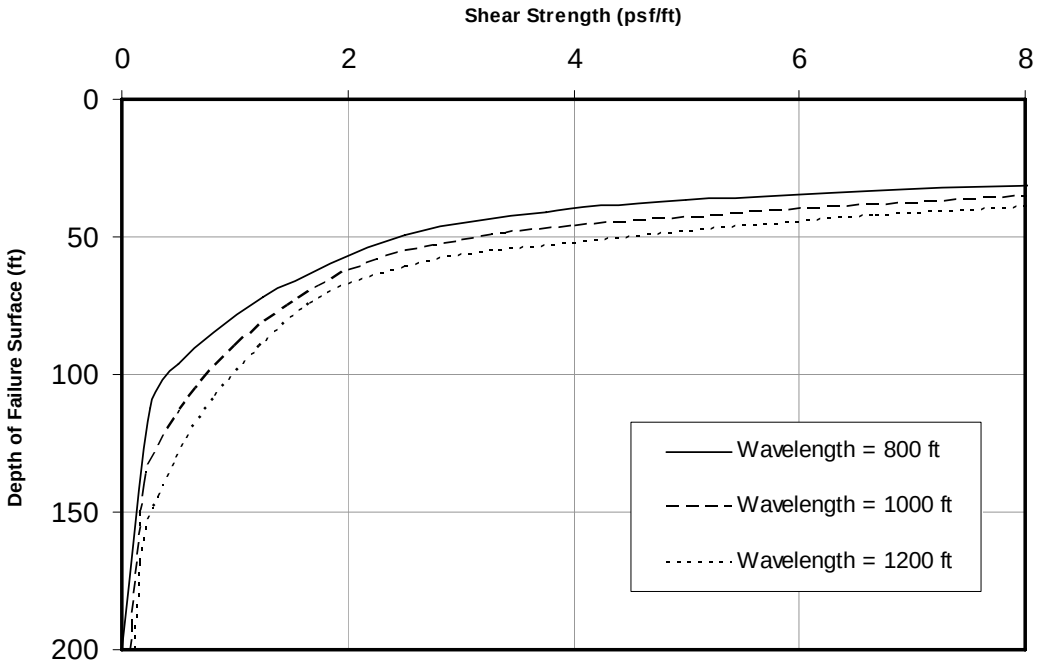

Figure 39. Depth of critical failure surface calculated using the limit equilibrium model as a function of soil shear strength and wavelength

The depth of the critical failure surface may vary when the soil shear strength is very nonlinear, as the failure will tend to occur where there is a reduction in strength. For nearly all soil profiles used in this study, however, the depth of the critical failure surface was less than 150 feet. In two cases where a strong upper crust of the soil extended very deep with weaker soil beneath (see shear strength profiles for South Pass Lease Block 30

and South Pass Lease Block 34 in Figure 13 and Figure 15, respectively) the critical failure surface was calculated to be about 175 feet deep.

Areal Extent of Mudslides

The analyses of mudslide behavior discussed so far in this section have been performed using the assumptions of linear wave theory, in which waves are assumed to be infinitely long in the direction perpendicular to the direction of motion. These two-dimensional models of waves work well to explore the relationship among wavelength, wave height and the initiation of mudslides. In order to investigate the influence of waves on the areal extent of mudslides, however, a three-dimensional model of waves is necessary in order to take into account the size and shape of the waves both perpendicular and parallel to the direction of motion.

The wave prediction program developed by Zhang et al. (1999) can simulate waves in three dimensions, so it was used to investigate the effects of wave geometry and directionality on the areal extent of mudslides. The program is described in the section entitled "Ocean Wave Data." Two three-hour simulations using the prediction program were performed using directional spectra from hurricane hindcasts at locations where mudslides were reported. One simulation was performed for Hurricane Ivan near Mississippi Canyon Lease Block 20, and one was performed for Hurricane Katrina near South Pass Lease Block 77. Values for the depth of the water, the slope of the sea floor, and the shear strength of the soil corresponded to the known values of these parameters for each respective site. Values for these parameters were assumed to be constant over each area analyzed. The only quantity that changed spatially in the simulation was the bottom pressure caused by the waves. The resulting patterns of mudslides for these simulations, represented by the locations for which the largest bottom pressure over the course of the three-hour simulation was sufficient to cause a factor of safety less than 1.0, are shown in Figure 40 and Figure 41.

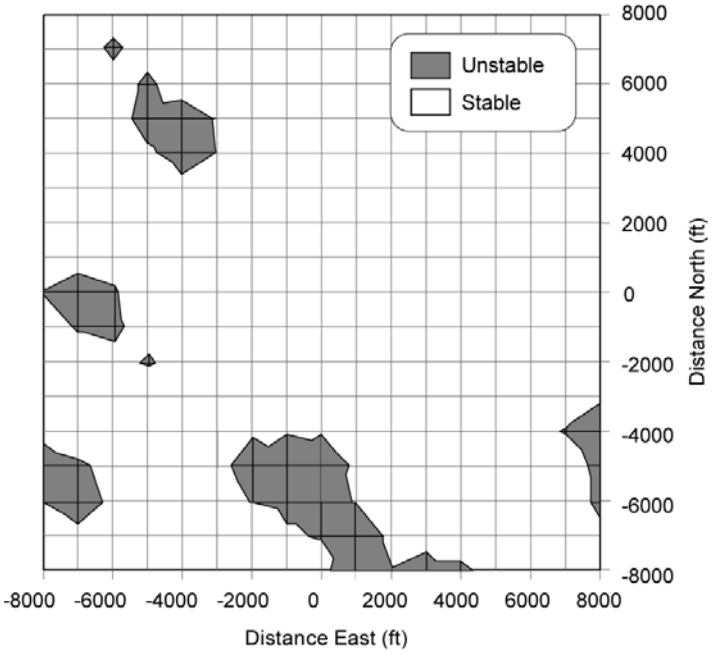

Figure 40: Simulated pattern of mudslides over lease block area with conditions at South Pass Lease Block 77 during Hurricane Katrina

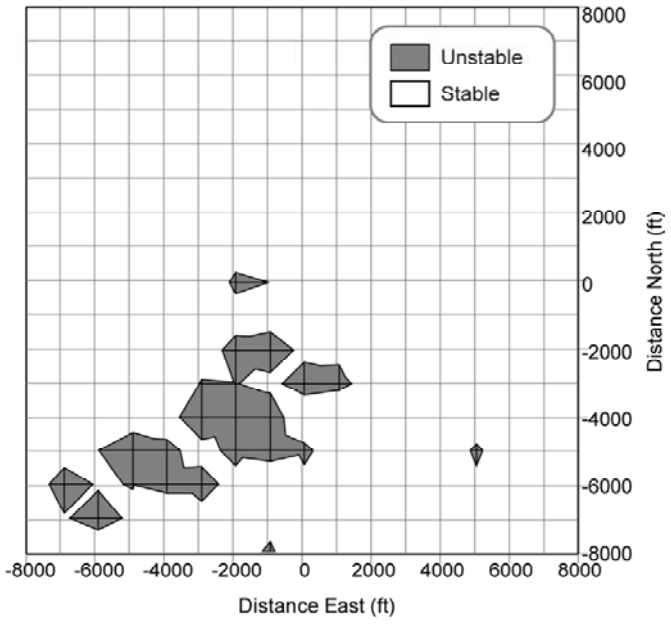

Figure 41: Simulated pattern of mudslides over lease block area with conditions at Mississippi Canyon Block 20 during Hurricane Ivan

The approximate sizes and shapes of the simulated mudslides shown in Figure 40 and Figure 41 mimic the patterns of the largest hurricane waves, with dimensions on the order of a few thousand feet. The patterns also look similar to post-hurricane surveys of actual mudslide features in the Mississippi Delta (Bea et al. 1980, Thompson et al. 2005, Walsh et al. 1006 and Hitchcock et al. 2005) and remarkably similar to many of the geologic features in the mudslide prone area described by Coleman et al. (1980) such as collapse depressions. Figures from Thompson et al. (2005) and Coleman et al. (1980) are shown in Figure and Figure. The areas of disturbed soil indicating mudslide activity (Figure 42) and collapse depressions (Figure 43) are outlined in the figures, as they are difficult to see in the scanned images.

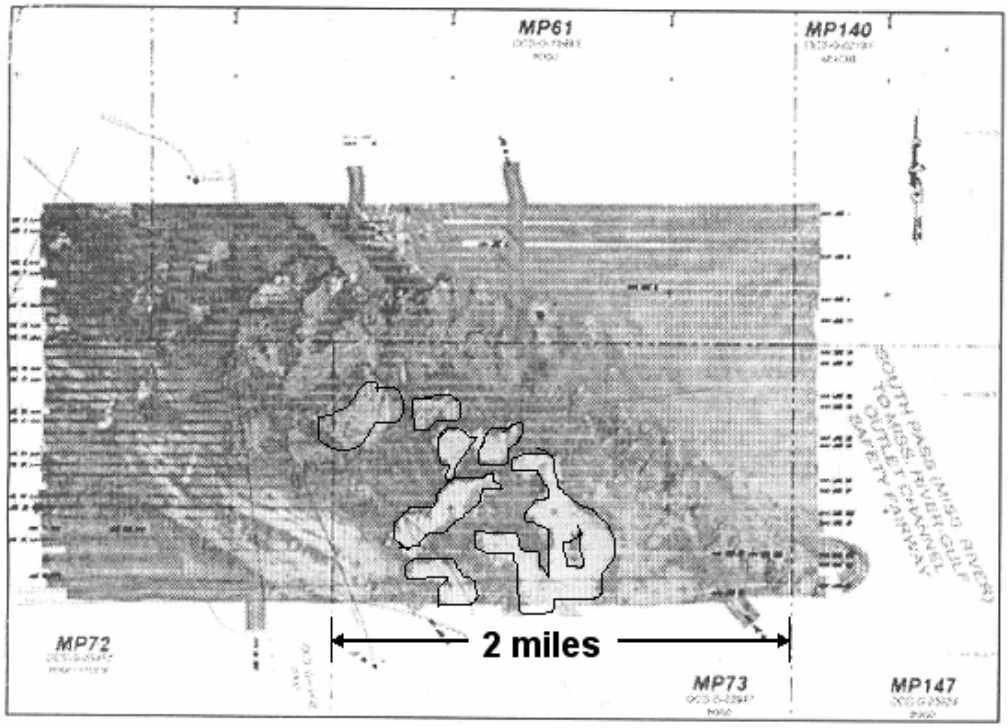

Figure 42. Side-scan sonar image in Main Pass Lease Blocks 72 and 73, showing soil disturbed by mudslide activity (from Thompson et al, 2005)

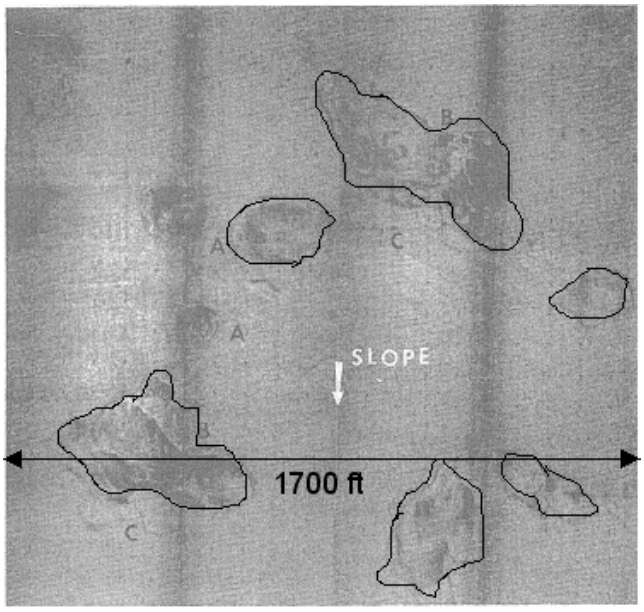

Figure 43. Side-scan sonar image showing collapse depressions from Coleman et al. (1980)

The simulated mudslides shown in Figure 40 and Figure 41 are relatively localized due to the significant variability in the hurricane waves; a wave large enough to induce a mudslide at one location may not be so large at a nearby location. Also, the soil shear strength profiles used in the simulations represent relatively weak soils, and the soil shear strength was assumed to be constant over the entire lease block-sized area over which the simulation was performed. In reality, the soil shear strength would vary throughout the lease block and would be stronger in some areas, making the portions of the areas that are affected by mudslides even smaller.

The simple limit equilibrium model is useful in making some important conclusions about mudslide behavior. Results of the parametric studies described in this section suggest that mudslides can only be caused by large storm waves, and that in much of the mudslide prone area, very intense hurricanes must occur in order to generate waves large enough to cause mudslides. The large storm waves required to cause mudslides have a low probability of occurrence in the Gulf of Mexico, and an even lower probability of occurrence in the mudslide prone area. The potential of storm waves to cause mudslides depends not only on the wave height, but also on the wave period. Results also show that except in portions of the mudslide prone area with the deepest water, slope angle is not a significant factor in mudslide vulnerability. Finally, the analyses performed suggest that the depth of the failure surface and the areal extent of mudslides is related to the lengths and widths of the storm waves that cause them. Mudslides are most likely localized features on the order of several thousand feet in lateral extent, and do not likely lead to large-scale, regional mudflows due to the very flat slopes in the mudslide prone area and the large amount of spatial variation in soil shear strength and wave height.

X. VERIFICATION OF LIMIT EQUILIBRIUM ANALYSIS

In order to check the results of the limit equilibrium model developed for this study and presented starting on page 21, analyses were compared with two other methods of analysis. The slope stability program UTEXAS4, which uses limit equilibrium procedures, was used to check results at two sites. In addition, an analysis was performed for one site using a layered continuum model to calculate displacements. The depth to which significant displacements occurred were then compared to the depth of failure determined from limit equilibrium analyses.

UTEXAS4 Slope Stability Program

Limit equilibrium analyses were performed for two sites using the Henkel-type model developed for this study and with the slope stability program UTEXAS4. Site-specific shear strength data were available at both sites. The first site is in Mississippi Canyon Lease Block 20, and analyses were performed using the wave height and period from the Hurricane Ivan hindcast. The second site is in South Pass Lease Block 77, and analyses were performed using the wave height and period from the Hurricane Katrina hindcast. Mudslides were reported in both Mississippi Canyon Lease Block 20 and South Pass Lease Block 77 for Hurricanes Ivan and Katrina, respectively. The limit equilibrium spreadsheet program included with this report, for which a user's guide is attached in Appendix B, was used to implement the limit equilibrium model developed for this study.

Input for UTEXAS4

Soil shear strength profiles for both sites were entered into UTEXAS4 as piecewise linear profiles. In order to define the profiles, a different material was defined each time the soil strength profile changed its slope with respect to depth, so the boundaries between the materials were at the depths of the known strength data points. Each material was assigned a linear increase or decrease in strength with depth equal to the slope of the soil shear strength at that location.

The ocean floor was defined in UTEXAS4 as a surface with a constant slope extending horizontally for 2000 feet. This horizontal dimension encompasses at least 1.5 wavelengths for a typical storm wave, and was selected in order to ensure that a typical critical circular failure surface would be within the defined slope geometry. The bottom pressure caused by the storm waves was entered into UTEXAS4 as a static distributed pressure with a sinusoidal shape.

Spencer's Procedure (Spencer, 1967) was chosen as the analysis method in UTEXAS4. Spencer's Procedure is a method of slices which satisfies all requirements for static equilibrium, and all side forces on slices are assumed to have the same inclination. The limit equilibrium model developed for this study also satisfies complete equilibrium due to the use of undrained shear strength and the resulting assumption that the soil friction angle, ϕ, is equal to zero. Theoretically, then, analyses using Spencer's Procedure and analyses using the limit equilibrium spreadsheet program (Appendix B) should result in identical critical circles and minimum factors of safety.

Comparison of Results

The results of the analyses performed using the limit equilibrium spreadsheet program and the analyses performed using UTEXAS4 are summarized in Table 7. The minimum factor of safety, the radius of the critical slip circle, and the depth to the bottom of the critical circle below the mudline are shown. It can be seen in Table 7 that the results found using the two programs agree very closely, both in terms of the value of the minimum factor of safety and the geometry of the critical failure circle.

Table 7. Comparison of results found using the limit equilibrium spreadsheet program and those found using UTEXAS4

	Minimum Factor of Safety		Radius of Critical Circle		Depth of Critical Circle	
Method of Analysis	MC-20	SP-77	MC-20	SP-77	MC-20	SP-77
Spreadsheet Program	0.974	0.764	711	370	145	70
UTEXAS4	0.981	0.782	711.5	368.8	146.2	68.5

Deformation Model

The second series of analyses (Nodine et al. 2007) was performed using a more complicated deformation model based on the theory of elastic continuum and comparing it with the limit equilibrium model. While the limit equilibrium model provides an indication of whether or not failure will occur, it does not give any indication of the magnitude of seafloor movements. The deformation model, however, can be used to solve for the displacements and stresses in the seafloor resulting from wave loading. Figure 44 shows a schematic of the deformation model, referred to as the layered continuum model. In this model equivalent linear, stress-dependent soil moduli are assigned based on a nonlinear Ranberg-Osgood stress strain curve (Pabor, 1981).

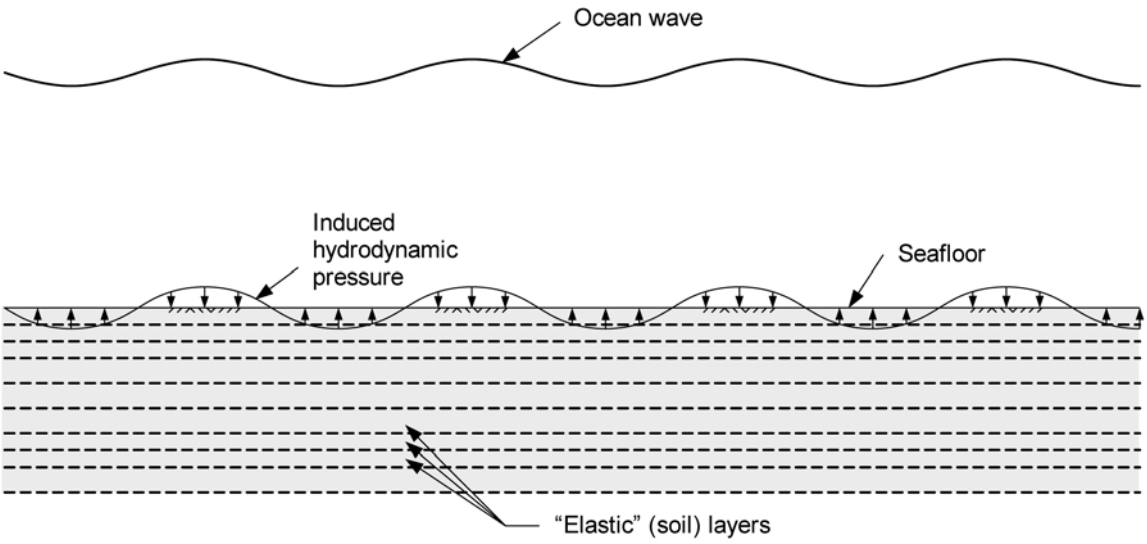

Figure 44. Layered continuum model for ocean-wave induced soil movements and stability (from Nodine et al. 2007)

Two different profiles of undrained shear strength were used to compare the limit equilibrium model with the layered elastic continuum model. Both soil strength profiles were from soil borings taken in South Pass Lease Block 70, near the site where a mudslide destroyed a platform during Hurricane Camille (Bea et al. 1983). The first profile, referred to by Bea et al. (1983) as a "soft" profile, has shear strength increasing linearly with depth at a rate of approximately 1.5 psf per foot to a depth of about 80 feet and at a rate of about 3 psf per foot thereafter. The second profile, referred to as a "stiff" profile, contains a strong crust overlying weaker material. The two soil profiles are shown in Figure 45.

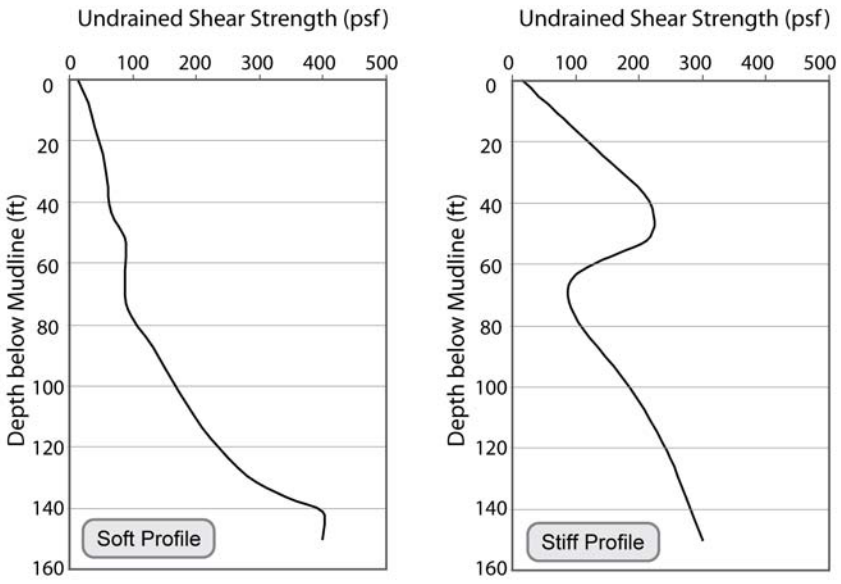

Figure 45. "Soft" and "stiff" soil profiles in South Pass Lease Block 70 (after Bea et al. 1983)

Analyses were performed using both the limit equilibrium and layered continuum models assuming a wave height of 55 feet with a period of 12.4 seconds for the "soft" profile, and a wave height of 68 feet with a period of 13.6 seconds for the "stiff" profile. The wave heights and periods used for the analysis are those that produced a factor of safety of approximately 1.05 based on limit equilibrium analysis for each respective soil profile. That is, the waves were selected to represent waves that are close to causing failure.

The variation in peak lateral displacement with depth found from the layered continuum analyses of the two soil profiles, as well as the depth to the bottom of the critical circle from the limit equilibrium analysis, are shown in Figure 46 and Figure 4747. The depths to which large lateral displacements occur correspond closely with the depth to the bottom of the critical circle from the limit equilibrium analysis (Figure and Figure 47). These results indicate that the geometry of the failure from both analyses is similar.

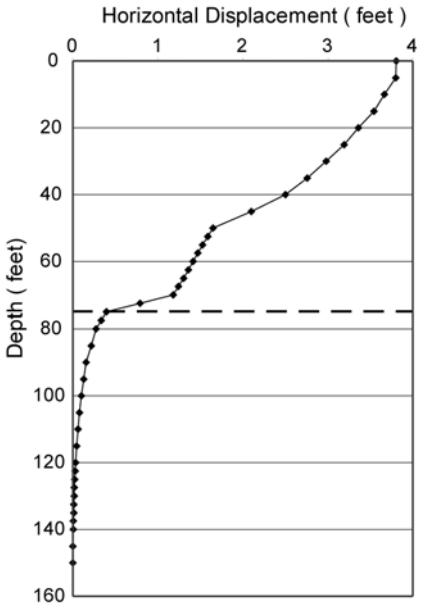

Figure 46. Maximum horizontal displacements for "soft" soil profile – Depth of critical circle shown by broken line. Wave height = 55 feet; Wave period = 12.4 seconds (from Nodine et al. 2007)

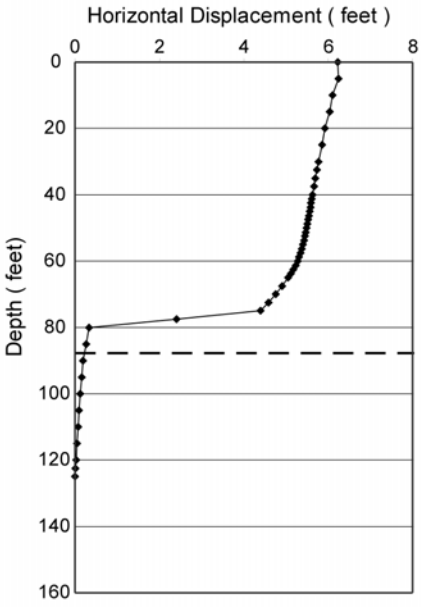

Figure 47. Maximum horizontal displacements for "stiff" soil profile – Depth of critical circle shown by broken line. Wave height = 68 feet; Wave period = 13.6 seconds (from Nodine et al. 2007)

To further compare the limit equilibrium and layered continuum slope stability models, analyses were performed assuming a variety of wave heights for each soil profile. The maximum shear strain in the soil found from the analyses with the layered continuum model plotted versus wave height are shown in Figure 48 and Figure 49. The two figures also indicate the wave heights that produce factors of safety of 1.0, 1.3, and 1.5, based on limit equilibrium analyses. The shear strain is small for factors of safety greater than 1.5, and becomes very large as factors of safety approach 1.0, which indicates impending failure.

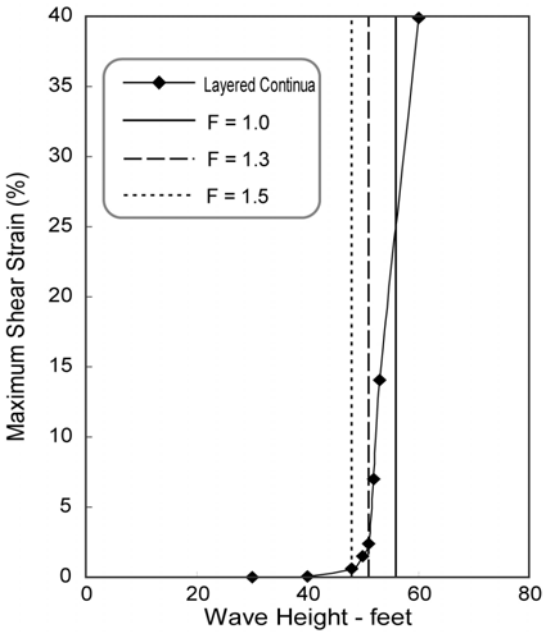

Figure 48. Variation in maximum shear strain with wave height for the "soft" soil shear strength profile (from Nodine et al. 2007)

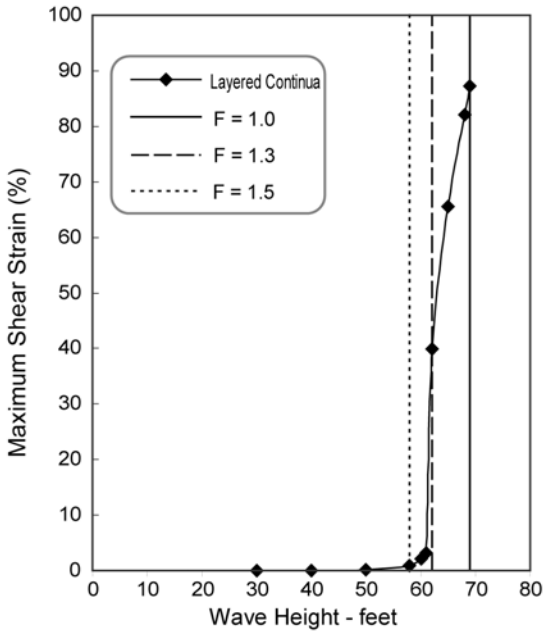

Figure 49. Variation in maximum shear strain with wave height for the "stiff" soil shear strength profile (from Nodine et al. 2007)

Results of the analyses performed using the limit equilibrium model and the more rigorous layered continuum model are very similar, both in terms of predicting the onset of failure and in predicting the geometry of the failure surface. These results help to verify the limit equilibrium model in terms of its ability to accurately model submarine slope behavior.

XI. MUDSLIDE VULNERABILITY ANALYSES

In order to investigate the mudslide vulnerability of the Mississippi Delta region of the Gulf of Mexico and to validate the limit equilibrium model, a series of analyses was performed to compare predicted mudslide vulnerability with actual mudslide occurrences in Hurricanes Ivan and Katrina. First, a regional analysis was performed in order to obtain an overall picture of the mudslide vulnerability throughout the Mississippi Delta region. Next, analyses were performed at the locations where mudslides were reported to find reasonable ranges in factors of safety and determine whether mudslides were expected at these locations. Site specific analyses were then performed at each site for which shear strength data were available to determine whether the limit equilibrium model would correctly predict where mudslides did and did not occur. A final analysis was performed to determine the mudslide vulnerability of the Gulf of Mexico outside the mudslide prone area.

Regional Analysis

In order to form an overall picture of how the mudslide potential predicted by limit equilibrium analyses compares with actual mudslide occurrences, seventy-three locations in a grid pattern across the Mississippi Delta region of the Gulf of Mexico were analyzed (Figure 50). Analyses were performed for the estimated maximum wave heights occurring at each location during a set of historical storms including Ivan and Katrina as well as Andrew, Lili and Rita. The grid points in Figure 50 match up with the hindcast grids used for Ivan and Katrina to account for spatial variations in the sea states.

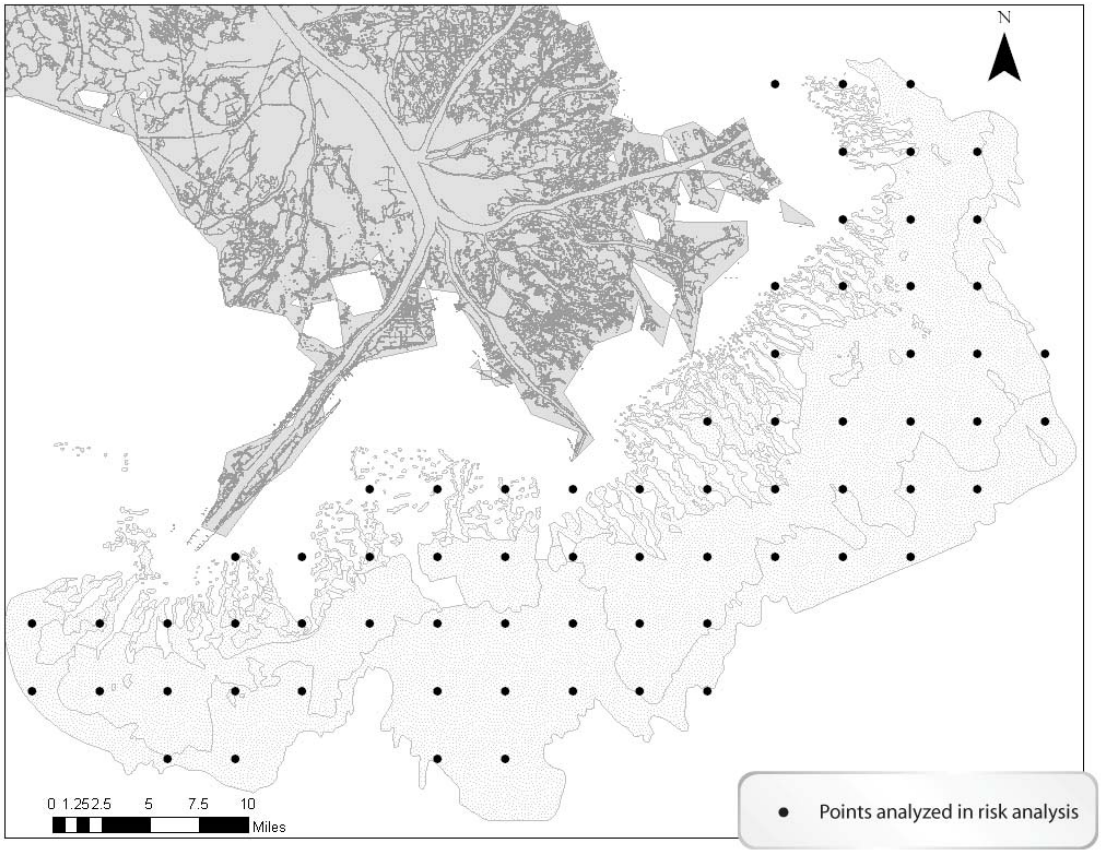

Figure 50: Grid points for regional analysis of mudslide vulnerability

In order to account for spatial variability in the shear strength of the soil across the Delta, a range of possible profiles of undrained shear strength were depth were used. A total of 21 different profiles were compiled from non-proprietary as well as proprietary sources (including the profiles shown on Figures 12 to 15). These borings are spaced across the Delta and are presumed to be representative of the range of soil conditions that exist. As discussed previously in GEOTECHNICAL PROPERTIES OF SUBMARINE CLAYS, the shear strength can vary significantly over relatively short distances (hundreds of feet) and there is clear relationship with the shear strength and mapped geologic features, such as mud lobes. Therefore, these 21 borings are assumed to provide a random sample of strength profiles, meaning that at any given location in the Delta we are equally likely to obtain one of these 21 profiles of undrained shear strength with depth.

The factor of safety was calculated at each grid location for each of the 21 soil shear strength profiles using the limit equilibrium method and the bathymetric and oceanographic data. The percentage of soil shear strength profiles that resulted in a factor of safety less than one was then calculated for each location to provide an indicator of the potential for wave-induced mudslides. For example, if less than 10 percent of the profiles resulted in a factor of safety less than one at a particular location in a particular hurricane, then the site could be regarded as relatively stable. Results for all sites were then contoured to produce the maps that indicate the relative stability over the entire region.

Hurricanes Ivan and Katrina

Contours of the percentage of shear strength profiles which resulted in a failure (factor of safety less than 1.0) during hurricanes Hurricanes Ivan and Katrina are shown in Figures 51 and 52. The four shaded areas depict regions where a mudslide would have been expected to occur during the peak of the hurricane for 0 to 10 percent, 10 to 50 percent, 50 to 90 percent, and 90 to 100 percent of the shear strength profiles. Higher percentages indicate areas of less relative stability, i.e., regions where mudslides would have been

more likely to occur. The locations of mudslides reported after the hurricanes are also shown superimposed on these figures. The area analyzed is bounded by the 50-foot water depth contour due to concerns in extrapolating the hindcast data into shallower water depths where seafloor interactions would become significant. The mudslide prone area delineated by Coleman et al. (1980) is outlined beneath the shaded areas.

In each hurricane, the locations with high predicted potential for mudslides, indicated by a high percentage of soil conditions for which failures are predicted, match well with the reported locations for mudslides (Figures 51 and 52). Also, the potential for mudslides increases as water depth decreases due to greater wave-induced bottom pressures.

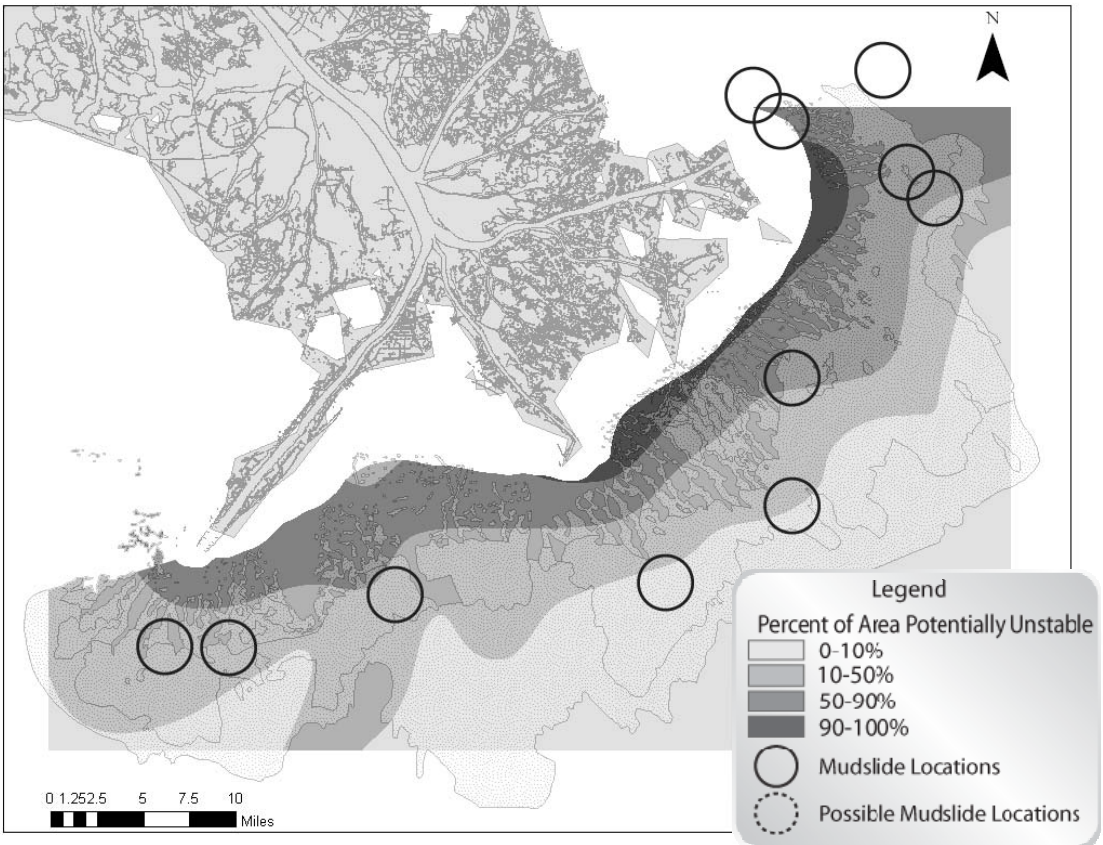

Figure 51. Contours showing the percentage of possible soil strength profiles resulting in a factor of safety less than 1.0 and locations of reported mudslides for Hurricane Ivan

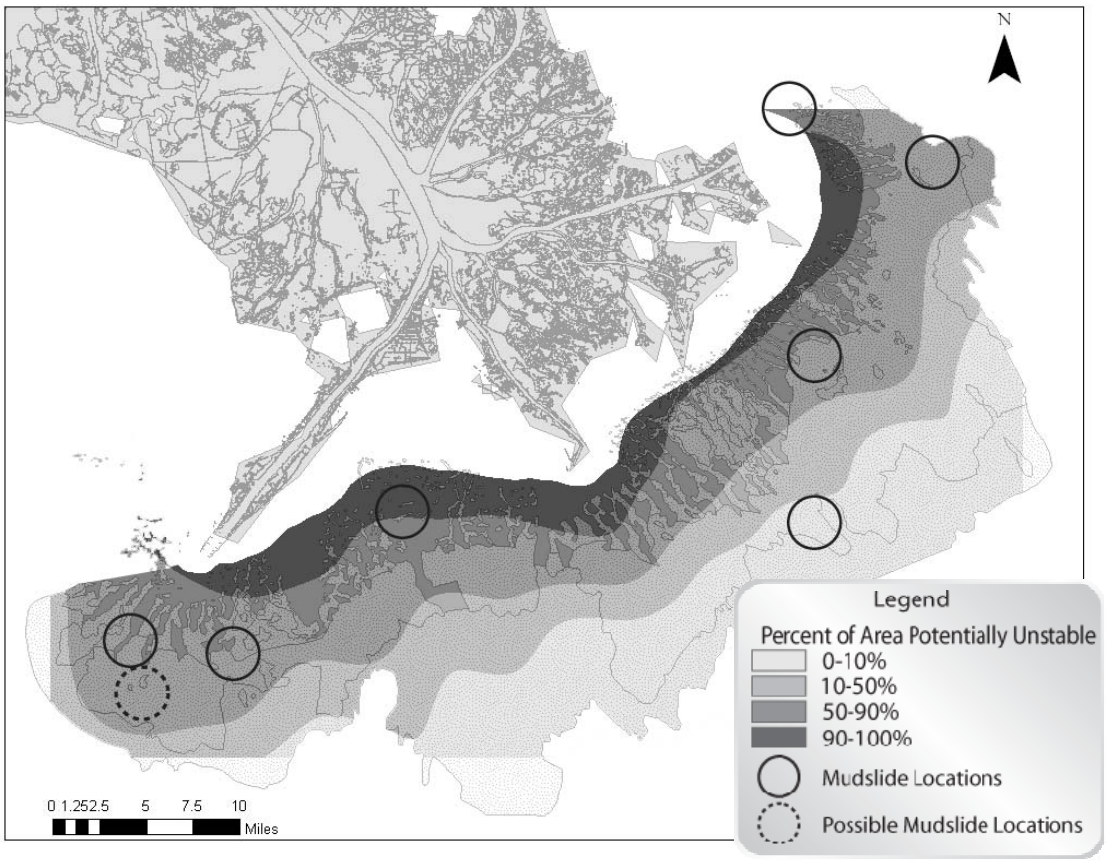

Figure 52. Contours showing the percentage of possible soil strength profiles resulting in a factor of safety less than 1.0 and locations of reported mudslides for Hurricane Katrina

In order to compare Hurricanes Ivan and Katrina, the map in Figure 53 was created showing the difference in the potential for mudslides between the two storms. The contours in Figure 53 were calculated by subtracting the percent of the area that was potentially unstable in Hurricane Katrina from the percent of the area that was potentially unstable in Hurricane Ivan.

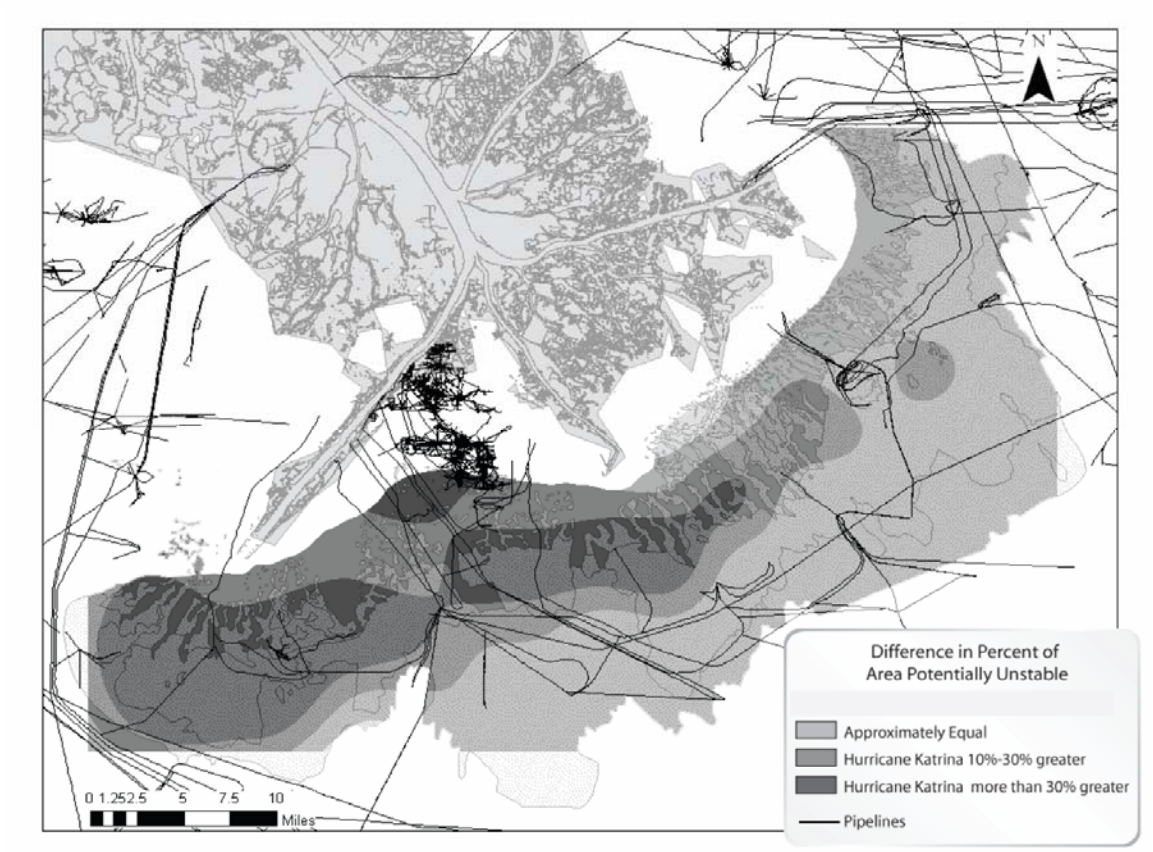

Figure 53. Difference in potentially unstable areas between Hurricanes Ivan and Katrina

Over most of the mudslide prone area, the potential for mudslides in Hurricanes Ivan and Katrina was similar (Figure 53). In the western portion and the shallower portion of the central area, Hurricane Katrina had a greater potential for mudslides than Hurricane Ivan. However, much of the area where Hurricane Katrina had a greater potential for mudslides is also an area where fewer pipelines are located (Figure 53). It is possible that mudslides occurred in these areas but that they did not damage any pipelines, and therefore were not reported.

Hurricane Katrina caused larger wave heights in the Mississippi Delta region than Hurricane Ivan, but much of the mudslide prone area still had similar vulnerability to

mudslides in Hurricane Ivan as in Hurricane Katrina. The main reason for this result is that Hurricane Ivan had very long wave periods.

The effects of Hurricane Ivan's long wave periods can be illustrated using a site at Mississippi Canyon Lease Block 20 as an example. The factor of safety is plotted as a function of maximum wave height and peak spectral period for the water depth (455 feet) and slope angle (3.5%) at the Mississippi Canyon Lease Block 20 site in Figure 54. The factors of safety for the wave conditions at the site for Hurricanes Ivan and Katrina are shown in Figure 54 as solid symbols (71 feet, 16.1 seconds for Hurricane Ivan and 84 feet, 15.2 seconds for Hurricane Katrina). Even though the maximum wave height at the site during Hurricane Katrina was 13 feet higher than the maximum wave height during Hurricane Ivan, the factors of safety calculated at the site are similar for the two storms (0.97 for Hurricane Ivan and 1.00 for Hurricane Katrina) due to the longer wave period in Hurricane Ivan.

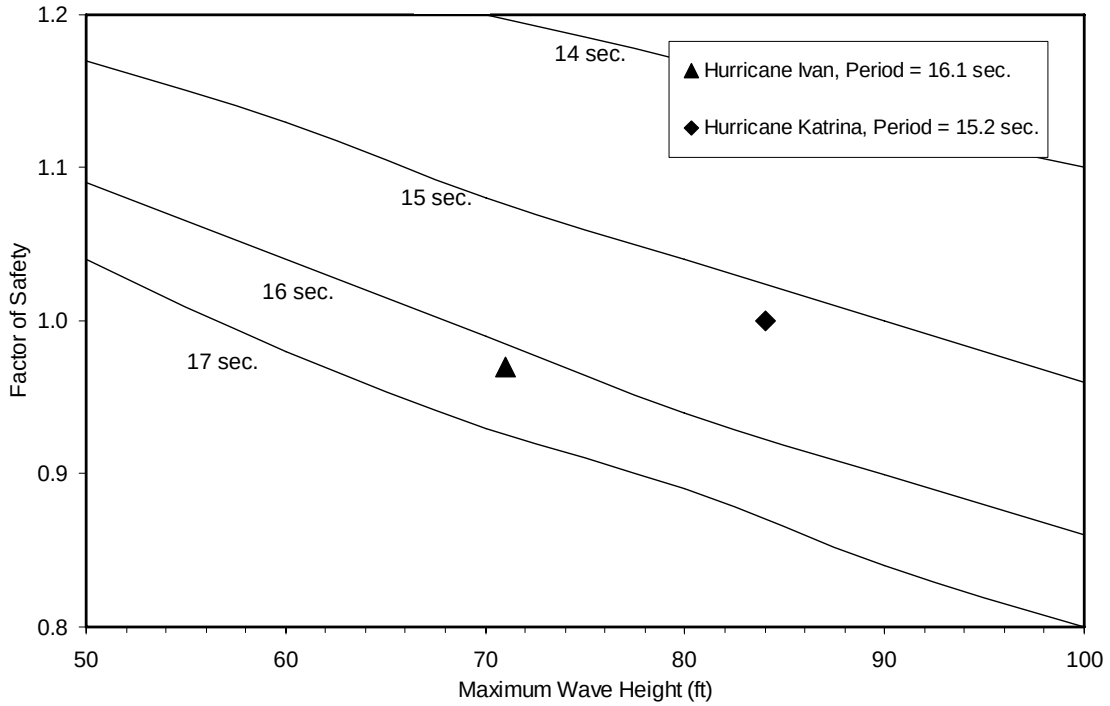

Figure 54. Factor of safety as a function of maximum wave height and peak spectral period for Hurricanes Ivan and Katrina at the Mississippi Canyon Block 20 site

Other Recent Hurricanes

The potential for mudslides was also computed for three other recent hurricanes: Andrew (1995), Lili (2002) and Rita (2005). These hurricanes are included for comparison because they did not cause significant amounts of mudslide activity. Contours for the percentage of shear strength profiles for which a failure would have been expected for Hurricanes Andrew, Lili, and Rita are shown in Figure 55 through Figure 57. The region analyzed for Hurricane Andrew, shown in Figure 55, is smaller than the regions analyzed for the other hurricanes because the available hindcast data for Hurricane Andrew (Cardone et al, 1992) were very sparse in this region.

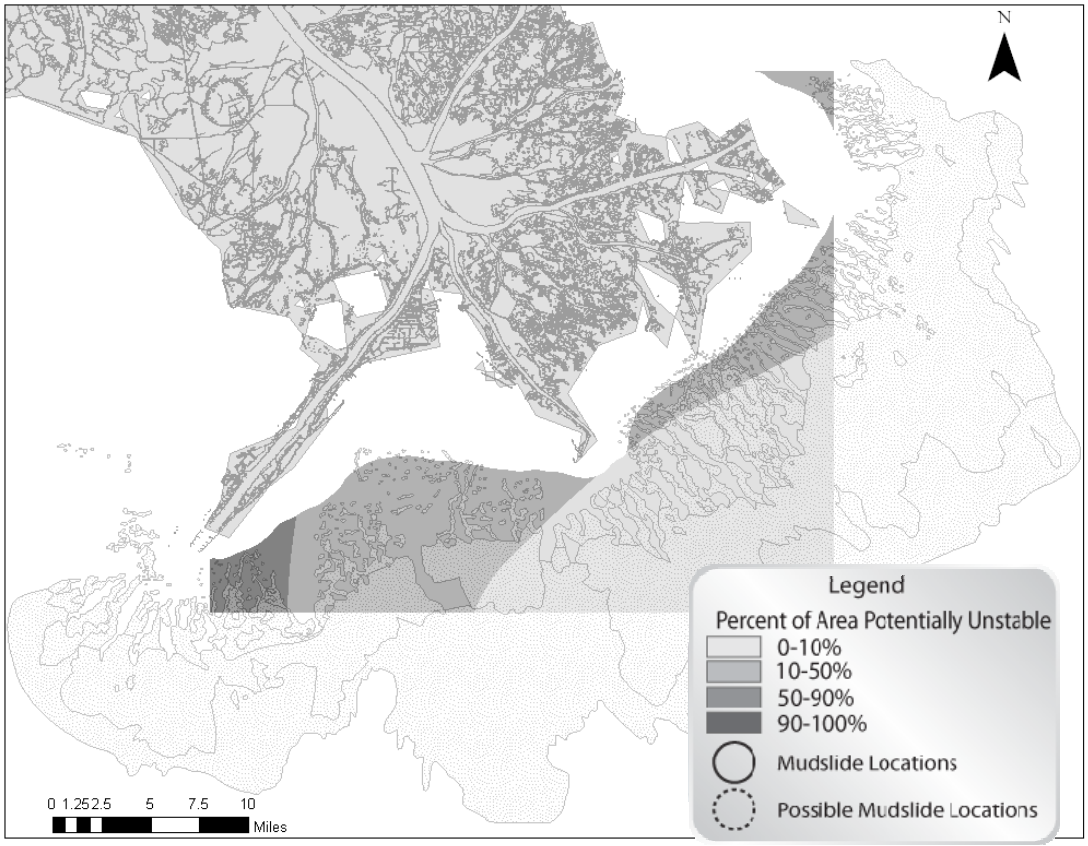

Figure 55. Contours showing the percentage of possible soil strength profiles resulting in a factor of safety less than 1.0 and locations of reported mudslides for Hurricane Andrew

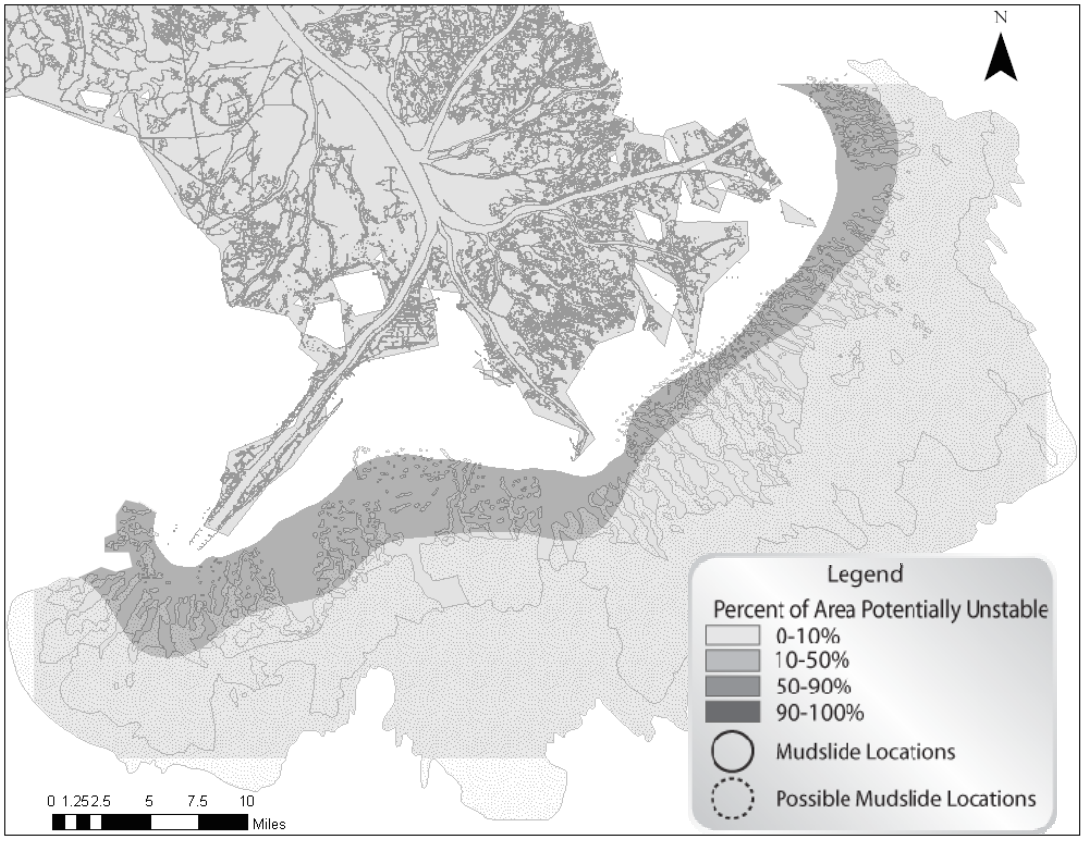

Figure 56. Contours showing the percentage of possible soil strength profiles resulting in a factor of safety less than 1.0 and locations of reported mudslides for Hurricane Lili.

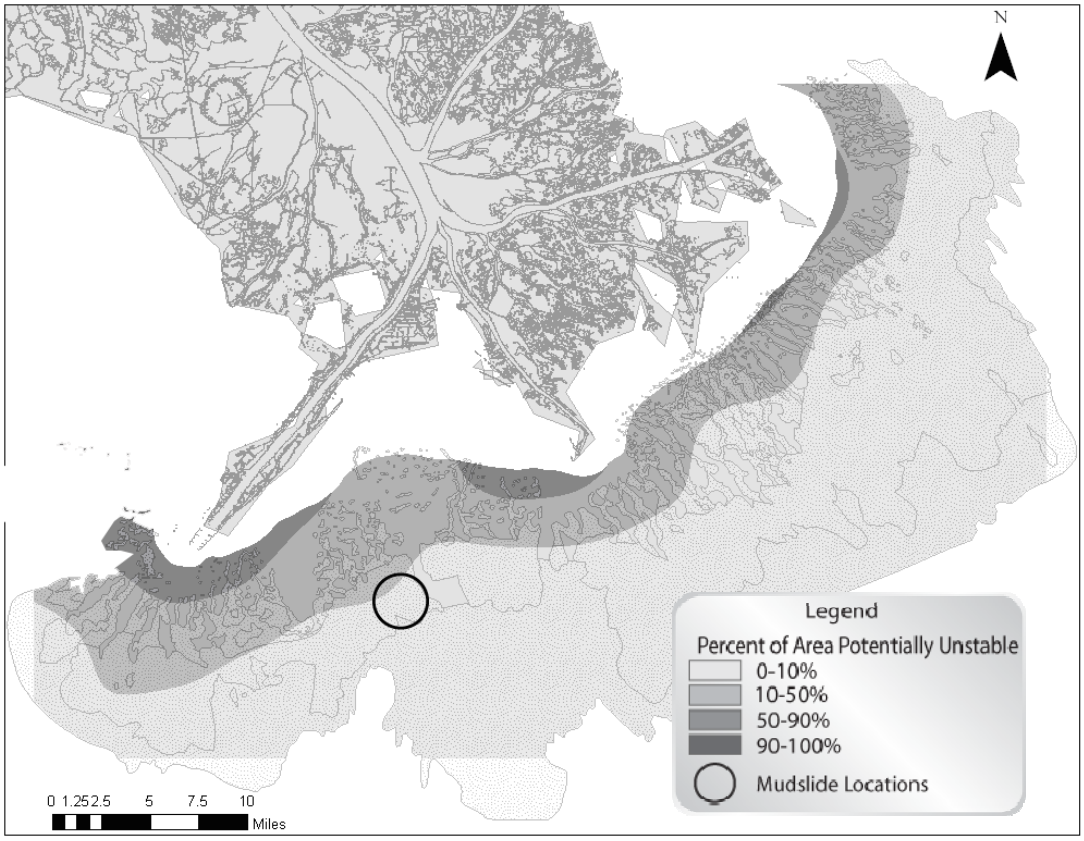

Figure 57. Contours showing the percentage of possible soil strength profiles resulting in a factor of safety less than 1.0 and locations of reported mudslides for Hurricane Rita

During the peaks of Hurricanes Andrew, Lili, and Rita, a mudslide would be expected for less than 10% of the possible soil strength profiles over most of the mudslide prone area (Figures 55 to 57). This amount of predicted mudslide activity is very small compared with that for Hurricanes Ivan and Katrina (Figures 51 and 52). The analysis therefore predicts that Hurricanes Ivan and Katrina would cause significantly more mudslide activity than the other three hurricanes, which is consistent with the experience.

Implications of the Regional Analyses

The regional analyses described above illustrate some important aspects of mudslide vulnerability in the Mississippi Delta region of the Gulf of Mexico. For all five of the

hurricanes analyzed, the areas with the highest mudslide vulnerability are the areas close to shore, in shallow water (Figures 51, 52 and 55 through 57). However, it can be seen in Figure 53 that much of the area in shallow water (less than about 100 feet) has very few pipelines. This shallow portion of the mudslide prone area generally corresponds with the area of collapse depressions and mudflow gullies delineated by Coleman et al. (1980). The mudslide prone area shown in Map 5 by Coleman et al. (1980, see Figure 7) is outlined beneath the shaded areas in Figures 51, 52 and 55 through 57, and collapse depressions are shown by individual, irregularly shaped zones of the mudslide prone area in shallow water. Collapse depressions are localized features on the order of hundreds of feet in areal extent and bear a strong resemblance to the mudslide features predicted using the irregular wave prediction program (Zhang, 1999) shown in Figure 40 and Figure 41. It is possible that the collapse depressions mapped by Coleman et al. (1980) represent individual slope failures caused by waves both during hurricanes and in smaller storms such as winter storms, since hurricane-sized waves are not required to cause mudslides in very shallow water.

The regional analysis results indicate that shallow water areas are more vulnerable to mudslides and pipeline damage. This conclusion is confirmed by the pipeline damage in the northeastern area of the mudslide prone area where there is a large number of pipelines in shallow water. Pipeline damage was reported in this area after both Hurricanes Ivan and Katrina, and one pipeline in this area has experienced mudslide damage four times in the past decade (Coyne and Wryzszczynski, 2006). Remembering that pipeline damage is being used as a primary indicator for mudslides in this study, the lack of reported mudslides in other shallow water areas within the mudslide prone zone may be due to the lack of pipelines routed through theses areas. Mudslides could have occurred in these areas as well, but pipeline routing to avoid these areas has been able to avoid this hazard.

Analyses at Locations of Mudslides

The potential for mudslides was also analyzed specifically at locations where mudslides were reported to assess if the factors of safety estimated for these locations indicated that mudslides were expected at these sites. The locations of mudslides caused by Hurricanes Ivan and Katrina are superimposed on maps of the mudslide prone area in Figures 8 and 9. Since there were not soil borings near each of these sites, the 21 shear strength profiles throughout the mudslide prone area were again used to characterize the impact of the possible variability in soil strengths. Factors of safety were calculated for all 21 soil shear strength profiles at each mudslide location, and the average and standard deviation for the factor of safety against mudslide initiation were determined at each location.

The factors of safety for sites at which mudslides were reported are plotted in Figure 58 and Figure 59 for Hurricanes Ivan and Katrina, respectively. Average values are represented by points, and the heavy vertical bars represent +/- one standard deviation above and below the average. The lighter bars above and below each point represent the full range in factors of safety calculated for each site. A factor of safety of 1.0 indicates the threshold below which a mudslide would be expected at a site. The mudslide sites plotted in Figure 58 and 59 are arranged from west to east across the mudslide prone area, and sites are identified by the abbreviation for their lease block (WD = West Delta, SP = South Pass, MC = Mississippi Canyon, and MP = Main Pass). Note that the mudslide reported in Mississippi Canyon Block 20 after Hurricane Ivan was not at the same location as the mudslide reported in that block after Hurricane Katrina; these locations are about 2 miles apart, and the mudslide reported after Hurricane Ivan was in 455 feet of water, while the mudslide reported after Hurricane Katrina was downslope in about 515 feet of water. The factors of safety calculated at the two sites are different because of these differences in their locations.

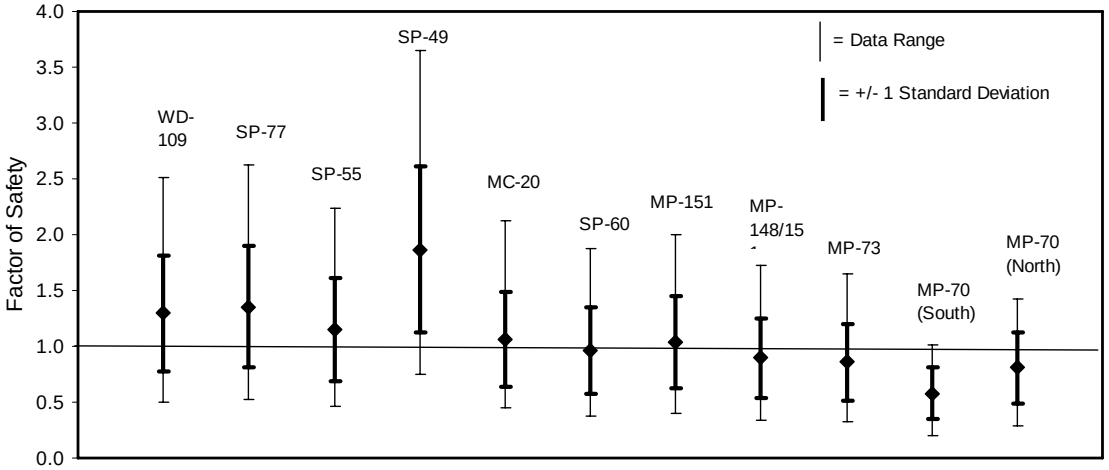

Figure 58. Average factors of safety with error bars showing plus and minus one standard deviation and the full range in factors of safety for sites where mudslides were reported during Hurricane Ivan

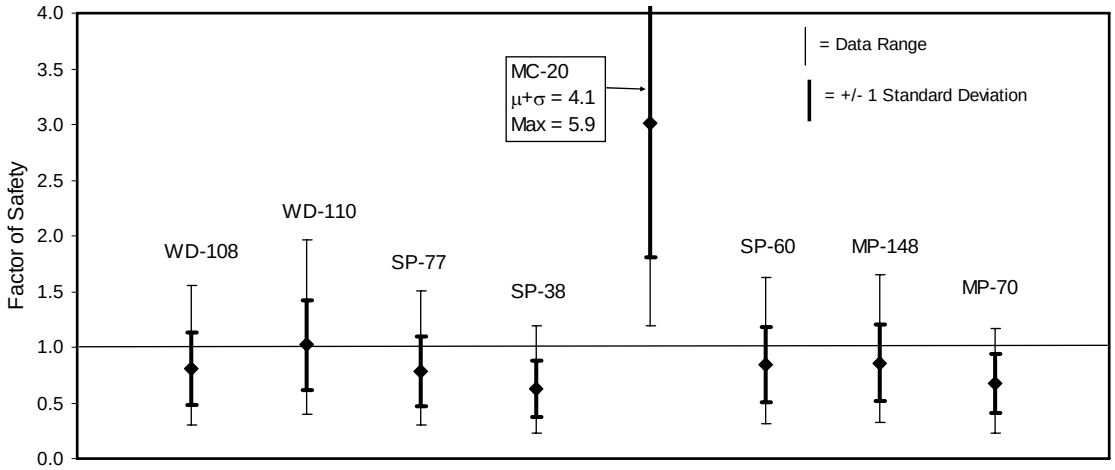

Figure 59. Average factors of safety with error bars showing plus and minus one standard deviation and the full range in factors of safety for sites where mudslides were reported during Hurricane Katrina

The ranges in factors of safety at the locations of mudslides shown in Figure 58 and Figure 59 are generally consistent with observed failures. In most cases, the average factor of safety is less than or equal to 1.0, and in nearly all cases the error bars showing plus- and minus-one standard deviation extend below 1.0. For Hurricane Ivan

(Figure 58), there is only one site (South Pass Lease Block 49) for which a factor of safety of 1.0 is not within one standard deviation of the average factor of safety; however, the minimum factor of safety calculated for this site is still below 1.0, so it is feasible that a mudslide could be expected within the range of known soil profiles.

The calculated factors of safety all average less than 1.0 for Hurricane Katrina, with the notable exception of the Mississippi Canyon 20 site (Figure 59). The minimum factor of safety at this site calculated from any of the 21 soil shear strength profiles was 1.2. Several factors could be responsible for this result. The damage to the pipeline was reported as having been caused by a mudslide, but perhaps the pipeline damage was due to some other event, and there was no mudslide due to strong soil at the site. Also, the slope angle of the bottom at this location is not known precisely. An estimate of 0.4 percent was used for the slope angle in this analysis based on regional bathymetry; however the slope angles in the vicinity are relatively variable, ranging from 0.3 to almost 2 percent (Figure 60). At the location shown on Figure 60 with a slope of 1.9 percent, the factor of safety is less than 1.0 for several of the possible shear strength profiles. Finally, the site-specific wave conditions and shear strength for the soil are being estimated based on regional information; small variations in either of these could readily explain the outlier in Figure 59.

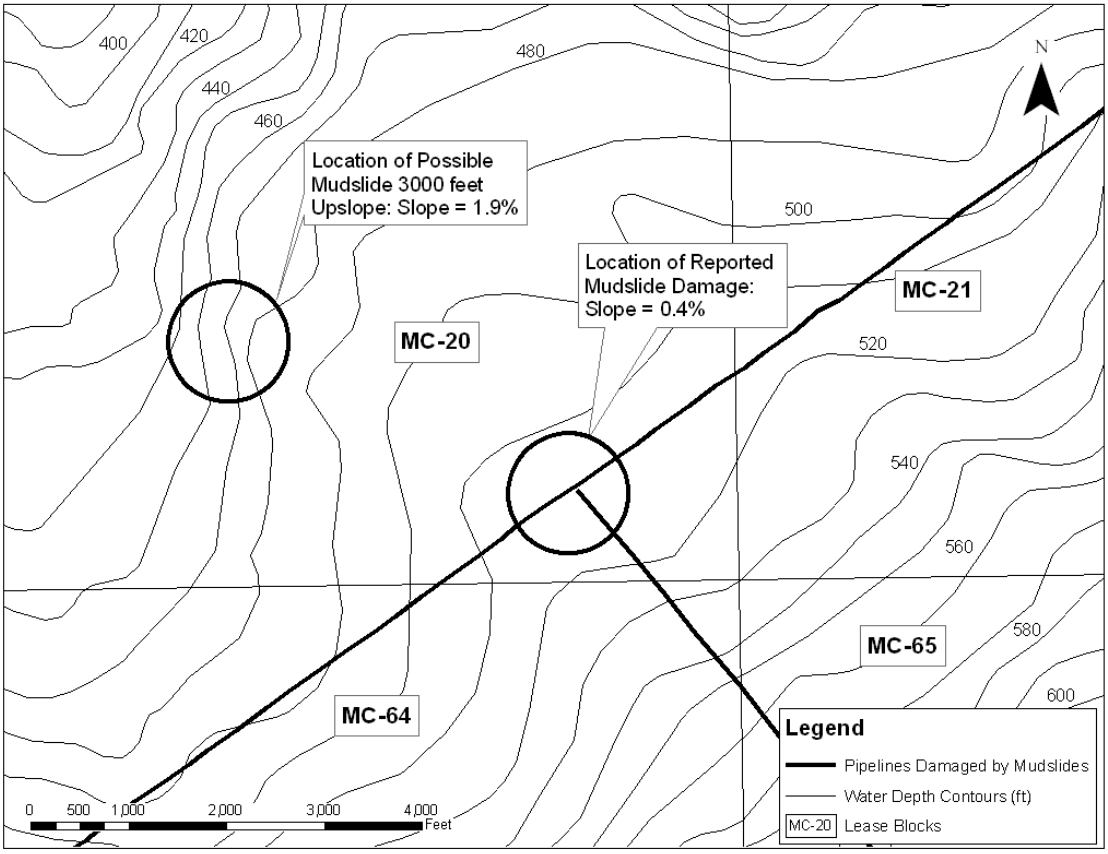

Figure 60. Detailed view of the site in Mississippi Canyon Lease Block 20 where a mudslide was reported after Hurricane Katrina

Site Specific Analyses

Lastly, factors of safety were calculated at each location where shear strength data were available within about 4,000 feet of a pipeline. The wave hindcast for Hurricanes Ivan and Katrina and water depth information presented previously were used. The calculated factors of safety are shown in Figure 61 and Figure 2 for Hurricanes Ivan and Katrina, respectively. In some locations, a range of safety factors is shown because two or three shear strength profiles were available nearby to that location. The symbols used in

Figure 61 and Figure 62 indicate where mudslides reportedly occurred and did not occur at locations for which factors of safety were calculated, based on the sources of mudslide damage described previously.

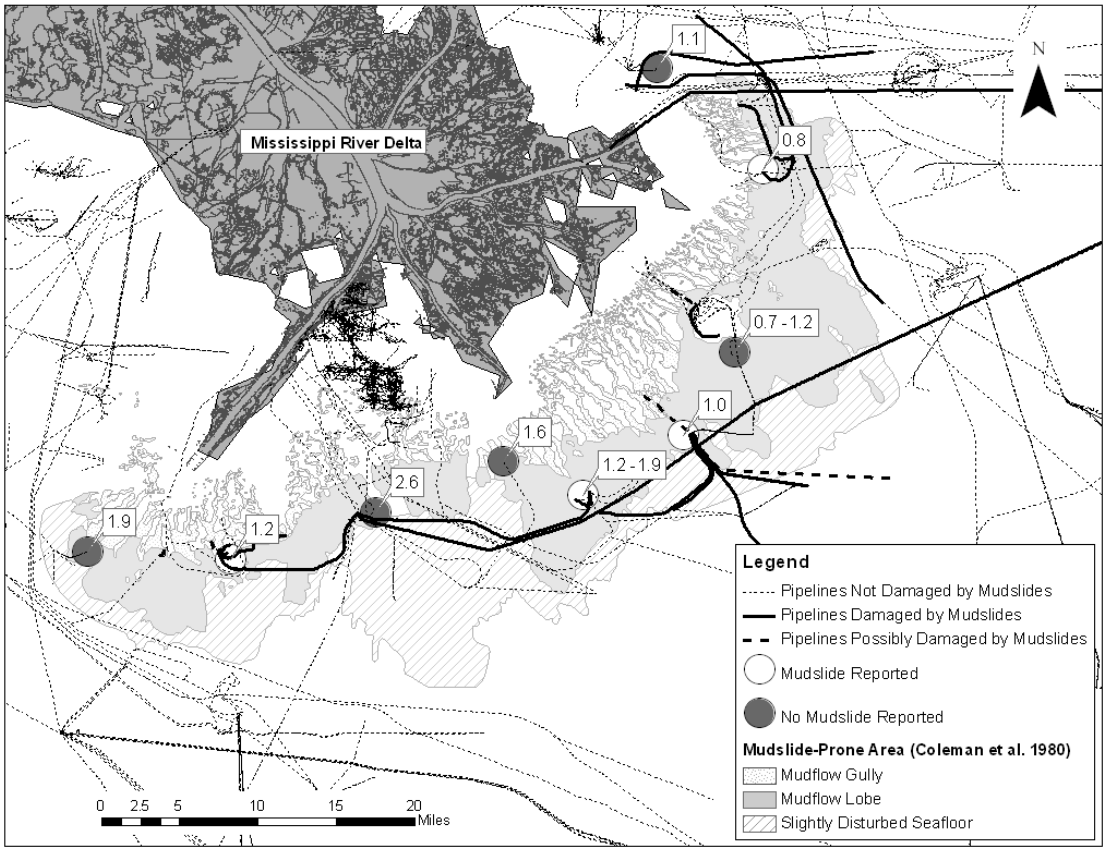

Figure 61. Site-specific analyses for Hurricane Ivan

Figure 61 shows that at the locations where no mudslides were reported after Hurricane Ivan, the factor of safety was either greater than 1.0 or the range of factors of safety extended above 1.0. These results are consistent with the lack of reported mudslides at these locations. However, at the two locations where mudslides were reported, the factor of safety is greater than 1.0.

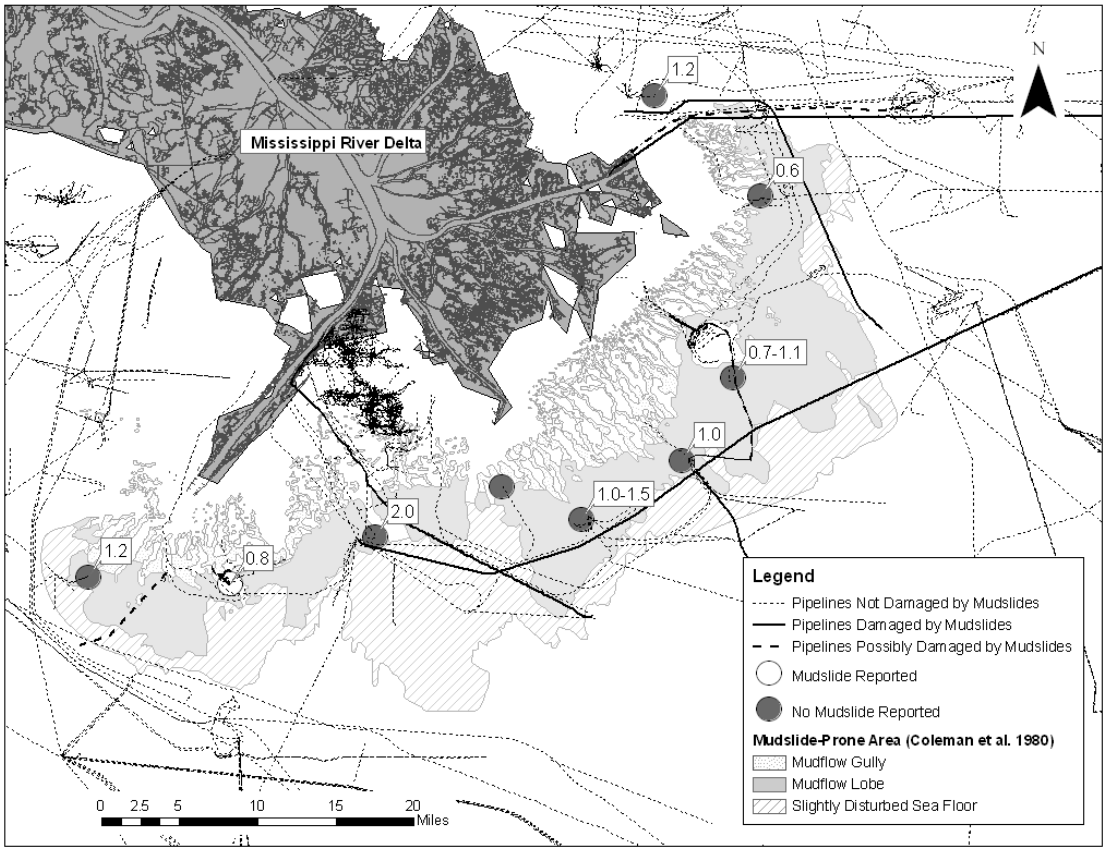

Figure 62. Site-specific analyses for Hurricane Katrina

Figure 62 shows that there is only one location where a mudslide was reported due to Hurricane Katrina and shear strength data were available nearby. The factor of safety there is 0.8, which is consistent with a mudslide occurring at this site. However, at one location where no mudslide was reported to date, the calculated factor of safety was 0.6 indicating that a mudslide would be expected.

Figure 63 summarizes the overall results for the site specific analyses. Most of the calculated factors of safety were less than 1.0 where mudslides were reported (3 out of 5 cases) and greater than 1.0 where mudslides were not reported 10 out of 14 cases). Therefore, Figure 63 demonstrates that the model for predicting the occurrence of mudslides is consistent with the available observations. When the factor of safety is near

1.0, there is a good chance that mudslides will be reported. When the factor of safety is much greater than 1.0, the chance for a mudslide to be reported is small. These results also imply that the occurrence of a mudslide may not necessarily cause damage to a pipeline that will be reported.

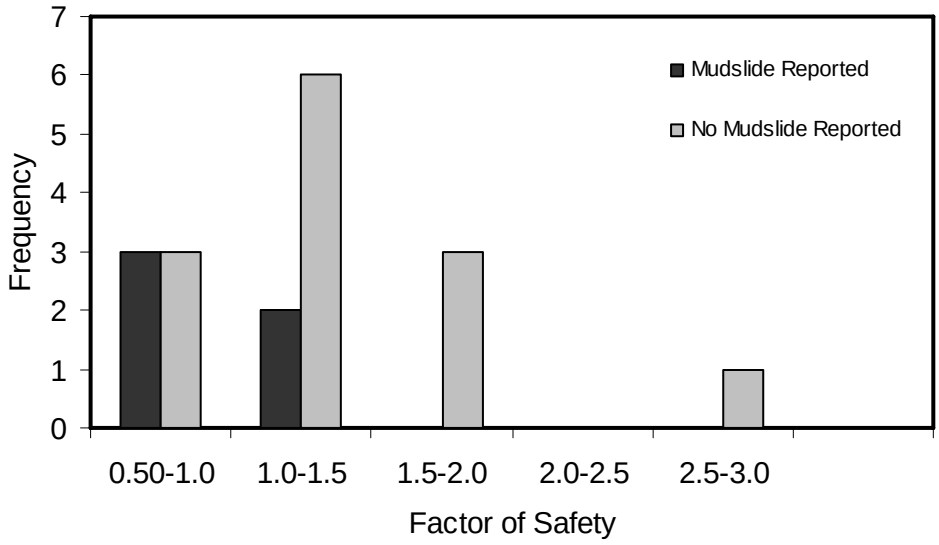

Figure 63. Frequencies of factors of safety calculated in site-specific analyses for Hurricanes Ivan and Katrina for locations where mudslides were and were not reported

There are several limitations in the site-specific analyses that should be considered in interpreting the results:

1. Mudslide locations occurrences and locations are not known precisely. It is possible that a mudslide occurred at a site, without damaging the pipeline and therefore was not reported. A mudslide that occurs at or very near to the location of a pipeline will not necessarily damage the pipeline. Pipelines can span over failed zones of soil, and pipelines can tolerate movements and being buried in a slide without rupturing. Nodine et al, (2007), Thompson et al. (2005), and Coyne and Wryzszczynski (2006) reported mudslides that occurred along pipelines without causing damage to the pipelines. It is possible that many similar incidents occurred in the mudslide prone area that went unnoticed. Also, a pipeline could be damaged by another cause that is incorrectly attributed to a mudslide.

2. Soil properties vary spatially. The undrained shear strengths for the soils in the Delta region are extremely variable and can differ significantly in borings located only a few hundred feet apart (see Figure 12 through Figure 15). Thus the shear strength at a nearby site may not be representative of the soils near the reported location of a mudslide.
3. The waves vary spatially in a sea state and the maximum wave conditions at a particular location are not known with certainty.

Beyond the Mississippi Delta

In order to determine whether mudslides might be expected to occur outside the mudslide prone area in the Mississippi Delta region of the Gulf of Mexico, an analysis was performed assuming soil shear strengths typical of other areas in the Gulf of Mexico. Outside the range of very soft, underconsolidated clays in the mudslide prone area, the undrained shear strength of the soil in the Gulf of Mexico is expected to increase with depth at a rate of at least 8 psf per foot (e.g., Quiros et al. 1983). Factors of safety were calculated for locations in the region extending from the mudslide prone area to the approximate latitude of the eyes of Hurricanes Ivan and Katrina when they passed near the mudslide prone area, using the hindcast wave data for each storm and an undrained shear strength profile with a nominal value of 50 psf at the mudline and an increase of 8 psf per foot. Contours of these factors of safety are shown in Figure 64 and Figure 65. There is no location where the factor of safety is less than 1.0. This observation is consistent with the observations from Hurricanes Ivan and Katrina in that all of the reported mudslides are in the mudslide prone area, where soil shear strengths are lower than 8 psf per foot.

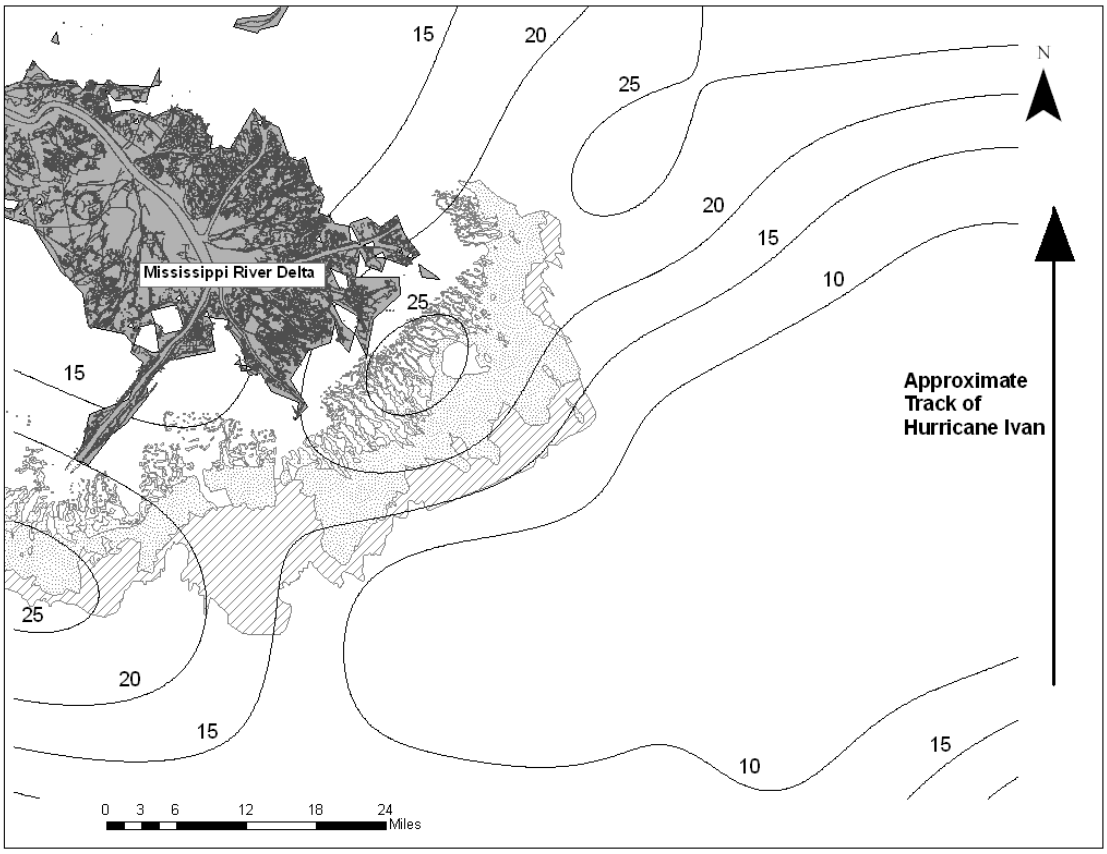

Figure 64. Contours of factors of safety calculated using the wave heights and periods from the Hurricane Ivan hindcast, assuming an undrained shear strength of 50 psf at the surface and increasing linearly with depth at the rate of 8 psf/ft

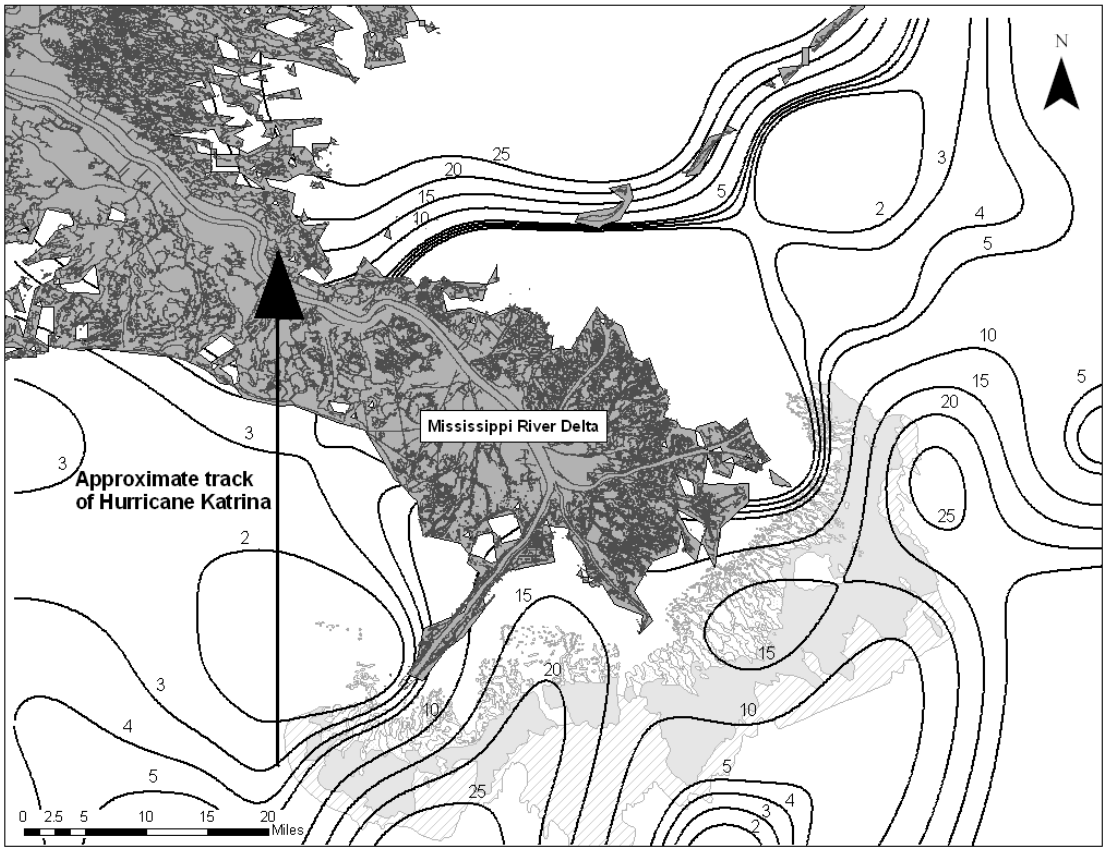

Figure 65. Contours of factors of safety calculated using the wave heights and periods from the Hurricane Katrina hindcast, assuming undrained shear strength of 50 psf at the surface and increasing linearly with depth at the rate of 8 psf/ft

Summary

The analyses described in this section indicate that the limit equilibrium model works well to predict the occurrence and non-occurrence of mudslides, particularly on a regional scale and when considering the uncertainty in soil shear strength. The results of the analyses also underscore conclusions about mudslide characteristics presented previously based on the theoretical model. The potential for mudslides increases as the water depths decreases, as the period of the ocean waves increases, and as the angle of the bottom slope increases.

XII. RISK ANALYSIS

Overview

The objective of this section is to produce maps that show the risk associated with mudslides in the Mississippi Delta. The risk includes both the probability that a mudslide occurs as well as the associated consequence if it impacts a facility, such as a pipeline or platform. In this analysis, we address both the probabilities that mudslides will occur and the probabilities that mudslides will impact platforms or pipelines. However, we do not explicitly consider the consequence associated with a mudslide impacting a facility.

The risk for mudslides is assessed by dividing the problem into a hazard, defined as wave-induced pressures acting on the sea floor, and a vulnerability, defined as the susceptibility of the sea floor to move under the applied bottom pressures. These components are then integrated to assess the annual probability that a mudslide will occur at a point, that at least one mudslide will occur within an area approximately the size of a lease block, and that a mudslide will impact an existing facility in the Delta. The intent is as much to develop a methodology for assessing the risk as it is to assess the risk. The results produced in this section correspond to a regional perspective and do not apply to a specific location where a detailed metocean analysis or geotechnical analysis has been conducted. However, the methodology is designed so that project-specific or site-specific information could readily be incorporated as input to the analysis.

Hazard Model for Wave-Induced Bottom Pressures

The hazard for wave-induced mudslides is defined by the magnitude and shape of pressures acting on the ocean floor. In a simplified, two-dimensional analysis, this hazard can be represented by the amplitude and length of the pressure wave, p_{max} and L/2, respectively, on Figure 66. The amplitude and length of the pressure wave are related to

the ocean waves as follows. The maximum pressure is approximated from the height and length of the ocean wave, H and L, the depth of the water, d, using linear wave theory with a correction factor to account for the three-dimensional shape of the wave, I_{3D} (the pressure ratio on Figs. 28 to 32):

$$p_{\max} = \frac{\gamma_w}{2}\left(\frac{H_{\max}}{\cosh\left(\frac{2\pi}{L_{H_{\max}}}d\right)}\right)I_{3D} \tag{17}$$

The maximum bottom pressure is assumed to occur below the largest wave, H_{max}, and its associated length, L_{Hmax}, occurring during a sea state. While it is possible that the maximum pressure could occur under a smaller wave with a longer wave length, the difference in p_{max} is expected to be negligible. The wave length associated with the largest wave is found by assuming that the period for the largest wave is approximated by 90 percent of the peak spectral period, T_p, for that sea state (Haring et al, 1976):

$$L_{H_{\max}} = \frac{g\left(0.9\times T_p\right)^2}{2\pi}\tanh\left(\frac{2\pi d}{L_{H_{\max}}}\right) \tag{18}$$

Note that Equation (18) provides an implicit expression for L_{Hmax}, meaning that it requires a numerical approach (trial and error) to find L_{Hmax} as a function of T_p.

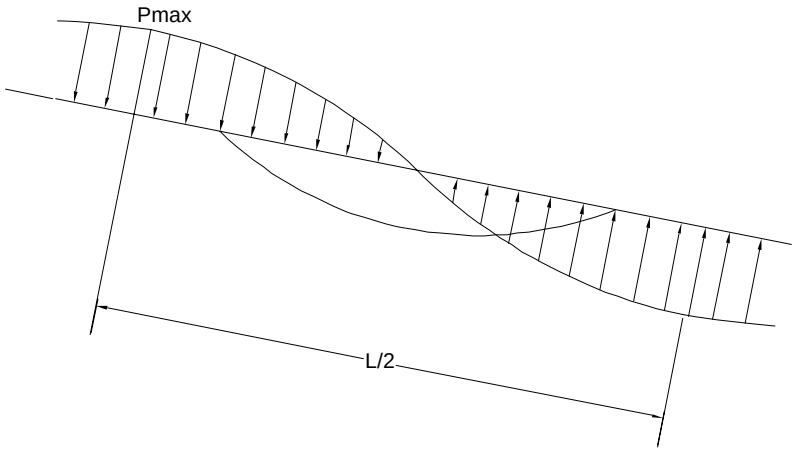

Figure 66. Representation of mud-slide hazard

Maximum Waves in Sea State

The maximum wave is estimated from the Forristall probability distribution (Forristall 1978), which describes the distribution of wave heights occurring during a sea state in the Gulf of Mexico that is characterized by a significant wave height. Since the upper tail of the Forristall distribution has an exponential shape, the probability distribution for the maximum wave height in a sea state is reasonably approximated using the Type I Extreme Value or Gumbel distribution:

$$F_{H_{\max}}\left(h_{\max}\right) = e^{-e^{-\alpha\left(h_{\max}-u\right)}} \tag{19}$$

where $F_{H_{\max}}\left(h_{\max}\right)$ is the cumulative distribution function for the maximum wave height, i.e., $P\left(H_{\max} \le h_{\max}\right) = F_{H_{\max}}\left(h_{\max}\right)$. The parameters α and u can be related to the mean

maximum wave height for the sea state, $\bar{H}_{\max}$, as follows by assuming that a 3-hour sea state contains approximately 1,000 waves:

$$\alpha = \frac{\pi}{\sqrt{6}}\left(\frac{1}{0.07\bar{H}_{\max}}\right) \tag{20}$$

$$u = \bar{H}_{\max} - \frac{0.577}{\alpha} \tag{21}$$

Note also that the mean maximum wave height for a sea state is approximately 1.75 times the significant wave height for a 3-hour sea state with 1,000 waves. An example of the probability distribution for the maximum wave occurring during a 3-hour sea state is shown on Figure 67.

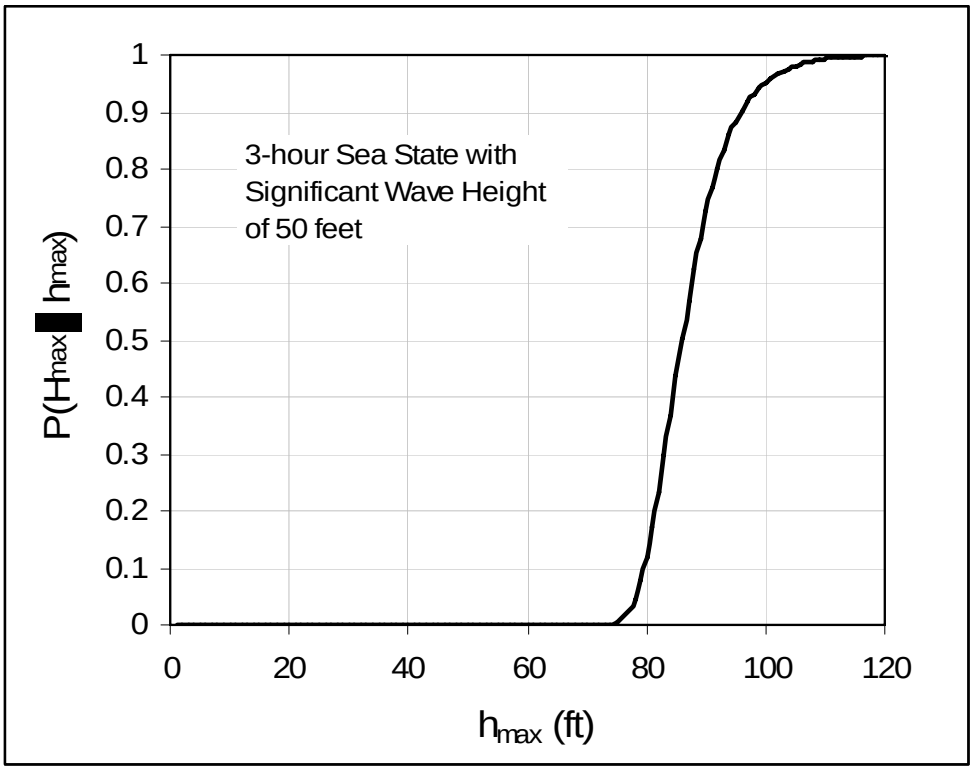

Figure 67. Probability distribution for maximum wave height in sea state

Sea States

To represent the possible sea states that may occur in the future in the mudslide prone area of the Mississippi Delta, API Bulletin 2INT-MET Interim Guidance on Hurricane Conditions in the Gulf of Mexico (API 2007) was used. This guidance provides a probabilistic description of possible 3-hour long sea states in terms of the mean maximum wave height and the peak spectral period as a function of water depth. An example of this information for three different water depths in the Central Gulf of Mexico, where the Mississippi Delta is located, is shown on Figure 68.

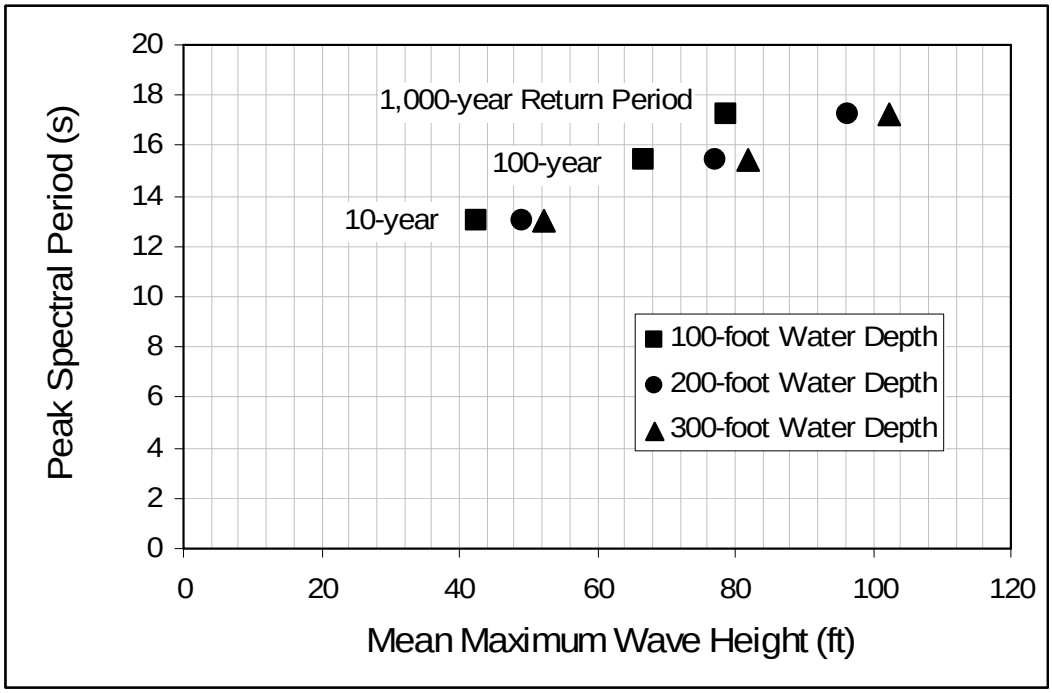

Figure 68. Probabilistic representation of sea states (API, 2007)

In order to simplify the probabilistic representation of wave heights and periods as a function of water depth, an approximate analytical expression was fit to the relationship between wave length (calculated from Equation 18 with the peak spectral period and the water depth) and mean maximum wave height for a range of return periods and water

depths. The data points on Figure 69 represent all of the possible combinations listed in API (2007) for mean maximum wave height and wave length for return periods ranging from 10 to 10,000 years and water depths ranging from 30 feet to 1,000 feet. The relationship between wave length and maximum wave height is fit reasonably well by a line (Fig. 69):

$$L_{H_{\max}} = \left(9.72\ ft/\ ft\right)\bar{H}_{\max} + 116\ ft \qquad (22)$$

where $\bar{H}_{\max}$ is the mean maximum wave height for a given sea state in feet and $L_{H_{\max}}$ is the associated wave length.

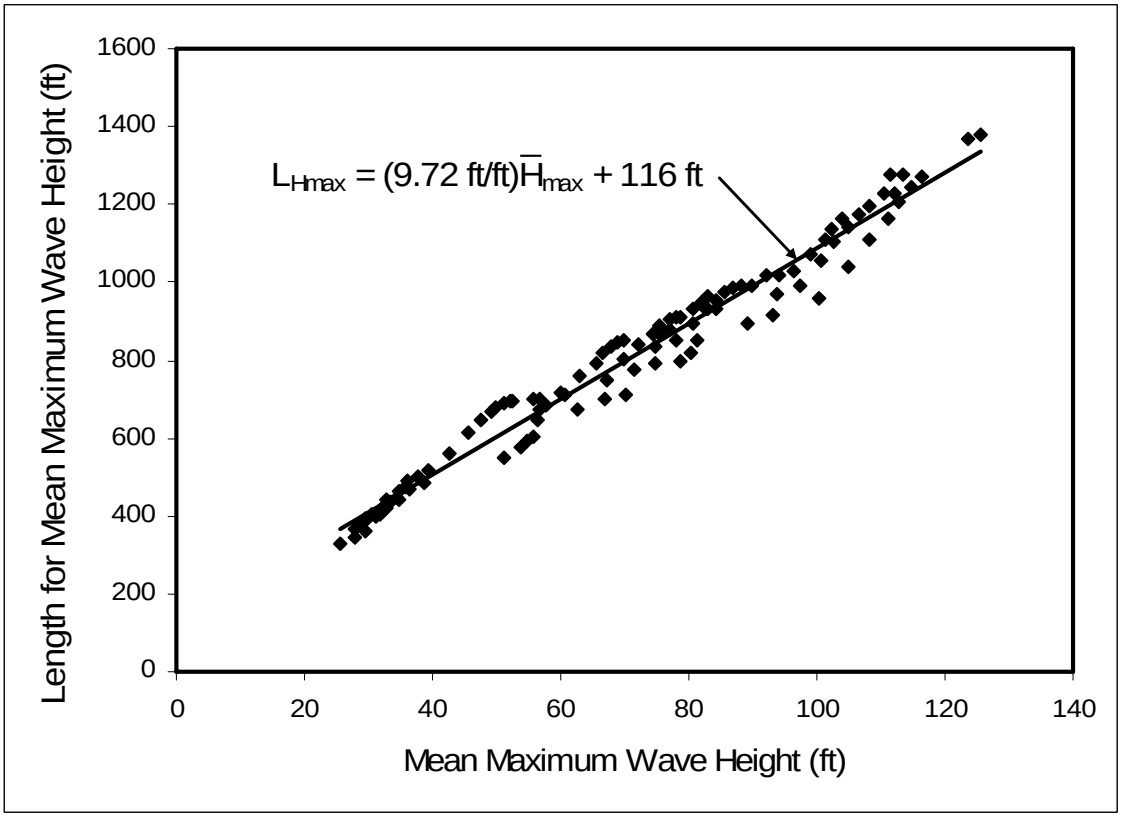

Figure 69. Approximated relationship between wave length and mean maximum wave height for all water depths

The variability in peak spectral period can be expressed as variability in the wave length for the maximum wave using Equation (18). Based on this approach, the following relationships between wave length and period were developed from historical hindcast data to characterize this variability:

$$\left(L_{H_{\max}}\right)_{\text{average - 1 standard deviation}} = \left(8.77\ ft/\ ft\right)\bar{H}_{\max} + 122\ ft \tag{23}$$

$$\left(L_{H_{\max}}\right)_{average} = \left(9.72\ ft/\ ft\right)\bar{H}_{\max} + 116\ ft \tag{24}$$

$$\left(L_{H_{\max}}\right)_{\text{average + 1 standard deviation}} = \left(10.7\ ft/\ ft\right)\bar{H}_{\max} + 111\ ft \tag{25}$$

Furthermore, a simplified representation of the probability of each relationship is that the average (Equation 24) has a probability of 0.5 and that the average plus and the average minus one standard deviation (Equations 23 and 25, respectively) each have a probability of 0.25. This approach approximately captures a normal or lognormal distribution of wave lengths for a given mean maximum wave height in a sea state.

The advantage to analytically relating wave length and wave height is that the probabilistic representation of possible sea states can be expressed directly as a probabilistic representation of the mean maximum wave height alone. To illustrate, the complement of the cumulative probability distribution for the mean maximum annual wave height to occur is shown on Figure 70 for different water depths; this information was obtained directly from API (2007) by calculating the annual probability that the

expected maximum wave height would be greater than a particular value from the inverse of the return period:

$$P\left(\bar{H}_{\max} > \bar{h}\right) = \frac{1}{\text{Return Period}} \tag{20}$$

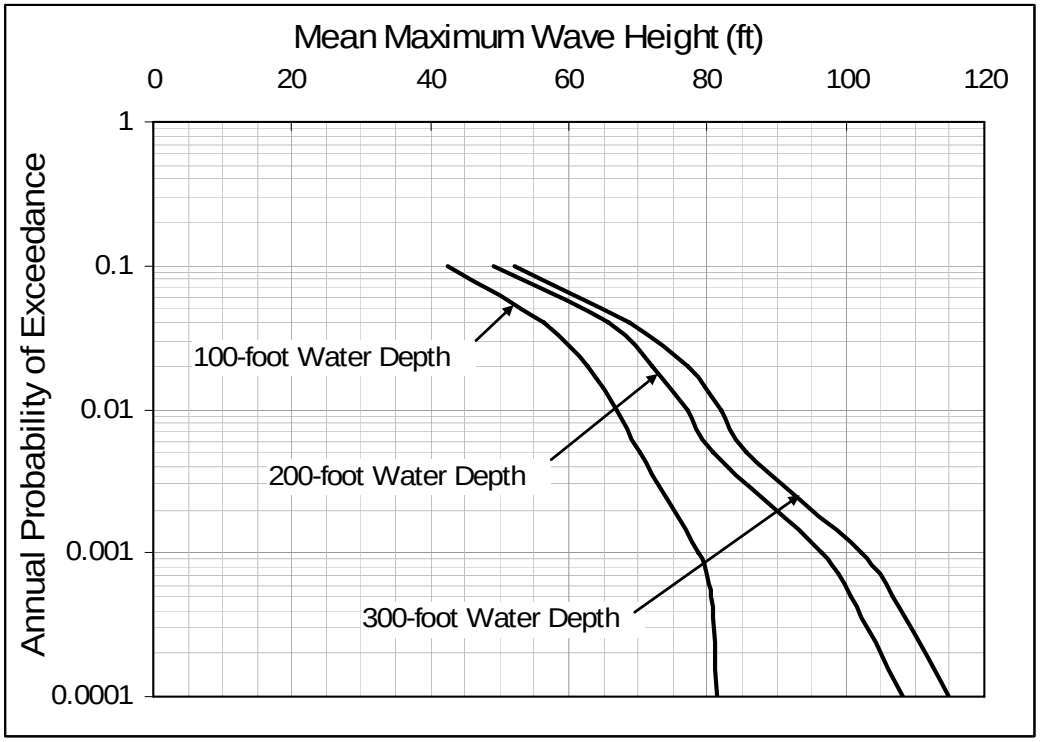

Figure 70. Annual probability distribution for mean maximum wave height (API 2007)

This information is then approximated by a discrete distribution of possible wave heights, as shown on Figure 71.

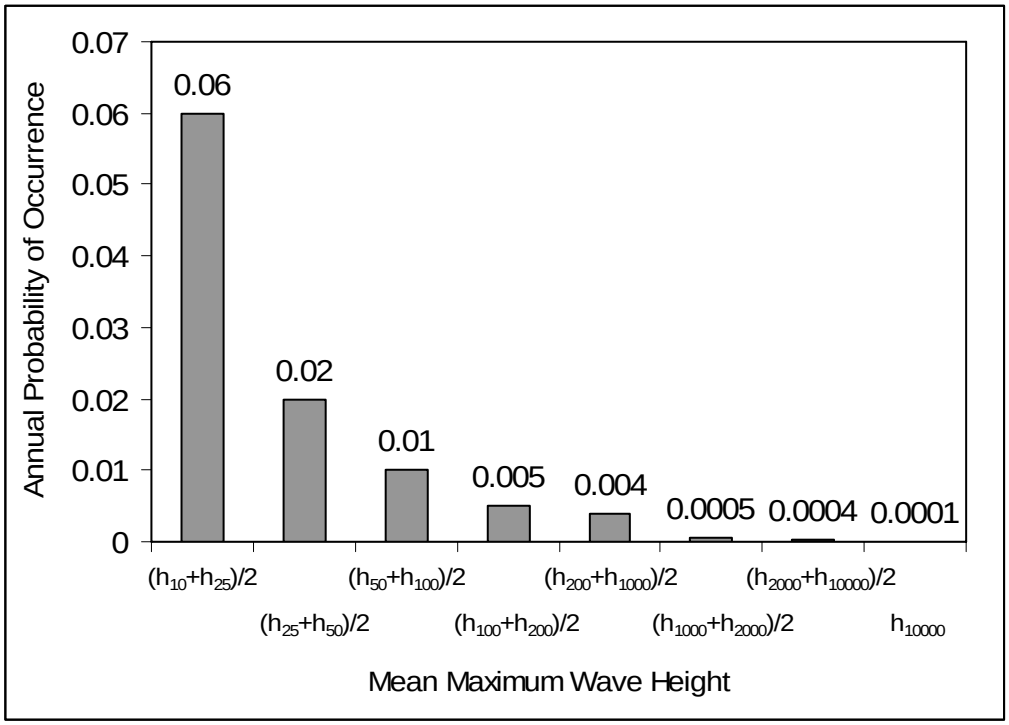

Figure 71. Approximate discrete probability distribution for mean maximum wave height for a given water depth (Note: h_t is the value for mean maximum wave height at that water depth corresponding to a return period t in Figure 70)

The final characteristic of the waves that affects the bottom pressure is the correction factor or pressure ratio in Equation (17), I_{3D}, which accounts for the reduction in the maximum bottom pressure due to the three-dimensional shape of the largest wave. Based on the analysis and results summarized on Figures 31 and 32, the variability in the pressure ratio from maximum wave to maximum wave is modeled using the simplified probability distribution shown on Figure 72.

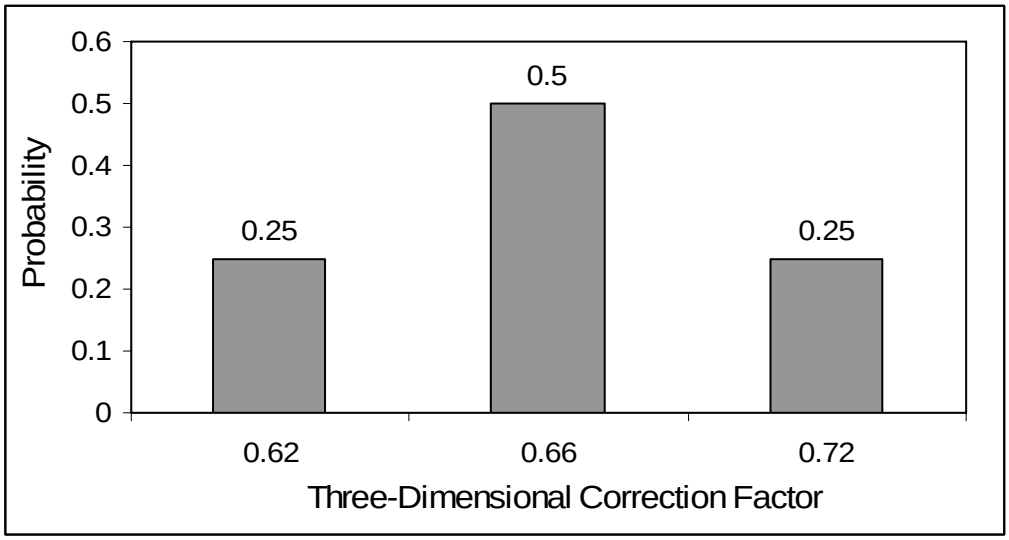

Figure 72. Approximate discrete probability distribution for bottom-pressure correction factor associated with maximum wave

Summary

The model to represent the hazard for wave-induced mudslides is summarized with the event tree shown on Figure 73. Each branch in the tree represents a possible value for a parameter describing the magnitude and shape of the wave-induced bottom pressures, and the number in parentheses is the probability of that particular value occurring. The first set of branches in Figure 73 characterizes the magnitude of the sea state in terms of the mean maximum wave height in a three-hour period. The probabilities for these values correspond to the probability of that mean maximum wave height occurring annually, and they depend on the water depth (e.g., Figure 70). For a given mean maximum wave height, the probability distribution of the maximum wave height during the three-hour sea state can be found from Equations (19), (20) and (21). The next set of branches in Figure 73 characterizes the wave length associated with the mean maximum wave height. There are three possible linear models relating wave length to the mean maximum wave height, given by Equations (23), (24) and (25). The final set of branches in Figure 73 characterizes the correction factor to account for the three-dimensional shape of the maximum wave in estimating the bottom pressure under the maximum wave. In total, the

event tree in Figure 73 consists of 8x3x3 = 72 possible combinations of parameters describing the sea state at a location.

The output of this event tree is the information needed to describe the magnitude and shape of the maximum bottom pressure during a storm: a probability distribution for maximum wave height H_{max}, $F_{Hmzx}(h_{max})$; a relationship between the wave length and the wave height, L_{Hmax}; and a bottom-pressure correction factor, I_{3D}. This information can be input into Equations (17) and (18) to obtain a probability distribution for the maximum bottom pressure, $F_{Pmax}(p_{max})$, and the associated wave length, L_{Hmax}. An example of this probability distribution is shown on Figure 74 for the combination of branches that is completed in the event tree on Figure 73 (i.e., a mean maximum wave height of $(h_{100} + h_{200})/2$, the average relationship between the wave length and wave height, $(L_{Hmax})_{avg.}$, and a pressure correction factor I_{3D} of 0.6) for a location in the Delta with a water depth of 200 feet. The probability that this location will see this particular combination of p_{max} and L_{Hmax} in a year is obtained by multiplying the respective probabilities of the three branches in Figure 73, 0.005x0.5x0.25 = 0.0006 per year.

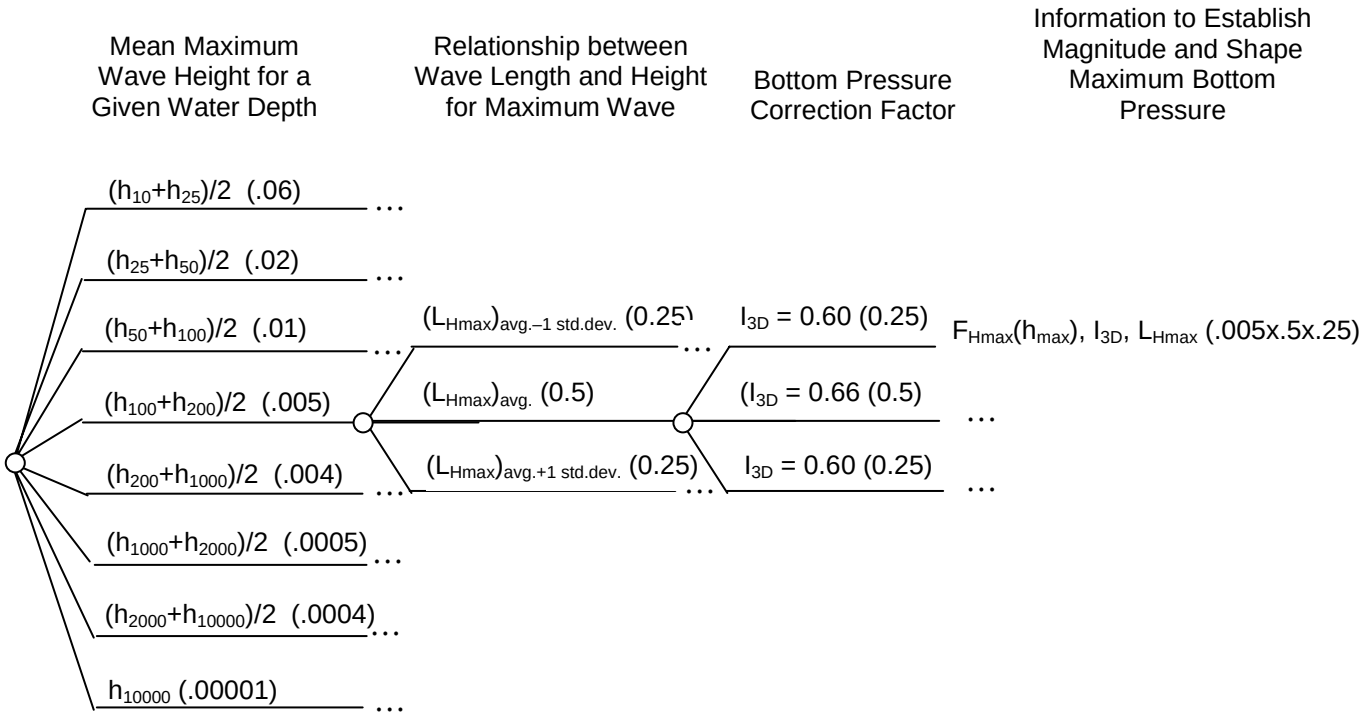

Figure 73. Event tree representing hazard for wave-induced mudslides

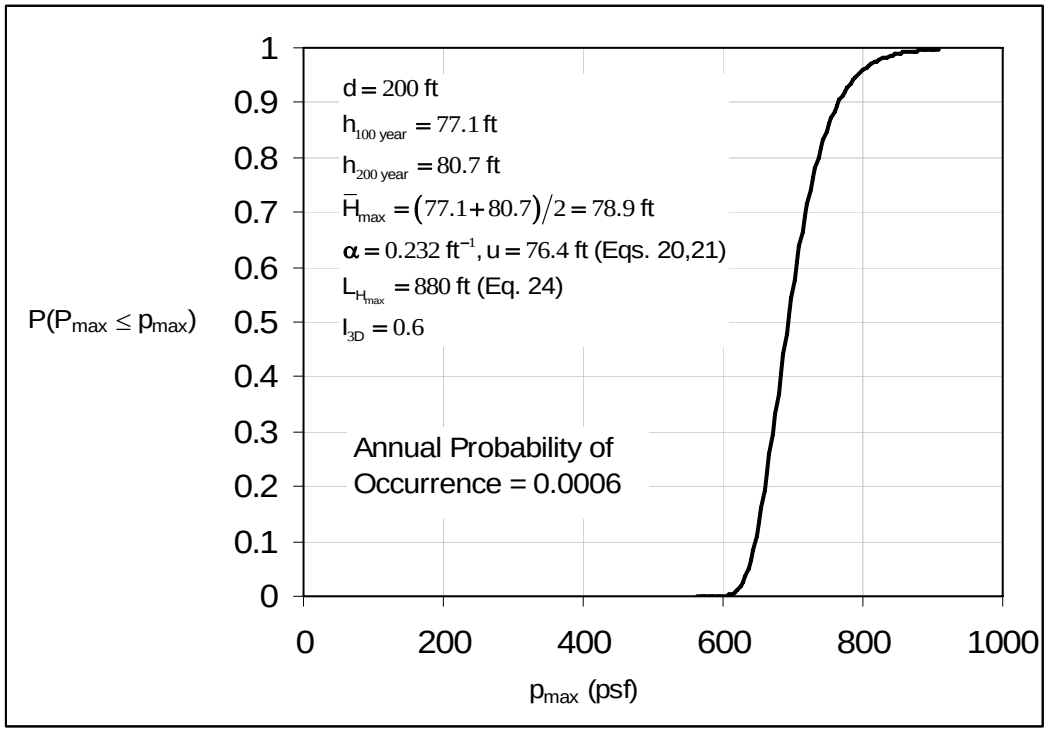

Figure 74. Example probability distribution for maximum bottom pressure and associated wave length for a location in 200 feet of water

Vulnerability Model for Wave-Induced Mudslides

The vulnerability for a wave-induced mudslide at a location is defined by the probability that the sea floor will fail when subjected to a particular sea state. Therefore, the input to this vulnerability is the information from the hazard analysis, such as Figure 74. For a given magnitude and shape of the pressures on the bottom, the vulnerability depends on the slope of the bottom and the profile of undrained shear strength with depth. The two-dimensional limit-equilibrium model described previously and implemented as a spreadsheet program (Appendix B) was used to characterize the vulnerability for a given bottom slope and profile of undrained shear strength. From this program, the threshold amplitude of bottom pressure that will cause a mudslide (i.e., a factor of safety just equal to 1.0) can be established for each wave length. An example of this threshold bottom pressure is shown on Figure 75 for a particular location with a given bottom slope and

profile of undrained shear strength versus depth. The threshold bottom pressure increases as the length of the bottom pressure wave increases because the critical slip surface is moving deeper into stronger soil.

From the relationship between threshold bottom pressure and wave length, the probability of a mudslide for a given sea state can be found as the probability that the maximum bottom pressure exceeds the threshold:

$$P\left(\text{Mudslide}\middle| P\left(P_{\max} \le p_{\max}\right), L_{H_{\max}}, \beta, s_u\left(z\right)\right) = 1 - P\left(P_{\max} \le p_{\max,\,\text{threshold}}\right) \tag{21}$$

where the possible combinations of $P\left(P_{\max} \le p_{\max}\right)$ and $L_{H_{\max}}$ are obtained from the event tree in Figure 73 (e.g., Figure 74 shows one combination), and β is the bottom slope and $s_u(z)$ is the profile of undrained shear strength versus depth. Therefore, the total annual probability of a mudslide can be obtained by summing up the probabilities for a given sea state over all possible sea states:

$$P_{annual}\left(\text{Mudslide}\middle| \beta, s_u\left(z\right)\right) = \sum_{\substack{\text{all combinations of} \\ P\left(P_{\max} \le p_{\max}\right) \text{ and } L_{H_{\max}}}} \left\{ \begin{array}{l} P\left(\text{Mudslide}\middle| P\left(P_{\max} \le p_{\max}\right), L_{H_{\max}}, \beta, s_u\left(z\right)\right) \\ \quad \times P_{annual}\left[P\left(P_{\max} \le p_{\max}\right), L_{H_{\max}}\right] \end{array} \right\} \tag{22}$$

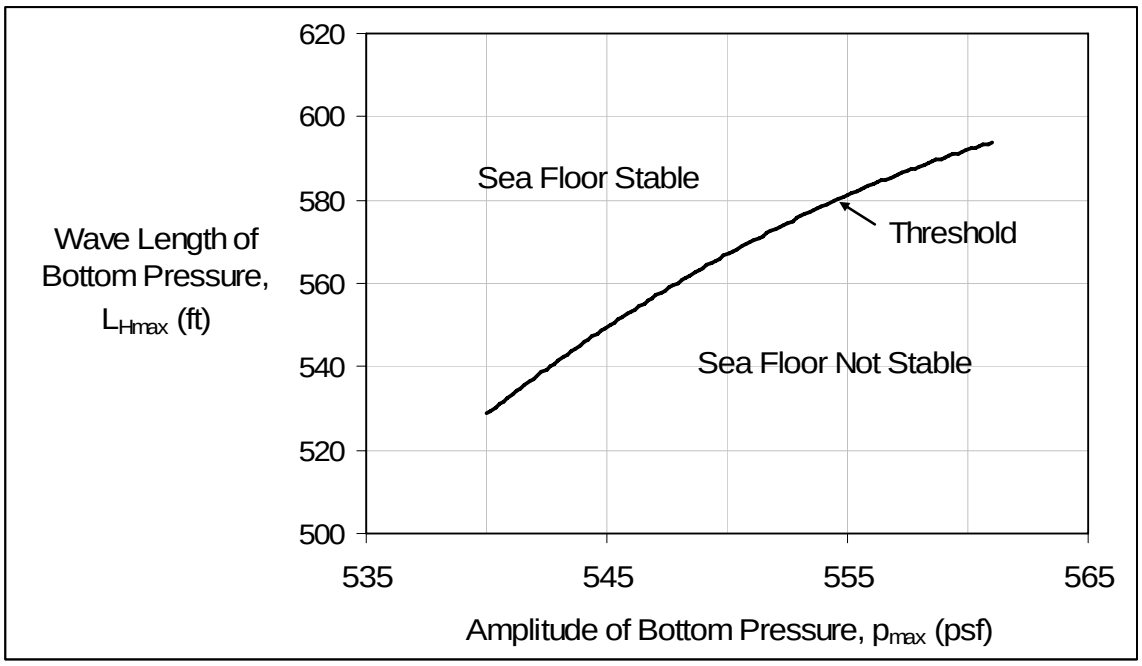

Figure 75. Bottom pressure threshold to cause a mudslide for a particular location in the Delta in 200 feet of water, with a bottom slope of 1 percent, and a profile of undrained shear strength with depth corresponding to the profile in Figure 12 labeled Main Pass 77

Variability in Undrained Shear Strength

The profile of undrained shear strength with depth is generally not known at a particular location and is extremely variable (e.g., Figures 12 to 15) across the Delta. In order to model this variability, the 21 profiles discussed earlier in MUDSLIDE VULNERABILITY ANALYSES were taken to represent a random sample of strength profiles, meaning that at any given location in the Delta we are equally likely to obtain one of these 21 profiles of undrained shear strength with depth. Therefore, the probability of a mudslide any given location in the Delta can be obtained as follows:

$$P_{annual}\left(\text{Mudslide}\middle|\beta\right)=\sum_{\text{all 21 profiles, }\left[s_u(z)\right]_i} P_{annual}\left(\text{Mudslide}\middle|\beta,\left[s_u(z)\right]_i\right)P\left(\left[s_u(z)\right]_i\right) \qquad (22)$$

where $P\left(\left[s_u\left(z\right)\right]_i\right)$ is equal to 1/21 for each of the possible 21 profiles. If site-specific boring information is available at a particular location, then Equation (22) can be adjusted by making the probability for that profile equal to 1.0 and the probabilities for all of the others 0.0. Probabilities may also be adjusted accordingly if there is uncertainty in the shear strength profile despite availability of site-specific shear strength data due to the small area represented by a single boring relative to the area of interest for a pipeline or a platform.

Risk Assessment

The risk analysis was conducted first by considering a point, then by considering a region of points approximately the size of a lease block, and finally by considering the locations of existing facilities that are located in the Delta.

Annual Probability of a Mudslide Occurring at a Point

Mudslide risk was assessed for seventy points or locations throughout the Mississippi Delta region of the Gulf of Mexico. The locations chosen were the same as the gridpoints used in the Hurricane Ivan hindcast (Cox et al, 2005), as shown on Figure 50 and repeated for convenience on Figure 76. Each location, or sub-region, represents approximately 11 square miles of area, which is nominally close to the 9-square-mile area for a typical lease block. The spacing of the locations shown in Figure 76 is considered to be fine enough to provide a realistic representation of the range of water depths and bottom slopes across the region. Within each of the sub-regions, the water depth and slope angle are assumed to be constant. The bathymetry used in the Ivan and Katrina mudslide analyses described previously was used in this analysis; it is assumed to represent the current conditions in the Delta. However, an updated bathymetric study of the entire region would be extremely helpful due to its dynamic nature and due to the possible changes that occurred in Hurricanes Ivan and Katrina.

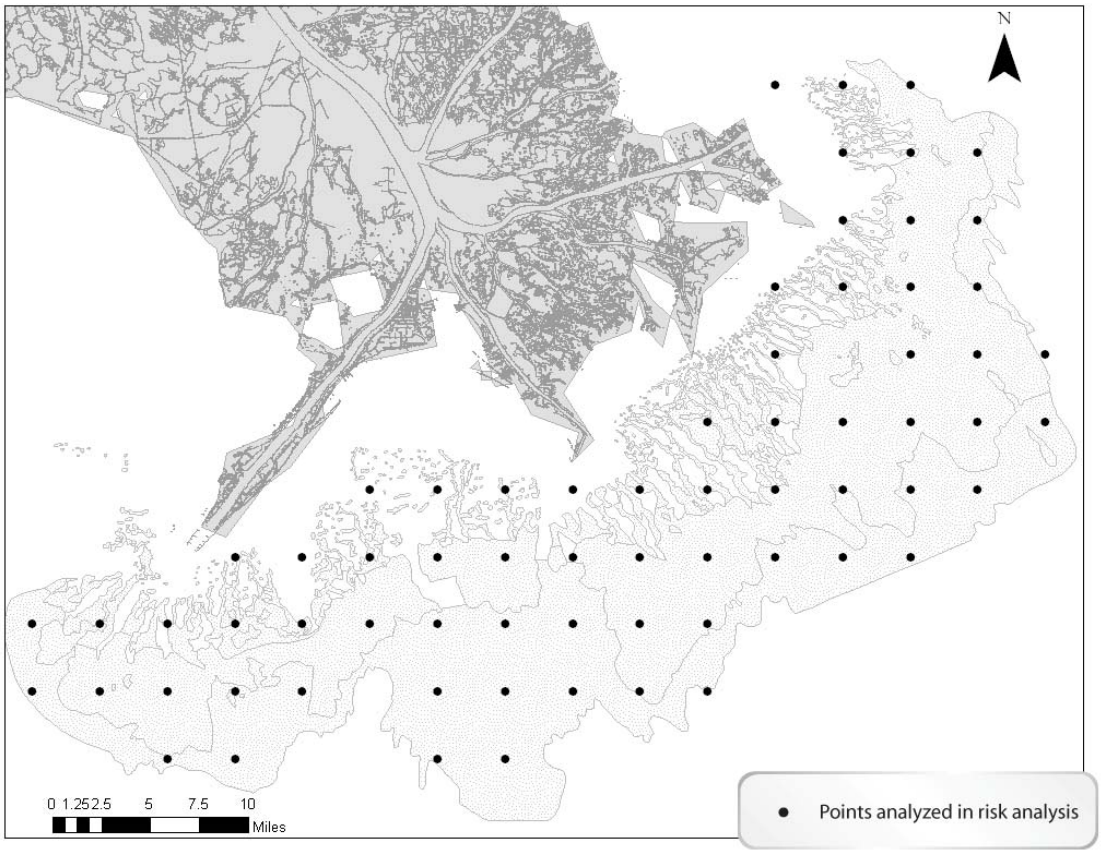

Figure 76: Locations of sub-regions analyzed for mudslide risk

For each of the sub-regions shown on Figure 76, the probability that a mudslide would occur annually was calculated from Equation 22. The results are shown as a return period versus location in the Delta on Figure 77. The differences in return period reflect differences in water depth, which affects both the maximum wave heights and the bottom pressures, and differences in bottom slope. The return periods for water depths between 200 and 400 feet are on the order of 10 to 100 years, which is consistent with at least three occurrences of mudslides in these water depths over the past 60 years: Hurricanes Camille, Ivan, and Katrina. The return periods for mudslides in water depths greater than

400 feet are on the order of 100 to 1,000 years. This estimate is also consistent with only one known occurrence over the past 60 years, Hurricane Ivan.

The practical meaning of information shown on Figure 77 is that an operator can use it to estimate the annual probability of a mudslide at the location of a particular facility, such as a platform. The term “location” here specifically corresponds to the area over which the maximum wave acts, which is approximately an area of roughly 4,000 feet by 4,000 feet (or several times the wavelength for the maximum wave). Therefore, this probability corresponds to a facility that is within a footprint that is several thousand feet across at most, such as a platform, and does not correspond to a facility that covers a much larger area of the Delta, such as a complex of platforms or a pipeline. The information on Figure 78 can also be used to determine the probability of at least one mudslide occurring over the lifetime of a facility:

$$P\left(\text{Mudslide at a Location over Lifetime}\right) = 1 - e^{-t/T} \cong t/T \qquad (23)$$

where t is the lifetime of the facility and T is the return period. For example, the probability of a mudslide occurring over a 30 year design life for a facility located where the return period for mudslides is 100 years is 26 percent.

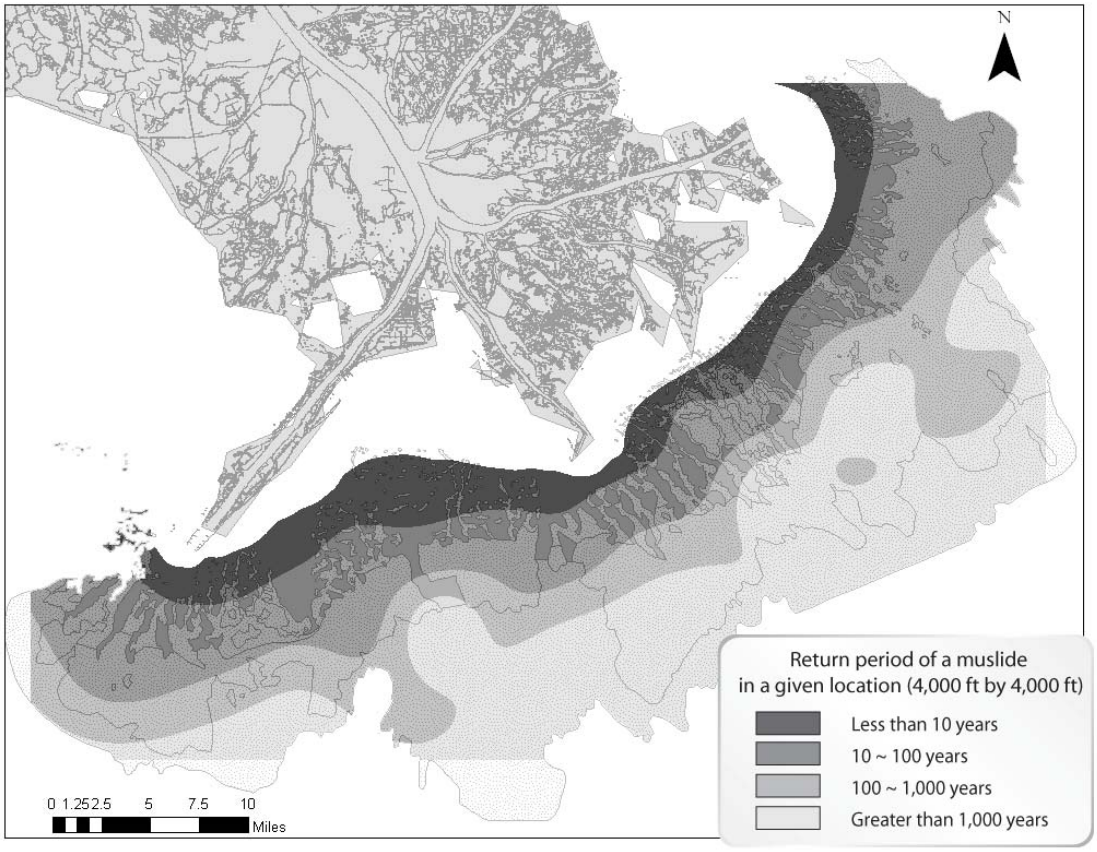

Figure 77: Return periods of a mudslide occurring at a point (4000 foot by 4000 foot area)

Annual Probability of a Mudslide Occurring in an Area

The event that at least one mudslide occurs over an area larger than roughly 4,000 by 4,000 feet is of interest in assessing the risk for a facility such as a pipeline or in assessing the risk associated with a group or fleet of facilities. We have extended the analysis to cover this type of event as follows:

1. The size of the storm (mean maximum wave height) and the period of the maximum wave (relative to the wave height) are assumed to be perfectly correlated among locations with the same depth, as a storm that affects one location will similarly affect other nearby locations and the relationship between

wave height and period tends to remain similar throughout an individual hurricane based on the hindcast data.

2. The probability that H_{max} was greater than the threshold value for and the bottom-pressure correction factor are assumed to be statistically independent between 4,000-foot by 4,000-foot locations in a given sea state in order to realistically model the variability in maximum wave heights at nearby locations in the same storm. This assumption is based on the size of an area that is affected by a single large wave.
3. The profile of undrained shear strength versus depth is also assumed to be statistically independent between 4,000-foot by 4,000-foot locations. This assumption is based on the observation that soil properties vary over relatively short distances (on the order of 1,000 feet or less) in the Delta.

With these assumptions, the statistically independent components of the risk analysis were modeled using a Bernoulli Sequence in order to calculate the probability of at least one mudslide occurring in an area of a given size. For a given sea state (mean maximum wave height and wave length), the probability that a mudslide would occur in a single 4,000-foot by 4,000-foot location for a given sea state was calculated as follows:

$$P\left(\text{Mudslide}\middle|\bar{H}_{\max}, L_{H_{\max}}, \beta\right) = \sum_{\substack{\text{all combinations of} \\ \left[s_u(z)\right]_i \text{ and } \left(I_{3D}\right)_j}} P\left(\text{Mudslide}\middle|\bar{H}_{\max}, L_{H_{\max}}, \beta, \left[s_u(z)\right]_i, \left(I_{3D}\right)_j\right) P\left(\left[s_u(z)\right]_i, \left(I_{3D}\right)_j\right) \quad (24)$$

Then, the probability of at least one occurrence of a mudslide over an area comprising n locations was calculated using the Bernoulli sequence:

$$P(\text{At Least One Mudslide} \mid \bar{H}_{\max}, L_{H_{\max}}, \beta) = 1 - \left[1 - P(\text{At Least One Mudslide} \mid \bar{H}_{\max}, L_{H_{\max}}, \beta)\right]^n \quad (25)$$

Finally, the annual probability of at least one mudslide occurring in a sub-region with n locations is obtained by summing the probabilities given a sea state over all of the possible sea states:

$$P_{annual}\left(\text{At Least One Mudslide} \middle| \beta\right) = \sum_{\substack{\text{all combinations of} \\ \bar{H}_{\max} \text{ and } L_{H_{\max}}}} P\left(\text{Mudslide} \middle| \bar{H}_{\max}, L_{H_{\max}}, \beta\right) P_{annual}\left(\bar{H}_{\max}, L_{H_{\max}}\right) \quad (26)$$

To illustrate the effect of an area of exposure larger than a 4,000-foot by 4,000-foot region, the probability of at least one mudslide occurring in each of the sub-regions shown on Figure 76 was calculated. Note that each 11-square mile sub-region in this analysis is nominally the size of a lease block and contains approximately 20 4,000-foot by 4,000-foot areas. The results are shown on Figure 78. The probability of at least one mudslide occurring in an area the size of a lease block is greater than the probability of a mudslide occurring in a particular 4,000-foot by 4,000-foot location because there are more opportunities for a large wave or a low shear strength profile to occur over the area of the lease block. This difference can be seen by comparing Figures 77 and 78; the regions corresponding to each interval of return period extend into deeper water in Figure 77 versus Figure 78.

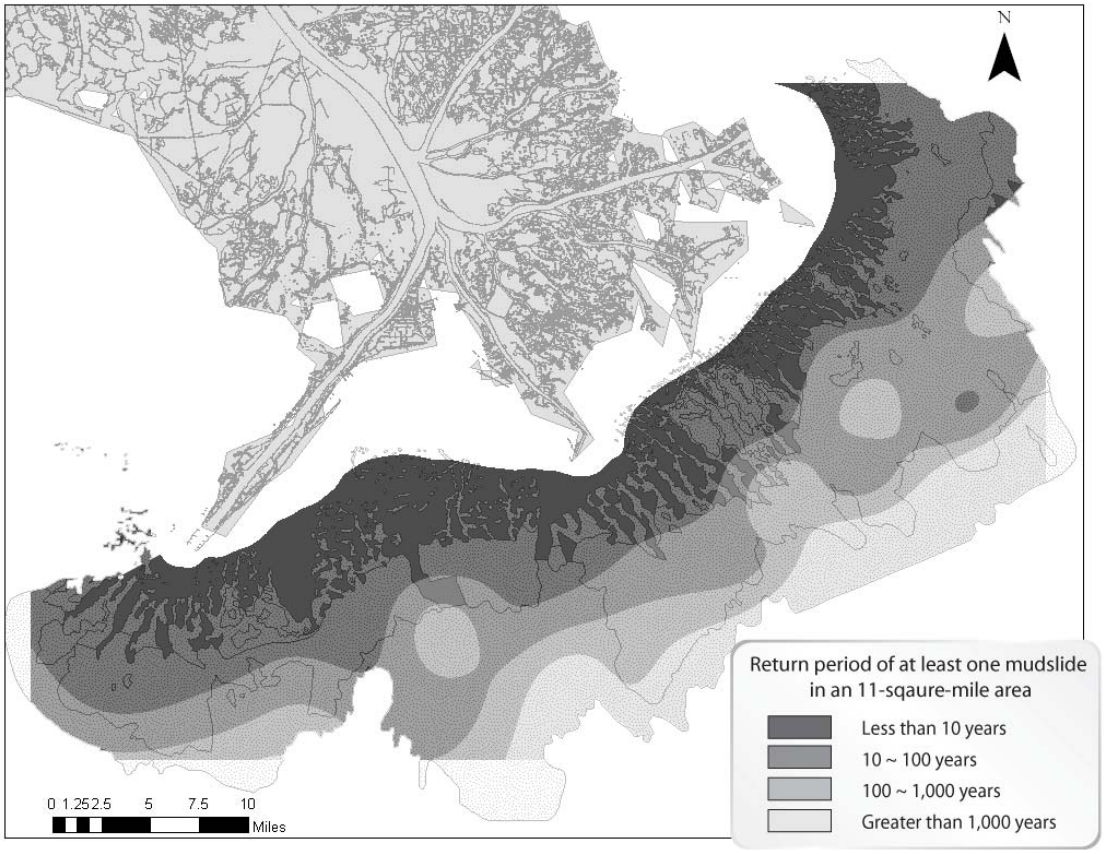

Figure 78: Return periods of at least one mudslide occurring in an 11-square-mile area (nominally the size of a lease block)

Annual Probability of Mudslides Impacting Pipelines

The occurrence of a mudslide itself is only of interest if it impacts a facility, that is, there is a consequence to the mudslide. Based on the existing pipeline infrastructure that exists in the Delta, the annual probability was calculated that a mudslide would impact a pipeline in each of the 70 sub-regions shown on Figure 76. This probability was calculated by determining in each sub-region the number of 4,000-foot by 4,000-foot areas out of the total of 20 that contain pipelines (e.g., Figure 4). For example, if 50 percent of a sub-region is covered with pipelines, then there are ten instead of 20 possible areas where a mudslide could impact a pipeline.

The estimated return periods of pipeline damage within each of the 11-square-mile areas in the Delta are shown in Figure 79. The return periods at each location are represented graphically by symbols of varying sizes, with the largest symbols corresponding to the shortest return periods (or highest annual probabilities of occurrence). Figure 79 represents a map of the risk to the oil industry as a whole. It combines the information about the probability of mudslides occurring in each sub-region together with the amount of pipeline infrastructure that is at risk. It is important to note that the occurrence of a mudslide near a pipeline does not necessarily mean that a pipeline will be damaged by a mudslide. A number of occurrences of mudslides that occurred near pipelines or moved pipelines but did not cause damage to the pipelines were described earlier in this report.

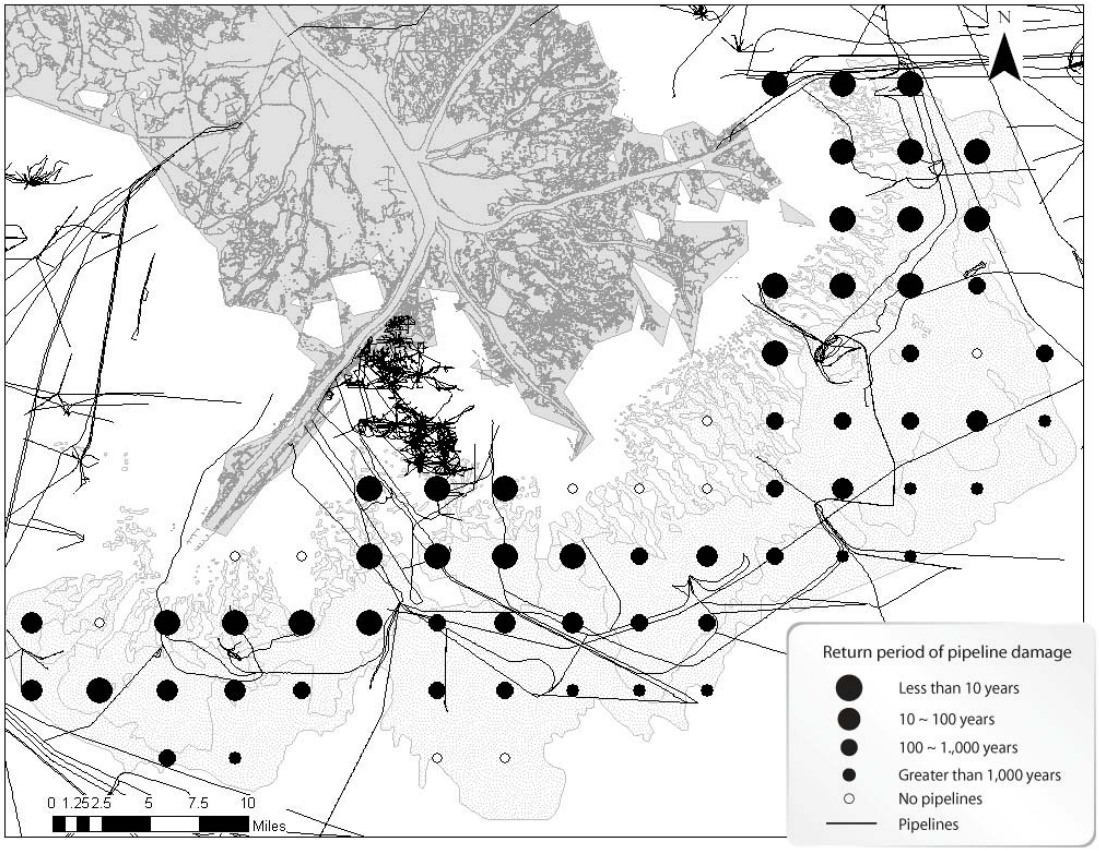

Figure 79: Return periods for mudslides impacting existing pipelines

This methodology could be extended to assess the risk for a particular pipeline as follows. First, the probability of at least one mudslide impacting it in each sub-region for a given sea state would be calculated depending on the percentage of area that the pipeline covers in each sub-region. Next, the probability that a mudslide impacts the pipeline across the whole region would be calculated for a given sea state from these individual sub-region probabilities by taking these events to be independent: the probability that the pipeline is impacted in at least one sub-region would be one minus the product of the probabilities that it is not impacted in each individual sub-region for that sea state. Finally, these probabilities for given sea states would be combined together for all of the possible sea states, as in Equation (26).

Conclusion

The risk of mudslides occurring and of mudslides impacting facilities has been assessed, and the results are shown as a series of maps on Figures 77, 78 and 79. The risk for mudslides increases as the water depth decreases, the slope of the bottom increases, and the amount of infrastructure in a particular area increases. The return periods for mudslides impacting pipelines range from less than 10 years to greater than 1,000 years and depend strongly on location.

Figure 37 showed the average relationship between maximum wave heights and peak spectral periods that were used in this risk analysis, and it was assumed that there was a unique one-to-one relationship between peak spectral period (and thus the maximum wave length) and the maximum wave height. The Ivan and Katrina data showed that lesser maximum wave heights at locations away from the hurricane track and the storm's eye also have the same long peak spectral periods. The assumption of the one-to-one relationship in effect ignores these other locations where the lesser maximum wave heights with the same peak spectral period may be large enough to cause a mudslide, and thus will tend to underestimate the frequency of occurrence of a mudslide. Given the wide bands on return periods shown in Figures 77 - 79, the inclusion of these other waves may not have a large impact on the result shown. However, this effect should be investigated.

The results of the risk analyses presented above are based on our understanding at present of hurricane characteristics and geotechnical conditions in the Delta. The results do not necessarily apply to a particular project where a site-specific met-ocean analysis and/or geotechnical analysis has been performed. However, the methodology could be applied on a project-specific basis by incorporating this information into the input.

XIII. CONCLUSION

The goal of this study was to use information obtained from recent hurricanes to investigate wave-induced mudslide activity in the Mississippi Delta region of the Gulf of Mexico. A list of the conclusions reached through this project is presented below.

- The data currently available suggest that all mudslides caused by recent large hurricanes occurred in or very near to the mudslide prone area delineated by Coleman et al. (1980). Most mudslides occurred in the mudflow lobe areas within the mudslide prone area, while a few occurred in the mudflow gully area.
- Hurricanes Ivan and Katrina probably caused similar amounts of mudslide activity.
- The simple limit equilibrium model used in this study works well to predict the factor of safety against mudslide initiation.
- Results of the simple limit equilibrium model agree well both with those found using an established slope stability computer program (UTEXAS4) and with a more rigorous layered continuum model, which calculates soil displacements.
- Site-specific analysis of mudslide vulnerability is challenging due to a lack of available shear strength data in the Mississippi Delta region of the Gulf of Mexico and the variation in soil shear strength even over short distances.
- Calculations performed using peak wave data (maximum wave heights and peak spectral periods) from hurricane hindcasts and assuming linear wave theory overestimate the pressure on the ocean floor caused by the wave due to the assumption that the wave is infinitely wide. A nonlinear wave simulation program by Zhang et al. (1999) was used to more accurately determine the bottom pressure. Bottom pressure was calculated using both linear wave theory and the irregular wave prediction program at 22 sites. The bottom pressure found using

the wave simulation program was on average 34% smaller than that found using linear wave theory, with a standard deviation of 6%.

- In most parts of the Mississippi Delta region of the Gulf of Mexico, mudslides can only be caused by very large storm waves and are therefore infrequent events. Only three major storms (Camille, Ivan, and Katrina) caused significant and widespread mudslide activity in the past 40 years.
- Wave period is an important factor in mudslide vulnerability. Waves in Hurricanes Ivan and Katrina had longer-than-average periods, and Hurricane Ivan, in particular, caused significantly more mudslide activity than other storms of its magnitude due to its very long wave periods.
- Slope angle is not a significant factor in mudslide vulnerability except in the deeper parts of the mudslide prone area (water depths greater than about 300 feet).
- Mudslide vulnerability is highest in shallow water and in areas with low shear strengths. Areas of the Mississippi Delta region of the Gulf of Mexico that have these characteristics have generally experienced mudslides in large hurricanes in the past, and it is likely that these areas will experience more mudslide activity in future storms.
- Mudslides are localized features, on the order of several thousand feet in lateral extent and about 50 to 150 feet deep. The areal extent and depth of mudslides are related to the lengths and widths of the storm waves that cause them. Mudslides are not likely to lead to large-scale, regional mudflows due to the very flat slopes in the mudslide prone area and the large amount of local variation in soil shear strength.
- The return periods for mudslides impacting pipelines range from less than 10 years to greater than 1,000 years and depend strongly on location. The risk for mudslides increases as the water depth decreases, the slope of the bottom increases, and the amount of infrastructure in a particular area increases.

Recommendations for Future Research

The most important limiting factor in this research was a lack of available undrained shear strength data in the Mississippi Delta region of the Gulf of Mexico. Hundreds of borings have been drilled in the Mississippi Delta, many of which include corresponding data on undrained shear strength, but most of these borings are proprietary and are not easily accessible. Work directed at creating a database of shear strength data throughout the Mississippi Delta region would be extremely useful for future studies of mudslide vulnerability. Shallow geologic cores are frequently collected and sonar surveys performed in the Mississippi Delta region for various studies. These methods often provide information on geologic features but not on shear strength. A comprehensive shear strength database would be useful to correlate values of shear strength with geologic features so that mudslide vulnerability might be estimated in areas where shear strength data are not available.

Another limiting factor in this research was a lack of high-quality data on mudslide occurrences. The Minerals Management Service pipeline damage lists (MMS, 2006) were the main source of information on mudslide occurrences, but these damage reports often included very little information on the areal extent, depth, and exact location of mudslides. Increased effort to collect and report detailed data on mudslide occurrences after hurricanes would be useful in future studies of mudslide vulnerability.

Linear wave theory involves simplifying assumptions that allow for rapid calculation of factors of safety against mudslide initiation. It was determined in this study, however, that linear wave theory significantly overestimates the pressures on the ocean floor caused by storm waves. An empirical correlation between bottom pressures calculated using linear wave theory and bottom pressures calculated using an irregular wave

prediction program (Zhang, 1999) was employed in this study. Development of a more accurate way to calculate bottom pressures using peak wave data would be useful.

The risk analyses of mudslide vulnerability presented in this report are based on available regional information for hurricane waves and soil properties. They should be updated as more information about waves and soil properties is obtained. In addition, they should be adapted for project-specific analysis by incorporating all available site-specific information on metocean conditions, bathymetry and soil properties.

The assumption of the one-to-one relationship between maximum wave height and peak spectral period ignores other locations in a given storm where lesser maximum wave heights with the same peak spectral period may be large enough to cause a mudslide, and thus will tend to underestimate the frequency of occurrence of a mudslide. The impact of this assumption on overall risks should be investigated.

REFERENCES

Arnold, P. (1973), "Finite Element Analysis—A Basis for Sea-floor Soil Movement Design Criteria," Proc. Offshore Technology Conference, Houston, Texas, OTC Paper No. 1900.

American Petroleum Institute (2007), "Interim Guidance on Hurricane Conditions in the Gulf of Mexico," API Bulletin 2, INT-MET, May, 2007.

Bea, R.G., Wright, S.G., Sircar, P., and Niedoroda, A.W. (1983), "Wave-Induced Slides in South Pass Lease Block 70, Mississippi Delta," Journal of Geotechnical Engineering, Vol. 109, No. 4.

Cardone, V. J., Cox, A. T., (1992), Hindcast Study of Hurricane Andrew (1992) Offshore Gulf of Mexico, Final Report by Oceanweather Inc., Cos Cob, CT.

Cardone, V.J., Cox, A. T. (2002), MMS Hindcast Study of Hurricane Lili (2002) Offshore Northern Gulf of Mexico, Final Report prepared for the MMS by Oceanweather Inc, Cos Cob, CT.

Cardone et al., (2006), "Hindcast Data on Winds, Waves, and Currents in Northern Gulf of Mexico in Hurricanes Katrina and Rita", Final Report prepared for the MMS by Oceanweather Inc., Cos Cob, CT.

Coleman, J.M., Prior, D.B., and Garrison, L. (1980), Minerals Management Service Open File Report 80-02, Maps 1-8.

Cox, A.T.,Cardone, V.J., Counillon, F., and Szabo, D. (2005), "Hindcast Study of Winds., Waves, and Currents in Northern Gulf of Mexico in Hurricane Ivan (2004)", Proc. Offshore Technology Conference, Houston, Texas, OTC Paper No. 17736.

Cox, A.T., Oceanweather, Inc., (2007), Personal Communication.

Coyne, M.J., and Dollar, J.J. (2005), "Shell Pipeline's Response and Repairs after Hurricane Ivan," Proc. Offshore Technology Conference, Houston, Texas, OTC Paper No. 17734.

Coyne, M.J., Shell Oil Products U.S., and Wrzyszczynski, M., Shell Exploration and Production Company (2006), Personal Communication.

Doyle, E.H. (1973), "Soil-Wave Tank Studies of Marine Soil Instability," Proc. Offshore Technology Conference, Dallas, Texas, OTC Paper No. 1901.

Dunlap, W., Holcombe, W., and Holcombe, T.(2004), Shear Strength Maps of Shallow Sediments in the Gulf of Mexico, OTRC Project Report, Library No. 09/04A126, Offshore Technology Research Center.

Forristall, G. Z. (1978), "On Statistical Distribution of Wave Heights in a Storm," *Journal of Geophysics Research,* 83, 2353-2358.

GEBCO, Inc. (2007), General Bathymetric Chart of the Oceans. http://www.ngdc.noaa.gov/mgg/gebco/

Haring, R.E., Osborne, A.R. and Spencer, L.P. (1976), "Extreme Wave Parameters Based on Continental Shelf Storm Wave Records," Proc. Fifteenth Coastal Engineering Conference, Honolulu, Hawaii, ASCE, Vol. 1, Ch. 10, July, pp. 151-170.

Haring, R. E. and Heideman, J.W. (1978), "Gulf of Mexico Rare Wave Return Periods," Proc. Offshore Technology Conference, Houston, Texas, OTC Paper No. 3230.

Henkel, D.J. (1970), "The Role of Waves in Causing Submarine Landslides," Geotechnique, Vol. 20, No. 1, pp. 75-80.

Hooper, J.R. (1980), "Crustal Layers in Mississippi Delta region of the Gulf of Mexico Mudflows." Proc. Offshore Technology Conference, Houston, Texas, OTC 3770.

Hooper, J.R. (1996), "Foundation Soil Motion in South Pass 47," Proc. Offshore Technology Conference, Houston, Texas, OTC Paper No. 1898.

Hooper, J.R. and Suhayda, J.N. (2005), "Hurricane Ivan as a Geologic Force: Mississippi Delta Front Seafloor Failures," Proc. Offshore Technology Conference, Houston, Texas, OTC Paper No. 17737.

Kraft, L.M., Jr., and Watkins, D.J. (1976), "Prediction of Wave-Induced Seafloor Movements," Proc. Fifteenth Coastal Engineering Conference, Honolulu, Hawaii, ASCE, Vol. 2, Ch. 49, July, pp. 1605-1623.

Ladd, C.C. and Foott, R. (1974), "New Design Procedure for Stability of Soft Clays," *Journal of the Geotechnical Engineering Division,* ASCE, Vol. 100, No. GT7, July, pp. 763-786.

Minerals Management Service (2005), List of pipelines damaged in hurricane Ivan by lease block, MMS Gulf of Mexico Region.

Minerals Management Service (2006), Pipelines in Gulf of Mexico Region, ArcInfo EEO File 8219-148, 409, 677.

Nodine, M.C., Gilbert, R.B., Wright, S.G., Cheon, J.Y., Wrzyszczynski, M., Coyne, M. and Ward, E.G. (2007), "Impact of Hurricane-Induced Mudslides on Pipelines," Proc. Offshore Technology Conference, Houston, Texas, OTC Paper No. 18983.

Pabor, P.A. (1981), "Numerical Analyses of Wave-Induced Seafloor Movements," M. S./ Thesis, The University of Texas at Austin, May 1981.

Patterson, M.M. (1974), "Oceanographic Data from Hurricane Camille," Proc. Offshore Tecnology Conference, Houston, Texas, OTC Paper No. 2109.

Prior, D.B. and Suhayda, J.N. (1979), "Application of Infinite Slope Analysis to Subaqueous Sediment Instability, Mississippi Delta," *Engineering Geology,* Vol. 14, pp. 1-10.

Quiros, G.W., Young, A.G. Pelletier, J.H., and Chan, J. H-C. (1983), "Shear Strength Interpretation for Gulf of Mexico Clays," Proc. Conference on Geotechnical Practice in Offshore Engineering, Austin, Texas, pp. 144-165.

Quiros, G.W. and Little, R.L. (2003), "Deepwater Soil Properties and Their Impact on the Geotechnical Program," Proc. Offshore Technology Conference, Houston, Texas, OTC Paper No. 15262.

Roberts, H.H., Cratsley, D.W., and Whelan, Thomas III (1976), "Stability of Mississippi Delta region of the Gulf of Mexico Sediments as Evaluated by Analysis of Structural Features in Sediment Borings," Proc. Offshore Technology Conference, Houston, Texas, OTC Paper No. 2425.

Schapery, R.A., and Dunlap, W.A. (1978), "Prediction of Storm-Induced Shear Bottom Movement and Platform Forces," Proc. Offshore Technology Conference, Houston, Texas, OTC Paper No. 3259.

Spencer, E. (1967), "A Method of Analysis of the Stability of Embankments Assuming Parallel Interslice Forces," *Geotechnique*, Great Britain, Vol. 17, No. 1, March, pp. 11-26.

Sterling, G.H. and Strobeck, E.E. (1973), "The Failure of the South Pass 70 B Platform in Hurricane Camille," Proc. Offshore Technology Conference, Houston, Texas, OTC Paper No. 1898.

Suhayda, J.N. (1996), “Oceanographic Design Data for South Pass Area Block 47,” Proc. Offshore Technology Conference, Houston, Texas, OTC Paper No. 7952.

Tang, W., Mesri, G. and Halim, I. (1992), “Uncertainty of Mobilized Undrained Shear Strength,” *Soil and Foundations*, Vol. 32, No. 4, December, pp. 107-116.

Thompson, J., Garrett, M., Taylor, M., and George, T. (2005), “Sonar surveys for pipeline inspection show extent of pipeline displacement and seafloor instability following Hurricane Ivan,” Proc. Offshore Technology Conference, Houston, Texas, OTC Paper No. 17738.

USACE (2006), Post-Katrina Intragency Hurricane Evaluation Task Force (IPET) report, U.S. Army Corps of Engineers.

Walsh, J.P., Corbett, D.R., Mallinson, D., Goni, M., Dail, M., Loewy, C., Marciniak, K., Ryan, K., Smith, C., Stevens, A., Sumners, B., and Tesi, T. (2006), “Mississippi Delta Mudflow Activity and 2005 Gulf Hurricanes,” Eos, Transactions, American Geophysical Union, Vol. 87, No. 44.

Ward, E.G., Borgman, L.E. and Cardone, V.J. (1978), “Statistics of Hurricane Waves in the Gulf of Mexico,” Proc. Offshore Technology Conference, Houston, Texas, OTC Paper No. 3229.

Wiegel, R.L. (1964), Oceanographical Engineering, Prentice Hall, Inc., Englewood Cliffs, NJ.

Winterstein, S.R. and Kumar, S. (1995), “Reliability of Floating Structures: Extreme Response and Load Factor Design.” Proc. Offshore Technology Conference, Houston, Texas, OTC Paper No. 7758.

Wright, S.G. and Dunham, R.S. (1972), "Bottom Stability Under Wave Induced Loads," Proc. Offshore Technology Conference, Houston, Texas, OTC Paper No. 1603.

Wright, S.G. (1976), "Analyses for Wave Induced Sea-Floor Movements," Proc, Offshore Technology Conference, Houston, Texas, OTC Paper No. 2427B.

Wright, S.G., Nodine, M.C., and Gilbert, R.B. (2007), “Submarine Slope Stability,” Proc. First North American Landslide Conference, Vail, Colorado.

Zhang, J., Yang, J., Prislin, I., Wen, J., and Hong, K. (1999), “Deterministic Wave Model for Short-Crested Ocean Waves, Part I. Theory and Numerical Scheme,” applied ocean Research, Vol.21, 167-188.

APPENDIX A - MUDSLIDES OCCURRENCES FROM THE MMS PIPELINE DAMAGE LIST

Most of the information on mudslide occurrences for this study was found in the MMS pipeline damage list. These damage reports in this list were reported by offshore pipeline and rig operators. This appendix includes a complete list of the damage reports corresponding to mudslides from Hurricanes Ivan and Katrina discussed in this study. Explanations of damage reports are provided where necessary. Damage reports are grouped by location. Damage reports at the same location are grouped together in the maps showing mudslide locations in the main body of this report (Figure 5 and Figure 6).

Most of the damage reports listed here have “Mud Slide” listed as the cause of damage. Those that do not are believed to have been caused by mudslides based on the location of the damage (in the vicinity of other mudslides), the damage description, or other information sources such as published reports or personal communication with industry representatives. These damage reports are shaded in gray.

Damage reports are copied exactly as they were published. Each row of the report was split into two lines so that it would fit onto the page.

Pipeline damage caused by mudslides in Hurricane Ivan

West Delta Block 109

SEGMENT	SIZE	PROD	Operator	ORIGIN			DESTINATION			Age	CAUSE		Damage	Damage Location	Location
				AREA	BLK	ID NAME	AREA	BLK	ID NAME		Prmry	Secndry			
14229	08	OIL	CHEVRON PIPE LINE COMPANY	WD	109	Capped End	WD	109	End	5	NH	Mud Slide	Other	Submerged Pipe	

REPORT DATE	Damage Description	Hurricane	REMARKS
19-Sep-04	Safety joint separated due to the mudflow from the hurricane.	Ivan	Hurricane Ivan

South Pass Lease Block 77

SEGMENT	SIZE	PROD	Operator	ORIGIN			DESTINATION			Age	CAUSE		Damage	Damage Location	Location
				AREA	BLK	ID NAME	AREA	BLK	ID NAME		Prmry	Secndry			
5750	26	GAS	TENNESSEE GAS PIPELINE CO	SP	77	A	SP	55	A	25	NH	Mud Slide	Other	Submerged Pipe	
5750	26	GAS	TENNESSEE GAS PIPELINE CO	SP	77	A	SP	55	A	25	NH	S/H	Pulled Apart	Departing Riser	
5773	10	BLKO	CHEVRON USA INC	SP	77	capped end	SP	77	end	26	NH	Mud Slide	Pulled	Receiving Riser	Other
6129	10	BLKO	CHEVRON USA INC	SP	77	Capped End	SP	77	Capped End	24	NH	Mud Slide	Pulled Apart	Receiving Riser	Tube Turn
12124	10	OIL	CHEVRON PIPE LINE COMPANY	SP	77	A	SP	55	A	28	NH	Mud Slide	Pulled	Departing Riser	
12170	08	BLKG	CHEVRON USA INC	SP	77	capped end	SP	77	end	8	NH	Mud Slide	Pulled	Receiving Riser	Other
9904	08	BLKO	CHEVRON USA INC	SP	58	D	SP	77	A	24	NH	S/H	Pulled Apart	Submerged Pipe	
6109	10	BLKO	CHEVRON USA INC	SP	77	Open End	SP	77	Open End	24	NH	S/H	Pulled	Submerged Pipe	

REPORT DATE	Damage Description	Hurricane	REMARKS
17-Sep-04	Pipeline has a leak about 100 yards from the SP 77 platform. Break away joint must be replaced and an investigation is underway to determine extent of damage.	Ivan	Hurricane Ivan
18-Mar-05	As a result of a mudslide, the PBSJ separted from SP77A structure, located 200 feet from the platform.	Ivan	Hurricane Ivan. Temporary repair made 5/9/05. PBSJ will not be available until Aug 2005. Temporary plan not approved by this office.
15-Dec-04	Due to mudslide pipeline separated and can only be located by divers 1500' from SP 77 A.	Ivan	Hurricane Ivan.
01-Oct-04	Pipeline parted at the riser on A structure. An investigation by divers determined the pipelin ewas buried 15' due to shifting bottom conditions. Divers searched for the end of the pipeline by jetting a probing, but were unable to find the end of the pi	Ivan	Hurricane Ivan. Permitted as a modification not a repair.
10-Nov-04	Line severed due to mudslide, found 6200' away from platform.	Ivan	Hurricane Ivan
15-Dec-04	Due to a mudslide pipeline separated and cannot be located until 3000' from SP 77 A.	Ivan	Hurricane Ivan
19-Nov-04	As a result of Hurricane Ivan, p/l developed a leak at the safety joint located ~20' from the receiving (SP 77 A end) riser, and the riser was pulled out 5' from the jacket leg at the -196' elev.	Ivan	
28-Feb-05	Pipeline completely destroyed, new pipeline installed SN 15049.	Ivan	Hurricane Ivan.

Segments 9904 and 6109 did not have mudslides listed as a cause of damage, but due to the numerous reports of nearby mudslide damage, it is likely that their damage was caused by the mudslide as well.

South Pass Lease Block 55

SEGMENT	SIZE	PROD	Operator	ORIGIN			DESTINATION			Age	CAUSE		Damage	Damage Location	Location
				AREA	BLK	ID NAME	AREA	BLK	ID NAME		Prmry	Secndry			
10711	20	GAS	ENTERPRISE FIELD SERVICES LLC	VK	817	A	SP	55	A	12	NH	Mud Slide	Apart	Submerged Pipe	

REPORT DATE	Damage Description	Hurricane	REMARKS
27-Oct-04	Mudslide at SP 55 severed pipeline from riser and moved the pipeline 6000' from the original location in some areas.	Ivan	Hurricane Ivan

South Pass Lease Block 49

SEGMENT	SIZE	PROD	Operator	ORIGIN			DESTINATION			Age	CAUSE		Damage	Damage Location	Location
				AREA	BLK	ID NAME	AREA	BLK	ID NAME		Prmry	Secndry			
6678	12	GAS	TENNESSEE GAS PIPELINE CO	SP	49	capped end	SP	55	capped end	23	NH	Mud Slide	Line Pulled Apart	Submerged Pipe	
6764	06	GAS	TENNESSEE GAS PIPELINE CO	SP	49	platform C	SP	50	12 SSTI	23	NH	Mud Slide	Line Ruptured	Submerged Pipe	
5625	10	G/O	CHEVRON PIPE LINE COMPANY	SP	49	capped end	SP	50	capped end	26	NH	Mud Slide	Line Pulled Apart	Departing Riser	Other

REPORT DATE	Damage Description	Hurricane	REMARKS
01-Jun-05	27,128 ft of pipe to be abandoned in place and replaced with new pipe in MP 50 and 51. x = 2,698,655.0 y = 72, 200.00 and x = 2.724,464.63 y = 70,200.0. New SN 15178 assigned to modified pipeline.	Ivan	Hurricane Ivan. Repair handled as a modification.
30-Jun-05	Line ruptured and filled with seawaters. PIpeline was decommissioned.	Ivan	Hurricane Ivan
27-Sep-04	Mudslide caused safety joint to break at SP 49 A and pipe is broken in SP 45. No pollution.	Ivan	Hurricane Ivan. 11/09/2004 entry: the ~20,000' section of pipeline located between SP 45 and SP 38 will be de-oiled by flushing the contents of the pipe in 3,000' increments through a coiled tubing head into approved containers using seawater and nitrogen

Mississippi Canyon Block 20

SEGMENT	SIZE	PROD	Operator	ORIGIN			DESTINATION			Age	CAUSE		Damage	Damage Location	Location
				AREA	BLK	ID NAME	AREA	BLK	ID NAME		Prmry	Secndry			
14312	03	BLKG	MARINER ENERGY INC	MC	65	Flange	MC	20	A	2	NH	Mud Slide			
13854	10	GAS	TOTAL E&P USA INC	MC	243	A	MC	20	20"SSTI	3	NH	Mud Slide	Pulled	Subsea Tie-In	
14313	03	UBEH	MARINER ENERGY INC	MC	20	A	MC	65	Splice		NH	Mud Slide	Pulled	Submerged Pipe	
14667	10	BLKO	TAYLOR ENERGY COMPANY	MC	21	B Platform	MC	20	A Platform		NH	Mud Slide	Unknown	Receiving Riser	Splash Zone
14668	08	BLKO	TAYLOR ENERGY COMPANY	MC	21	Plat "B"	MC	20	Plat "A"		NH	Mud Slide	Unknown	Receiving Riser	Splash Zone
14669	08	BLKG	TAYLOR ENERGY COMPANY	MC	21	Plat "B"	MC	20	Plat "A"		NH	Mud Slide	Unknown	Receiving Riser	Splash Zone
14670	06	TEST	TAYLOR ENERGY COMPANY	MC	21	Plat "B"	MC	20	Plat "A"		NH	Mud Slide	Unknown	Receiving Riser	Splash Zone
14671	04	GAS	TAYLOR ENERGY COMPANY	MC	20	Plat "A"	MC	21	Plat "B"		NH	Mud Slide	Unknown	Departing Riser	Splash Zone
7296	06	OIL	TAYLOR ENERGY COMPANY	MC	20	Valve	MC	65	Flange	22	NH	Mud Slide	Other	Departing Riser	Other
7178	12	GAS	TRANSCONTINENTAL GAS PIPE LIN	MC	65	Capped End	MC	108	End	21	NH	Mud Slide	Unknown	Departing Riser	
12712	06	BLKG	WALTER OIL & GAS CORPORATION	MC	65	capped end	MC	20	A	5	NH	S/H	Unknown	Receiving Riser	
10909	08	G/C	W & T OFFSHORE INC	SP	72	platform A	MC	20	platform A	10	NH	S/H	Unknown	Receiving Riser	

REPORT DATE	Damage Description	Hurricane	REMARKS
17-Sep-04		Ivan	e-mail from B. Dinger 9/17/04 indicated that p/l probably parted either at the MC 20 A riser or at the safety joint. The source, MC 66 SS Well #1 is S-I downhole and the tree vaves are closed.
28-Dec-04	Line moved 207 ft from the current trunkline tie-in point.	Ivan	Hurricane Ivan
08-Oct-04		Ivan	Hurricane Ivan
20-Sep-04	MC 20 "A" platform toppled and the extent of the pipeline damage is unknown at this time.	Ivan	Hurricane Ivan
20-Sep-04	MC 20 "A" platform toppled in storm, extent of pipeline damage unknown at this time.	Ivan	Hurricane Ivan
20-Sep-04	MC 20 "A" toppled in storm, the extent of the pipeline damage is unknown.	Ivan	Hurricane Ivan
20-Sep-04	MC 20 "A" toppled in storm, extent of pipeline damage is unknown at this time.	Ivan	Hurricane Ivan
20-Sep-04	MC 20 "A" platform toppled in storm, extent of damage is unknown at this time.	Ivan	Hurricane Ivan
20-Sep-04	MC 20 "A" Platform was toppled over, extent of pipeline damage is unknown until diver investigation is complete.	Ivan	Hurricane Ivan
29-Sep-04	MC 20 A platform toppled in storm, extent of damage unknown.	Ivan	Hurricane Ivan
29-Sep-04	MC 20 A platform toppled in storm, extent of damage is unknown.	Ivan	Hurricane Ivan
20-Sep-04	MC 20 A toppled in storm.		

A platform was toppled by a mudslide in Mississippi Canyon Block 20 during Hurricane Ivan. The pipelines damaged at this location were all connected to the platform, so most of the pipeline damage was probably directly caused by the movement of the platform. Segments 12712 and 10909 did not have mudslides listed as the cause of damage, but it is assumed that their damage is associated with the same mudslide.

South Pass Lease Block 60

SEGMENT	SIZE	PROD	Operator	ORIGIN			DESTINATION			Age	CAUSE		Damage	Damage Location	Location
				AREA	BLK	ID NAME	AREA	BLK	ID NAME		Prmry	Secndry			
4715	08	OIL	SHELL OIL COMPANY	SP	70	C	SP	60	A	28	NH	S/H	Unknown	Submerged Pipe	
3655	10	GAS	SPN RESOURCES LLC	SP	60	A	SP	6	F/S		NH	S/H	Line Pulled Apart	Submerged Pipe	

REPORT DATE	Damage Description	Hurricane	REMARKS
24-Feb-05	Pipeline severed, currently gather more data on where the pipeline severed and where it is currently located.	Ivan	Hurricane Ivan
11-Nov-04	Following Hurricane Ivan, p/l failed integrity test and bubbles were observed ~1/4 mi from SP 60 A. Sidescan sonar subsequently determined p/l to be parted w/ends ~1827' apart.	Ivan	

Segment 4715 was reported as a mudslide through personal contact with representatives from Shell Oil Company. Segment 3655 is believed to have been damaged by a mudslide due to its vicinity to segment 4715.

Main Pass Lease Block 151

SEGMENT	SIZE	PROD	Operator	ORIGIN			DESTINATION			Age	CAUSE		Damage	Damage Location	Location
				AREA	BLK	ID NAME	AREA	BLK	ID NAME		Prmry	Secndry			
13543	18	OIL	EQUILON PIPELINE COMPANY LLC	MC	474	A	MP	70	F/S	3	NH	S/H	Apart	Submerged Pipe	

REPORT DATE	Damage Description	Hurricane	REMARKS
23-Sep-04		Ivan	Hurricane Ivan-for repair procedure see other entry for 9/23/04.

The mudslide in Main Pass Lease Blocks 151 and 148, which severed Shell's Nakika pipeline, was described by Coyne et al. (2005).

Main Pass Lease Block 151/148

SEGMENT	SIZE	PROD	Operator	ORIGIN			DESTINATION			Age	CAUSE		Damage	Damage Location	Location
				AREA	BLK	ID NAME	AREA	BLK	ID NAME		Prmry	Secndry			
4283	18	GAS	SOUTHERN NATURAL GAS COMPANY	MP	151	18 SSTI	MP	62	26 SSTI	32	NH	Mud Slide	Line Pulled Apart	Submerged Pipe	
6144	06	GAS	GULF SOUTH PIPELINE COMPANY LP	MP	72	F/S	MP	151	18 SSTI	24	NH	Mud Slide	Line Pulled Apart	Subsea Tie-In	
8628	08-10	GAS	CHEVRON USA INC	MP	77	A	MP	151	18 SSTI	22	NH	Mud Slide	Line Pulled Apart	Submerged Pipe	

REPORT DATE	Damage Description	Hurricane	REMARKS
02-Nov-04	18" pipeline is completely separated 15ft North of MP 151 block valve and three pipeline tie-ins are damaged in MP 72, 151 and 77.	Ivan	Hurricane Ivan
01-Aug-05		Ivan	Hurricane Ivan.
15-Feb-05	PBSJ broke due to a mudslide, line was found 500 feet away. Modification submitted for the repair procedure.	Ivan	Hurricane Ivan

Main Pass Lease Block 72/73

SEGMENT	SIZE	PROD	Operator	ORIGIN			DESTINATION			Age	CAUSE		Damage	Damage Location	Location
				AREA	BLK	ID NAME	AREA	BLK	ID NAME		Prmry	Secndry			
11015	18	OIL	BP PIPELINES (NORTH AMERICA) I	MP	225	A	MP	69	F/S	10	NH	S/H	Other	Submerged Pipe	

REPORT DATE	Damage Description	Hurricane	REMARKS
30-Sep-04	Pipeline has moved 3000 feet from the original as-built location and is resting up against Chevron's MP 144 Platform. Major displacement is from MP 143 to MP 265. 3 holes at the Nakika pipeline crossing were found.	Ivan	Hurricane Ivan.

The mudslide in Main Pass Lease Blocks 72 and 73 was described by Thompson et al. (2005). An image of the mudslide scars at this location is shown in Thompson et al. (2005). The damage report above refers to where BP's Main Pass Oil Gathering (MPOG) System pipeline moved due to other mechanisms (possibly bottom currents) in deeper water at Main Pass Lease Block 144. The pipeline was displaced slightly at the location of the mudslide, but a damage report was not submitted to MMS for the incident.

Main Pass Lease Block 70

SEGMENT	SIZE	PROD	Operator	ORIGIN			DESTINATION			Age	CAUSE		Damage	Damage Location	Location
				AREA	BLK	ID NAME	AREA	BLK	ID NAME		Prmry	Secndry			
14948	12	OIL	SHELL OFFSHORE INC	MP	290	Flange	MP	72	F/S	37	NH	S/H	Other		

REPORT DATE	Damage Description	Hurricane	REMARKS
06-May-05	Pipeline crossing damage	Ivan	Hurricane Ivan

The mudslide that caused a leak in Segment 14948, Shell's Odyssey 12" pipeline, was described by Coyne et al. (2005).

Pipeline damage caused by mudslides in Hurricane Katrina

West Delta Block 110

SEGMENT	SIZE	PROD	Operator	ORIGIN			DESTINATION			Age	CAUSE		Damage	Damage Location	Location
				AREA	BLK	ID NAME	AREA	BLK	ID NAME		Prmry	Secndry			
15007	08	OIL		WD	109	A	WD	125	12" SSTI	5	NH	S/H	Unknown		

REPORT DATE	Damage Description	Hurricane	REMARKS
19-Dec-05	Damage description not provided by operator.	Katrina	Hurricane Katrina

Segment 15007 is located in the mudflow lobe area, and no information about the damage was provided in the damage report. It is possible, then, that the pipeline was damaged by a mudslide.

South Pass Lease Block 77

SEGMENT	SIZE	PROD	Operator	ORIGIN			DESTINATION			Age	CAUSE		Damage	Damage Location	Location
				AREA	BLK	ID NAME	AREA	BLK	ID NAME		Prmry	Secndry			
15050	08	LIFT	CHEVRON USA INC	SP	77	A	SP	77	C	1	NH	Mud Slide	Line Pulled Apart	Receiving Riser	
15049	10	BLKO	CHEVRON USA INC	SP	77	C	SP	77	A	1	NH	Mud Slide	Line Pulled Apart	Departing Riser	
5773	10	BLKO	CHEVRON USA INC	SP	77	capped end	SP	77	capped end	26	NH	Mud Slide	Line Pulled Apart	Submerged Pipe	
12170	08	BLKG	CHEVRON USA INC	SP	77	capped end	SP	77	capped end	8	NH	Mud Slide	Line Pulled Apart	Submerged Pipe	

REPORT DATE	Damage Description	Hurricane	REMARKS
08-Feb-06	Riser parted on C structure, divers found the end of the pipe 128' from structure.	Katrina	Hurricane Katrina
08-Feb-06	10" riser parted at C structure, divers were able to find the end of the 10" pipe 36' from the structure.	Katrina	Hurricane Katrina
07-Feb-06	Line separated and moved 3068' from SP 77 A Structure. Will be handled as a modification/partial decommission	Katrina	Hurricane Katrina
07-Feb-06	Line parted and found 3977' from SP 77 A Structure. Will be handled as a modification/partial decommissioning.	Katrina	Hurricane Katrina

Mississippi Canyon Block 20

SEGMENT	SIZE	PROD	Operator	ORIGIN			DESTINATION			Age	CAUSE		Damage	Damage Location	Location
				AREA	BLK	ID NAME	AREA	BLK	ID NAME		Prmry	Secndry			
13854	10	GAS	TOTAL E&P USA INC	MC	243	A	MC	20	20"SSTI	3	NH	Mud Slide	Other	Subsea Tie-In	

REPORT DATE	Damage Description	Hurricane	REMARKS
22-Nov-05	Significant damage at SSTI to VKGS pipelines	Katrina	

South Pass Lease Block 60

SEGMENT	SIZE	PROD	Operator	ORIGIN			DESTINATION			Age	CAUSE		Damage	Damage Location	Location
				AREA	BLK	ID NAME	AREA	BLK	ID NAME		Prmry	Secndry			
3655	10	GAS	SPN RESOURCES LLC	SP	60	A	SP	6	F/S		NH	Mud Slide	Line Pulled Apart	Departing Riser	Below Splash Zone
15060	10	BLKO	TAYLOR ENERGY COMPANY LLC	MC	21	B	SP	60	F		NH	S/H	Other	Submerged Pipe	
15158	06	OIL	DEVON LOUISIANA CORPORATION	SP	70	Capped end	SP	60	Capped end		NH	S/H	Unknown	Submerged Pipe	
38	06	OIL	ARCO PIPE LINE COMPANY	SP	60	B	SP	60	A	34	NH	S/H	Line Pulled Apart	Departing Riser	Above Splash Zone
47	12	GAS	SPN RESOURCES LLC	SP	60	C	SP	60	A		NH	S/H	Other	Departing Riser	
6526	04	NGER	SPN RESOURCES LLC	SP	60	F	SP	60	D	24	NH	S/H	Other	Departing Riser	

REPORT DATE	Damage Description	Hurricane	REMARKS
28-Nov-05	The lowest riser clamp is located at the -144 elevation. The riser is bent just below the riser clamp and is sheared off just downstream of the pipe bend at the base of the riser. There is a gap of 74.5' of missing pipe and the downstream section of the	Katrina	Hurricane Katrina
26-May-06	Pipeline crossing with SN 11449 mats displaced and pipeline displaced.	Katrina	Hurricane Katrina
16-Feb-06	Pipeline was under construction and not yet connected when hurricane hit. 7350' section of pipe could not be located. Burried below mudline and to be abandoned in place. Repalcemnt pipe to be installed and new SN 15598 to be assigend to pipeline under par	Katrina	Hurricane Katrina
19-Dec-05	Riser is broken just above the J-tube.	Katrina	Hurricane Katrina
19-Dec-05	Riser standoff broken	Katrina	
19-Dec-05	Standoff brace broken.	Katrina	

There was one damage incident reportedly caused by a mudslide in South Pass Lease Block 60 (Segment 3655) but five other pipelines in the vicinity were reported damaged. It is possible that these incidents were caused by mudslides as well.

Main Pass Lease Block 70

SEGMENT	SIZE	PROD	Operator	ORIGIN			DESTINATION			Age	CAUSE		Damage	Damage Location	Location
				AREA	BLK	ID NAME	AREA	BLK	ID NAME		Prmry	Secndry			
14948	12	OIL	SHELL OFFSHORE INC	MP	290	Flange	MP	72	F/S	37	NH	S/H	Other	Submerged Pipe	
11926	10	OIL	CHEVRON PIPE LINE COMPANY	MP	299	FP	MP	71	F/S	35	NH	S/H	Unknown		

REPORT DATE	Damage Description	Hurricane	REMARKS
06-Feb-06	Pipeline damaged in MP 70.	Katrina	Hurricane Katrina
19-Dec-05	No description provided by operator	Katrina	Hurricane Katrina Deoiling procedure approved 4/20/

The damage to segment 14948 was caused by a mudslide, according to representatives from Shell Oil Company. The It is possible that the damage to nearby segment 11926 was also caused by a mudslide, as no damage description was provided.

Unknown Location

SEGMENT	SIZE	PROD	Operator	ORIGIN			DESTINATION			Age	CAUSE		Damage	Damage Location
				AREA	BLK	ID NAME	AREA	BLK	ID NAME		Prmry	Secndry		
10711	20	GAS	ENTERPRISE FIELD SERVICES LLC	VK	817	A	SP	55	A	12	NH	Mud Slide	Line Pulled Apart	Submerged Pipe

REPORT DATE	Damage Description	Hurricane	REMARKS
20-Oct-05	Line pulled apart and moved in 2 locations.	Katrina	Hurricane Katrina.

Segment 10711 begins far east of the Mississippi Delta in the Viosca Knoll area, and terminates at South Pass Lease Block 55. It was reportedly severed by mudslides at two locations during Hurricane Katrina, but neither of the locations was specified. It is likely that the damage occurred in either Mississippi Canyon Block 20 or in South Pass Lease Block 55, as mudslides have been known to occur in these locations, but the damage may have occurred anywhere within the mudslide prone area.

APPENDIX B - USER'S GUIDE FOR THE LIMIT EQUILIBRIUM SPREADSHEET PROGRAM

The spreadsheet program that was developed for this study is included with this report as a Microsoft Excel file. The spreadsheet program can be used to calculate a factor of safety against mudslide initiation for any site where the undrained shear strength varies in a piecewise linear pattern with depth.

The input parameters for the spreadsheet include:

- Slope angle (β)
- Water depth (d)
- Wavelength (L)
- Wave height (h)
- Submerged soil unit weight (γ'_s)
- Water unit weight (γ_w)
- Any soil shear strength profile with up to 50 data points
- A range of trial circle heights (h) – see Figure B1

Assumptions incorporated into the limit equilibrium model include:

- Slip surface is circular
- Soil unit weight, γ'_s, is constant
- The slope, β, is uniform
- Soil layers run parallel to the slope
- Bottom pressure, p_{max}, is calculated using linear wave theory (assumes a rigid sea floor)

The spreadsheet calculates the minimum factor of safety for a site by calculating the factors of safety for various slip circles. The size of the circle is dictated by its radius, R, and the height, h, of its center point above the slope, as shown in Figure B1.

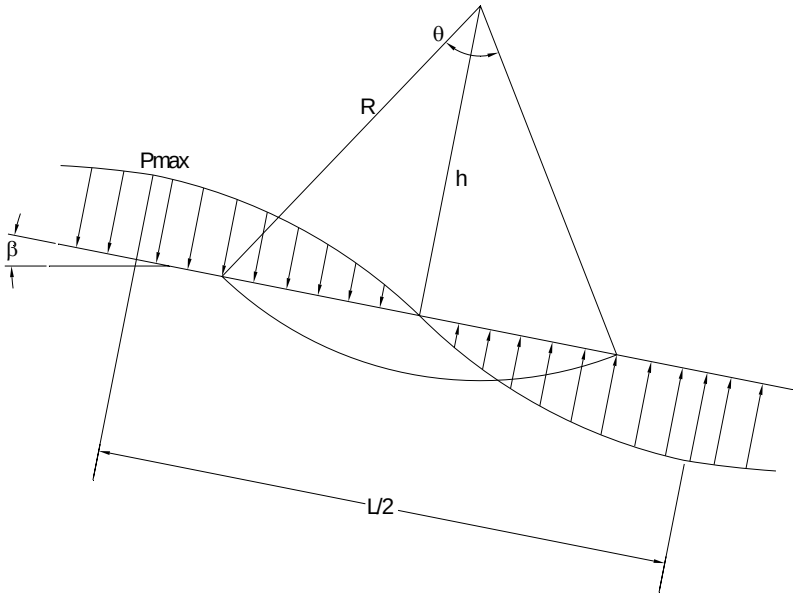

Figure B1. Model geometry

The user interface for the spreadsheet program is shown in Figure B2. For simplicity, the shear strength profile is defined by only six data points. The user can enter up to 50 data points to define the shear strength profile in the spreadsheet program.

Slope Angle (rad)	Water Depth (ft)	Wavelength (ft)	Wave Height (ft)	Submerged Soil Unit Wt. (pcf)	Water Unit Wt. (pcf)	Maximum Wave Pressure (psf)
β	d	L	H	γ'_s	γ_w	p_{max}
0.0100	**350**	**1000**	**70**	**30.0**	**64**	490.80

Minimum Factor of Safety = **0.80**

Trial Heights, h (ft)	Corresponding Factors of Safety
50	0.936
100	0.852
150	0.815
200	0.801
250	0.804
300	0.807
350	0.818
400	0.833
450	0.852
500	0.874
550	0.899

Shear Strength Profile

Critical height, h (ft)	Depth (ft)	Shear Strength (psf)	Radius of circle, r (ft)	Factor of Safety, F
200	**0**	**50**		
	50	**105**	**250**	**0.99**
	100	**139**	**300**	**0.81**
	150	**167**	**350**	**0.80**
	200	**175**	**400**	**0.82**
	250	**196**	**450**	**0.91**

Figure B2. User interface for the spreadsheet program

All cells requiring user input are highlighted blue in the spreadsheet program and are highlighted light gray in the figures contained in this Appendix. English units are listed for all values in the spreadsheet, but SI units can be used as long as units are consistent.

Steps to Using the Spreadsheet Program

1. ***Initial input and calculated values***

Initial input values are typed into the spreadsheet in the cells shown circled in Figure B3. The contents of the various cells in which data are entered are described further below. The resulting values calculated in the spreadsheet program are also described. The equations used for all calculations are shown in the main body of this report.

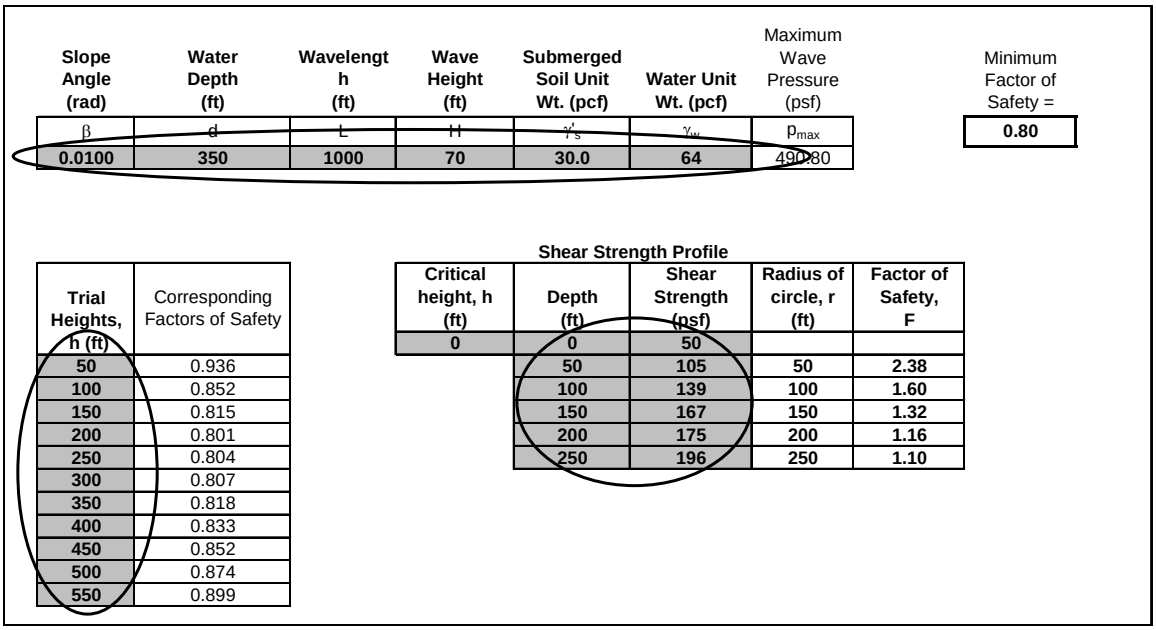

Slope Angle (rad)	Water Depth (ft)	Wavelength (ft)	Wave Height (ft)	Submerged Soil Unit Wt. (pcf)	Water Unit Wt. (pcf)	Maximum Wave Pressure (psf)
β	d	L	H	γ'_s	γ_w	p_{max}
0.0100	350	1000	70	30.0	64	490.80

Minimum Factor of Safety = **0.80**

Trial Heights, h (ft)	Corresponding Factors of Safety
50	0.936
100	0.852
150	0.815
200	0.801
250	0.804
300	0.807
350	0.818
400	0.833
450	0.852
500	0.874
550	0.899

Shear Strength Profile

Critical height, h (ft)	Depth (ft)	Shear Strength (psf)	Radius of circle, r (ft)	Factor of Safety, F
0	0	50		
	50	105	50	2.38
	100	139	100	1.60
	150	167	150	1.32
	200	175	200	1.16
	250	196	250	1.10

Figure B3. Locations of initial input values

Site Parameters

The slope angle (in radians), water depth, wavelength, wave height, submerged unit weight of soil, and unit weight of water for the site are entered into the cells shown circled in Figure B4. The equation to calculate wavelength from wave period is presented in the main body of the report, Equation 15.

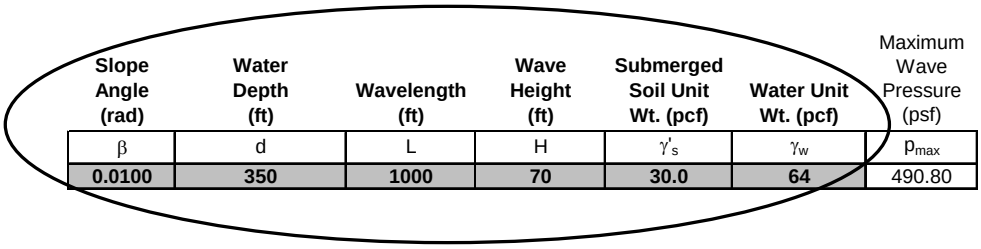

Slope Angle (rad)	Water Depth (ft)	Wavelength (ft)	Wave Height (ft)	Submerged Soil Unit Wt. (pcf)	Water Unit Wt. (pcf)	Maximum Wave Pressure (psf)
β	d	L	H	γ'_s	γ_w	p_{max}
0.0100	350	1000	70	30.0	64	490.80

Figure B4. Site parameters

The maximum pressure caused by the wave on the sea floor, shown circled in Figure B5, is calculated from the water depth, wavelength, wave height, and unit weight of water.

Slope Angle (rad)	Water Depth (ft)	Wavelength (ft)	Wave Height (ft)	Submerged Soil Unit Wt. (pcf)	Water Unit Wt. (pcf)	Maximum Wave Pressure (psf)
β	d	L	H	γ'_s	γ_w	p_{max}
0.0100	**350**	**1000**	**70**	**30.0**	**64**	490.80

Figure B5. Maximum pressure on the sea floor

Undrained Shear Strength Profile

The variation in undrained shear strength with depth is entered into the cells shown circled in Figure B6. Up to fifty points can be entered into the spreadsheet program to describe the shear strength profile.

Shear Strength Profile

Critical height, h (ft)	Depth (ft)	Shear Strength (psf)	Radius of circle, r (ft)	Factor of Safety, F
0	**0**	**50**		
	50	**105**	**50**	**2.38**
	100	**139**	**100**	**1.60**
	150	**167**	**150**	**1.32**
	200	**175**	**200**	**1.16**
	250	**196**	**250**	**1.10**

Figure B6. Shear strength profile

Trial Circle Heights

A number of trial heights for the centers of circles are entered into the cells shown circled in Figure B7. The factor of safety associated with each trial height will be calculated in the column to the right of the designated heights. The height of the critical circle (that with the lowest factor of safety) will be chosen from among the trial heights entered. For the Gulf of Mexico sites investigated, the critical circle height was typically between 200 and 500 feet. Accordingly, 50 to 100 feet is a good starting value for the heights. The factor of safety is not particularly sensitive to height. Thus, the increment between heights can be relatively large. Increments between 25 and 100 feet are sufficient. The example below uses a starting height of 50 feet, a maximum height of 550 feet, and increments of 50 feet. The critical factor of safety of 0.801 falls within the range of heights specified. Notice the small change in factor of safety (0.801-0.936) over the large range in height.

Trial Heights, h (ft)	Corresponding Factors of Safety
50	0.936
100	0.852
150	0.815
200	0.801
250	0.804
300	0.807
350	0.818
400	0.833
450	0.852
500	0.874
550	0.899

Figure B7. Trial heights

Once the initial input values have been entered, the minimum factor of safety is displayed in the upper right corner of the spreadsheet, in the cell shown circled in Figure B8.

Slope Angle (rad)	Water Depth (ft)	Wavelength (ft)	Wave Height (ft)	Submerged Soil Unit Wt. (pcf)	Water Unit Wt. (pcf)	Maximum Wave Pressure (psf)
β	d	L	H	γ'_s	γ_w	p_{max}
0.0100	**350**	**1000**	**70**	**30.0**	**64**	490.80

Minimum Factor of Safety = **0.80**

Trial Heights, h (ft)	Corresponding Factors of Safety
50	0.936
100	0.852
150	0.815
200	0.801
250	0.804
300	0.807
350	0.818
400	0.833
450	0.852
500	0.874
550	0.899

Shear Strength Profile

Critical height, h (ft)	Depth (ft)	Shear Strength (psf)	Radius of circle, r (ft)	Factor of Safety, F
0	**0**	**50**		
	50	**105**	**50**	**2.38**
	100	**139**	**100**	**1.60**
	150	**167**	**150**	**1.32**
	200	**175**	**200**	**1.16**
	250	**196**	**250**	**1.10**

Figure B8. Factor of safety calculated from initial input values

2. *Check that the factor of safety is a minimum*

To verify that the factor of safety calculated is a minimum factor of safety for the given set of input parameters, the minimum factor of safety must be located in the column labeled "Corresponding Factors of Safety," as shown in Figure B9. The column shows the factors of safety corresponding to each of the trial heights. The minimum factor of safety must lie somewhere within the range of heights designated as input.

Trial Heights, h (ft)	Corresponding Factors of Safety
50	0.936
100	0.852
150	0.815
200	0.801
250	0.804
300	0.807
350	0.818
400	0.833
450	0.852
500	0.874
550	0.899

Figure B9. Minimum factor of safety within range of heights

If the minimum factor of safety corresponds to either the maximum or the minimum trial height, the range of trial heights must be changed. For example, if the trial heights shown in Figure B9 began at 400 feet rather than at 50 feet, the range of heights and corresponding factors of safety would be as shown in Figure B10.

Trial Heights, h (ft)	Corresponding Factors of Safety
400	0.833
450	0.852
500	0.874
550	0.899
600	0.927
650	0.957
700	0.989
750	1.024
800	1.062
850	1.102
900	1.130

Figure B10. Minimum factor of corresponding with minimum height

The lowest factor of safety shown in this case would appear to be 0.833, while in reality

the minimum factor of safety is 0.801. In order to ensure that the factor of safety calculated is a minimum, lower trial heights should be entered.

3. ***Selection of the critical circle and computation of its properties***

Once the height of the critical circle has been determined, the depth and radius of the circle can be calculated and the variation in factor of safety with circle depth can be examined. To compute the properties of the critical slip circle, the height corresponding to the minimum factor of safety must be typed into the box labeled "Critical Height," as shown in Figure B11.

Slope Angle (rad)	Water Depth (ft)	Wavelength (ft)	Wave Height (ft)	Submerged Soil Unit Wt. (pcf)	Water Unit Wt. (pcf)	Maximum Wave Pressure (psf)	Minimum Factor of Safety =
β	d	L	H	γ'_s	γ_w	p_{max}	**0.80**
0.0100	**350**	**1000**	**70**	**30.0**	**64**	490.80	

Trial Heights, h (ft)	Corresponding Factors of Safety
50	0.936
100	0.852
~~150~~	~~0.815~~
200	0.801
~~250~~	0.804
300	0.807
350	0.818
400	0.833
450	0.852
500	0.874
550	0.899

Shear Strength Profile

Critical height, h (ft)	Depth (ft)	Shear Strength (psf)	Radius of circle, r (ft)	Factor of Safety, F
200	**0**	**50**		
	50	**105**	**250**	**0.99**
	100	**139**	**300**	**0.81**
	150	**167**	**350**	**0.80**
	200	**175**	**400**	**0.82**
	250	**196**	**450**	**0.91**

Figure B11. Critical circle height entered in to table to calculate circle properties

Once the critical circle height has been entered, the radius for a circle corresponding to each depth in the shear strength profile is calculated by subtracting the depth from the circle height. The factors of safety for slip circles extending to each depth are calculated. The radii and factors of safety are shown circled in Figure B12.

Slope Angle (rad)	Water Depth (ft)	Wavelength (ft)	Wave Height (ft)	Submerged Soil Unit Wt. (pcf)	Water Unit Wt. (pcf)	Maximum Wave Pressure (psf)
β	d	L	H	γ'_s	γ_w	p_{max}
0.0100	**350**	**1000**	**70**	**30.0**	**64**	490.80

Minimum Factor of Safety = **0.80**

Trial Heights, h (ft)	Corresponding Factors of Safety
50	0.936
100	0.852
150	0.815
200	0.801
250	0.804
300	0.807
350	0.818
400	0.833
450	0.852
500	0.874
550	0.899

Shear Strength Profile

Critical height, h (ft)	Depth (ft)	Shear Strength (psf)	Radius of circle, r (ft)	Factor of Safety, F
200	**0**	**50**		
	50	**105**	**250**	**0.99**
	100	**139**	**300**	**0.81**
	150	**167**	**350**	**0.80**
	200	**175**	**400**	**0.82**
	250	**196**	**450**	**0.91**

Figure B12. Radii and factors of safety for slip circles extending to each depth in the shear strength profile

In order to find the properties of the critical slip circle, the value of the minimum factor of safety from the top of the spreadsheet must be located in the table of factors of safety shown circled in Figure B12. The corresponding radius and depth can then be found. In the example shown in Figure B13, the critical slip circle has a depth of 150 feet and a radius of 350 feet.

Slope Angle (rad)	Water Depth (ft)	Wavelength (ft)	Wave Height (ft)	Submerged Soil Unit Wt. (pcf)	Water Unit Wt. (pcf)	Maximum Wave Pressure (psf)
β	d	L	H	γ'_s	γ_w	p_{max}
0.0100	**350**	**1000**	**70**	**30.0**	**64**	490.80

Minimum Factor of Safety = **0.80**

Trial Heights, h (ft)	Corresponding Factors of Safety
50	0.936
100	0.852
150	0.815
200	0.801
250	0.804
300	0.807
350	0.818
400	0.833
450	0.852
500	0.874
550	0.899

Shear Strength Profile

Critical height, h (ft)	Depth (ft)	Shear Strength (psf)	Radius of circle, r (ft)	Factor of Safety, F
200	**0**	**50**		
	50	**105**	**250**	**0.99**
	100	**139**	**300**	**0.81**
	150	**167**	**350**	**0.80**
	200	**175**	**400**	**0.82**
	250	**196**	**450**	**0.91**

Figure B13. Identification of properties of the critical slip circle

APPENDIX C - WAVE AMPLITUDE AND PRESSURE ANIMATIONS

Two thirty-second animation files in avi format are included with this report. One animation shows the amplitudes of the waves on the ocean surface, and the other shows the corresponding pressures caused by the waves on the ocean floor. The animations are for directional spectra for the peak of Hurricane Ivan, and they correspond to a site that has a water depth of 259 feet. The animations cover an area of 5000 feet by 5000 feet, about the size of one oil lease block. It can be seen in these animations that both the amplitudes and bottom pressures are variable in time and space. Waves may increase or decrease in amplitude as they move, causing the maximum bottom pressure experienced at one location to be different from that at a nearby location.